Chair of Leightweight Systems

Materials Science Department

Faculty of Natural Sciences and Technology

The AMASE Master Programme

Master Thesis

Ultrasound Monitoring of CFRP-Aluminum Hybrid Joints

submitted by

Ezgi Erdogan

on April 2019

Advisor
Prof. Dr.-Ing. Hans-Georg Herrmann

Supervisor
M. Sc. Stephan Bechtel

Reviewer
Prof. Dr. rer. nat. Ralf Busch

DECLARATION OF AUTHENTICITY

I hereby confirm that this thesis is my own work and that I have documented all sources used.

Saarbrücken, 15 April 2019

_____

Ezgi Erdogan

ACKNOWLEDGEMENTS

First and foremost, I would like to thank my advisor Prof. Dr. Hans-Georg Hermann for giving me the opportunity to write this thesis at the chair of lightweight systems.

My sincere thanks to Prof. Dr. Ralf Busch for reviewing my master thesis.

I owe my gratitude to my supervisor M. Sc. Stephan Bechtel for his valuable help, patience and the time he invested into my thesis.

Sincere thanks are given to everyone in AMASE programme for the unlimited help they have given during my studies.

I would like to deeply thank Dilege, Esmeray, Gülfem, Didem, Çağlar and Başak for their valuable friendship.

Also, I am indebted to Sema for her support and encouragement during my time in Germany.

I would like to thank Michael for his support and patience. He made it possible to complete my studies.

Finally, I would like to express my gratitude to my family for their endless support, especially to my father for encouraging my scientific curiosity.

ABSTRACT

In this work, shear horizontal (SH) guided ultrasonic waves are investigated as a means to monitor adhesively bonded hybrid structures. Aluminium alloy and carbon fiber reinforced polymer (CFRP) single lap joints are produced using co-curing method. Co-curing is a single step joining method, which uses the excess resin from the impregnated laminate to establish the adhesive bonding. SH guided waves are generated and detected by electromagnetic acoustic transducers (EMAT) in a pitch-catch mode. EMATs are placed on the aluminium part of hybrid single lap joint test pieces. First, the initial state of stress free joints are investigated by comparing them to a reference waveform. It is found that the bonding affects the shape and amplitude of the wave packet; thus, carries information regarding the bonding area. Then, the hybrid test pieces are investigated under quasi-static, incremental step and dynamic loading. The results indicate that the failure event can be clearly detected by SH guided wave monitoring. Moreover, gradual change of the waveforms during the incremental step and dynamic loading can be linked to damage propagation of the adhesive joint.

Table of Contents

List of Abbreviations and Symbols

A	Area of the overlap (mm)
b	Width of the overlap (mm)
B	Magnetic field
c_g	Group velocity (mm/µs)
c_L	Longitudinal wave velocity (mm/µs)
c_p	Phase velocity (mm/µs)
c_T	Shear wave velocity (mm/µs)
CFRP	Carbon fiber reinforced polymer
δ_{ij}	Kronecker delta
d	Guided wave propagation medium thickness (mm)
ε_{ij}	Strain tensor
e	Electron charge
$\underline{E}$	Electric field
EMAT	Electromagnetic acoustic transducer
Ep#	Epoxy matrix hybrid sample
φ	Scalar displacement field
f	Frequency (MHz)
$\underline{f}_L$	Lorentz force
F_a	Force amplitude (N)
F_{fail}	Failing load (N)
F_m	Mean force (N)

H	Vectorial displacement field
J_e	Electron eddy current density
k	Wave number
l_o	Length of the overlap (mm)
λ , μ	Lame constants
n_e	Electron density
N	Ion density
m	Electron mass,
NDT	Non-destructive testing
ρ	Density (kg/m^3)
R	Reflection coefficient
σ_{ij}	Stress tensor
τ_B	Shear stress (MPa)
τ	Mean time of electron-ion collision
τ_B	Shear strength of the adhesive joint (MPA)
T	Transmission coefficient
TP#-#	Thermoplastic matrix hybrid sample
u_i	Particle displacement in the x_i direction
$\underline{u}$	Ion displacement.
US	Ultrasonics
$\underline{v}_e$	Mean electron velocity
VIP	Vacuum infusion process
ω	Angular frequency
Z	Acoustic impedance ($kg/m^2 s$)
Z_e	Ion charge

1. INTRODUCTION

Adhesively bonded aluminium alloy and carbon fiber reinforced polymer hybrid structures were investigated using ultrasonic shear horizontal (SH) guided waves, while subjected to quasi-static load, incremental step load and dynamic load tests. Hybrid structures had a single lap joint configuration, where bonding was established by co-curing using vacuum infusion process. SH guided waves were generated and detected by electromagnetic acoustic transducers (EMATs). The goal of the experiments is to monitor changes within the adhesive joints during the mechanical loading and predict the failure of the joints.

1.1 MOTIVATION

Adhesive joints (also termed as adhesively bonded joints, bonded joints) are widely used in various industries as an alternative to other joining methods [1]. However, its use as primary load carrying structures has been restricted due to lack of knowledge of the adhesion mechanisms, difficulties regarding the reliable testing and evaluation of the adhesive joint quality and performance [2]. The reason is the sensitivity of the joints quality to the vast amount of parameters involved every step in its life cycle.

Adhesive joints have many advantages over their counterparts. One of the advantages of using adhesives as a joining method is to join dissimilar materials with complicated geometries, which results in structures called *Hybrid structures*. Hybrid structures are combining the "unique and desirable" features of both materials [3]. Especially in industries with lightweight design concerns, hybrid structures have been increasingly utilized. For example, hybrid structures made of metal and CFRP (Carbon Fibre Reinforced Polymer) are chosen to combine favourable mechanical properties of metals, such as high strength and ductility, with high specific strength and stiffness of CFRP [4]. However, the qualitative and quantitative characterization of these type of adhesive joints remains an issue.

Joints are generally the weakest points in structures [5]. Depending on the stress state and service conditions, adhesive joints with the same material combination can have different failure modes at different rates [6]. Since adhesively bonded joints are often subjected to shearing loads and fail under such loads [7], it has been seeked to increase their

performance in terms of shear properties [8]. Thus, methods for shear property measurement and damage evaluation under shear load have been researched extensively.

Various analytical, numerical and empirical methods have been developed for the stress analysis and shear strength estimations of the adhesive joints. However, these methods postulate simplified assumptions regarding joint geometry, material parameters, load transfer and stress state, boundary conditions [9] or environmental conditions. Besides, various defects might pre-exist within the adhesive layer, which can have a great impact on the adhesive shear properties.

Non-destructive testing (NDT) of adhesive joints aim to obtain a correlation between strength of the joint and some mechanical, physical or chemical parameters without causing any change in the joint [10]. NDT methods can be used for monitoring the bonding during production, for bond quality assessment after production and for condition monitoring during the service. Depending on the joints material and geometry, product cycle stage, and the parameters to be estimated, some of the NDT methods can be more suitable than others.

Ultrasonic NDT methods are considered most suitable for adhesive joints [7]. A family of ultrasonic (US) waves, named guided waves, are known to provide more characteristic information about the interface of the adhesive joints, in addition to being able to propagate long distances [11]. Thus, they can be used in condition monitoring, as they can be generated and captured remotely [8]. US methods, utilizing *shear horizontal* (SH) guided waves interacting with the adhesive joints, have potential to provide information about the existence of defects, their location and types, as well as, mechanical characteristics of the adhesive layer and the bonded joint. However, in order to correlate these quantitative and qualitative properties of adhesive joints to the experimental data obtained from US-SH guided wave inspection, analytical and numerical analysis of wave propagation is required (i.e., solving an inverse problem) [12].

The lowest symmetrical SH mode (SH_0) is often used for adhesive joint investigation. The reason is that they have appealing characteristics such as, exhibiting no dispersion behaviour, uniform particle displacement in thickness direction and low probability of mode conversion when interacting with defects [13]. Therefore, SH guided waves potential for evaluation of not only adhesive joints, but also any type of guided medium has been investigated in various studies. In some cases, SH waves interaction with adhesive joints

were successfully correlated to the interfacial and cohesive properties of the adhesives [7][8][14][15] (see Section 2.3).

Furthermore, generating and capturing SH waves with specific type of transducers, named meander-line coil *electromagnetic acoustic transducer* (EMAT), brings several advantages to the adhesive joint inspection. These advantages are contactless generation of the SH waves and not requiring coupling medium [16].

Current technology of shear horizontal guided wave US systems for the evaluation of adhesive joint is presented in State of the Art (Section 2.3). It is revealed that the reliable quantitative characterisation of the joints to predict in service performance remains a challenge. Therefore, in this thesis, the aim is to find the applicability and the limits of the shear horizontal guided waves on condition monitoring of the hybrid structures by exposing them to quasi-static and cyclic loading.

1.2 OUTLINE

First, the relevant theoretical background regarding the adhesive joints and ultrasonic waves are supplied focusing on the materials and methods that were used during the experimentation (Chapter 2). It is aimed to give the relevant information for the main objective of the experiments and for the interpretation of the results. The state of the art for investigating adhesively bonded joints through SH guided waves is presented.

In Chapter 3, the production of test samples, equipment for the experimentation and methodology for the analysis is explained. The technical details for the production and experimental equipment is elaborated in the appendices.

Next, the results are discussed, comparing with literature findings (Chapter 4). A compilation of the results is presented in the appendices.

Finally, in Chapter 5 the question of applicability of US SH guided waves for condition monitoring of hybrid structures is tried to be answered. Challenges are elaborated, with an outlook on the possible research implication, for the complementary answer to the question.

2. THEORY

In this thesis, carbon fibre reinforced polymer (CFRP) and aluminium alloy (AA6082) hybrid structures were monitored by using the ultrasonic non-destructive method under various mechanical loads. The hybrid structure test samples were produced as a single lap joint geometry using an adhesive bonding method. Shear horizontal (SH) guided waves were used for the ultrasonic monitoring. In this section, the relevant topics are detailed more within the scope of used materials, conditions, tests and methods during the experimentation.

First, starting with the hybrid structures, adhesive bonding technology is presented. Concepts for adhesion, bond-line defects, stress state and failure of single lap joints are detailed. An overview of the hybrid structure production and the quality assessment methods for the adhesive joints is given.

Secondly, ultrasonic non-destructive testing is introduced focusing on the electromagnetic acoustic transducer (EMAT). This technology is used to generate SH guided waves in the aluminium part. The general information for the related concepts of US NDT is given, and the theoretical background regarding shear horizontal guided wave propagation in solids and EMAT working mechanism are detailed.

Finally, after introducing the relevant theoretical background the state of the art for SH guided waves on inspection of adhesively bonded joint is elaborated.

2.1 HYBRID STRUCTURES & ADHESIVELY BONDED JOINTS

The structures made by joining different types of materials are called “hybrid structures”. The aim is to combine the desirable features of distinct materials to obtain high performance structures. There are various methods for joining hybrid structures, such as, mechanical fastening, welding, adhesive bonding, etc. Joining methods specific to aluminium alloys and CFRP are reviewed and compared in the work of Pramanik et. al. (2017) [3]. This work gives an overview of different joining methods, which explains the variety in terms of joining and load transfer mechanisms. Moreover, combining some of the methods (combination of joining methods is named hybrid joints) are also utilized in joining of hybrid structures. However, it is pointed out that there is neither an established model to predict the properties for these joints nor established guidelines for the

comparison of the joint properties produced using different joining techniques.

All of the joining methods or their combinations have superiorities and weaknesses over each other. Nevertheless, all of them are employed to achieve the same goal; increased performance of the joints. The reason is that the joints are often the weakest point of the hybrid structures [17].

When solely adhesives are used, joints are named adhesive joints. Some advantages of the adhesive joints have raised interest in them in assembling processes, especially in the aerospace industry [2]. Advantages and disadvantages of adhesive joints over its counterparts are summarized below [3][18][19][20].

Advantages are:

- No stress concentrations are introduced as in mechanically fastened joints (e.g rivets, bolts...) .
- On the bonded area relatively continuous stress distribution can be achieved.
- It is possible to join dissimilar materials like metals and composites.
- Electrolytic and galvanic corrosion between metal adherends can be prevented, because the adhesive acts as a sealant.
- During application it causes less thermal stress compared to welding.
- Complicated geometries can be joined.
- It can be used to reduce weight for light-weight structures.

Disadvantages are:

- Adhesives have lower thermal, chemical and environmental resistance.
- They usually require surface treatment of the adherend.
- It is an irreversible process; therefore, disassembling can cause damage on the adherends, unlike some mechanical fasteners.
- Curing of the adhesives may increase the time for production cycle and requires control as it can affect the joint quality.
- There is a lack of knowledge in evaluation methods (e.g. limited NDT methods for joint evaluation) .
- Due to lack of knowledge in adhesives, it is preferred mostly in secondary structures.
- There are recycling issues.

Although there is a lack of knowledge in adhesives, various factors are known to affect the adhesively bonded joints quality and performance. Therefore, the design of adhesive joints as well as the quality and performance evaluation is a complicated task, as the

consideration of numerous parameters involved, starting from production of the joints until failure during service life time, is required [2][21].

In this thesis, in a broad sense, it is aimed to assess the performance of the adhesively bonded aluminium-CFRP hybrid structures with a single lap joint (SLJ) geometry that are subjected to mechanical loading. In order to give an in-depth understanding for the *performance* of the adhesively bonded joint, next sections are devoted to the relevant theoretical background of adhesives (section 2.1.1, 2.1.2, 2.1.3, 2.1.4).

2.1.1 Adhesive Bonding

In bonded joints, load transmission between joint materials (i.e. adherends or substrates) is achieved rather uniformly. The reason for this load transmission behaviour is the continuous contact between adhesive and adherends, as a result of 'adhesion'. Although the assumption of uniform stress distribution is debatable [22]; when compared to mechanically fastened joints, they have rather continuous stress distribution (Figure 1).

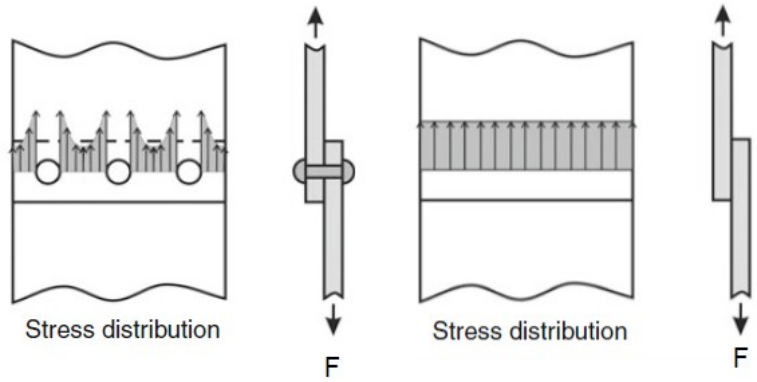

Figure 1. Stress distribution of riveted joint (left) and adhesively bonded single lap joint (right) under tension. [18]

Adhesion refers to the adhesive forces (or intermolecular forces) between adhesive and adherend molecules that causes attraction, i.e. *adhering*. When intermolecular forces are within a single material, then the phenomena is referred to as *cohesion*. The mechanism behind adhesion is explained by various theories, namely, physical adsorption, diffusion, electrostatic, mechanical interlocking and weak boundary layer theories. However, all these theories are considered to contribute to the strength of the joint [3]. Likewise, they are considered to give a partial understanding of a more complex and comprehensive adhesion model [23].

The illustration for the regions of the adhesive joint is presented in Figure 2. The interface is a two-dimensional hypothetical [6] boundary layer between the adhesive and the adherend. The volume bounded by two boundary layer (or adherend surfaces) is called bond-line. In various literature bond-line is also referred to as glueline, adhesive layer and adhesive bond [20][24][25]. For bonded lap joints, the bonding area can be referred to as *overlap area* as well. Adhesive theories give different explanation to interaction of the adherend and adhesive molecules in the vicinity of the interface. The region between the adhesive and adherend is called *interphase*, whose properties are different than the bulk adhesive and adherend material. The interphase properties are not constant; on the contrary, they exhibit a gradient in material properties.

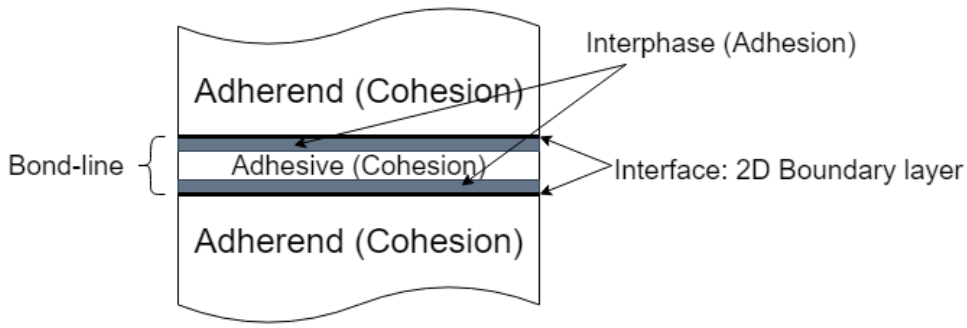

Figure 2. Regions within adhesive joint: Bond-line, interphase (3D) and interface (2D).

Adhesive properties arise from the combination of adhesive bulk material properties and the interphase properties, where interaction between adherend & adhesive take place. Therefore, anything that might hinder the adhesion mechanism and cohesion of the adhesive will have an influence on the adhesive properties, and by extension the joints properties. In other words, adhesive properties together with the adherend properties contribute to the strength of the bonded joint. Yet, there are other factors that affect the mechanical strength of the joints; such as environmental conditions, joint geometry and the residual internal stress [21]. Furthermore, the manufacturing process of the joint has an effect on the adhesive joint, as it can alter the adhesive properties of the joint. The manufacturing process of adhesive joints includes surface treatment of adherends, application and curing of the adhesives. Hence, the surface state of the adherends is one of the main contributors to the joint strength, while it has a direct affect on adhesion (see Section 2.1.4.1).

The joints strength is sensitive to the integrity of the adhesive layer [25], due to its influence on the stress distribution in the joint. Consequently, any defect that compromises

the integrity of the joint will have an effect on its strength. In the next section (Section 2.1.2), different types of defects within bonded joints are introduced.

2.1.2 Defects in a Adhesively Bonded Joint

Defects can occur during the manufacturing process of the bonded joint or during the service life, even though all measures are taken to prevent them [2]. Depending on the type and placement within the joint, they can have an effect on the cohesive or the adhesive strength. Defects of the bond-line can be on the interface or within the adhesive layer. Interfacial defects are surface unbonds and disbonds. Adhesive defects are voids, porosity, pure cure and cracks. A compilation of possible bond-line defects is illustrated in Figure 3.

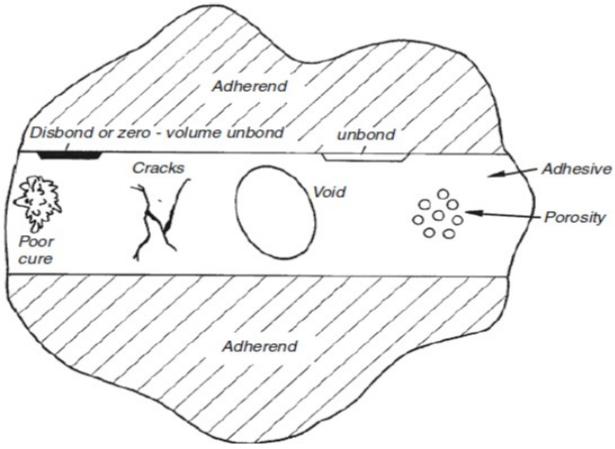

Figure 3. Typical bondline defects in adhesively bonded joint [18].

Bond-line defects are [25]:

- Porosities caused by trapped volatiles or air in adhesive,
- Voids, with higher volume compared to porosity, caused by entrapped air or gas in the adhesive,
- Adhesive cracks caused by stress,
- Poor cure resulting from inappropriate application of the adhesive system,
- Surface unbond, i.e. void on the interface, resulting from inappropriate application of adhesive system,
- Zero-volume unbonds (also known as kissing bonds, weak bonds or disbonds) resulting from insufficient surface preparation or curing.

Kissing bonds occur on the interface, where the adherend and the adhesive are in contact

(i.e. zero volume), but with little or no bonding; hence, adhesion. Marty et al., Decourcelle and Kellar (as cited by Ehrhart et al. [2]) established the definition of a kissing bond with the following characteristics;

> *"- strength measured with a lap shear test must be below 20% of the nominal bond strength,*
>
> *- the mode of failure must be of adhesive type,*
>
> *- the weak bond must be undetectable from normal bonds by using classical NDT techniques."*

When the adherends are composites and the joints are produced by co-curing method (see Section 2.1.4), voids can be observed in the substrates as well [26].

For the quality assessment, detecting the defects qualitatively and quantitatively during the life cycle of joint is important [27]. By creating material discontinuities and stress concentration, defects affect the stress distribution within the joint, consequently can affect the mechanical performance. There are various non-destructive testing (NDT) methods for detecting joint defects. However, in this thesis only the details for US methods are elaborated (Section 2.2).

2.1.3 Mechanical Performance of Bonded Joints

The mechanical performance of a bonded joint is only evaluated by destructive tests, since NDT methods failed to assess mechanical parameters for quality control [24]. Different joint configurations such as single lap, double lap, butt joints and many others can be used for strength assessment under various loads and conditions. Tests for different joint configuration are all standardized by the German Institute for Standardization (DIN) and European Standards (EN) in predefined conditions, covering every step such as test sample preparation, storage of test samples, testing conditions for reproducible results. During the experiments, single lap joint (SLJ) configuration was used, therefore theoretical details are confined to this type of joints. Before elaborating more on the joints stress state, failure types and fracture modes are introduced.

2.1.3.1 Failure Types and Fracture Modes

Bonded joints can fail adhesively, cohesively or combination of both. Adhesive failure (also known as interfacial failure) occurs on the interface. In this type of failure, adherend surface is free of adhesive on macroscopic level. However, due to existence of the

interphase region this kind of failure is not observed in practise [6]. This is illustrated in Figure 4. Both failed surfaces have remaining of other material in microscopic scale.

Cohesive failure can occur either on the adherend or on the adhesive. In cohesive failure of the adhesive, there is adhesive remaining on both of the adherend surface that is observable in macroscopic scale. In mixed failure, overlap adherend surfaces can be partially free of adhesive. Failure types indicate the adhesive joint quality. Interfacial failure can indicate insufficient surface treatment, while cohesive failure of the adhesive can indicate poor strength of the bulk adhesive [28].

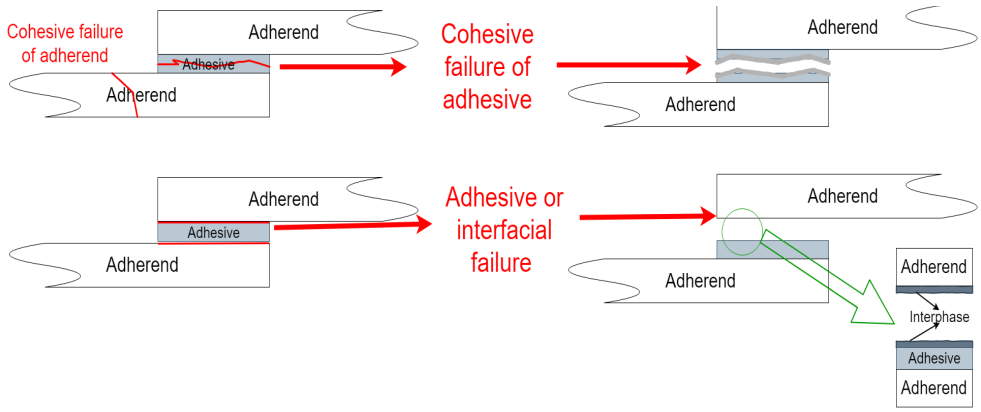

Figure 4. Adhesive and cohesive failure illustration (with close up view of interphase).

Principle fracture modes are illustrated in Figure 5, all of which can be observed in single lap joints [28]. Mode I occurs due to peel forces; mode II occurs due to shear forces applied along a plane; and mode III occurs under shear force applied around an axis [28].

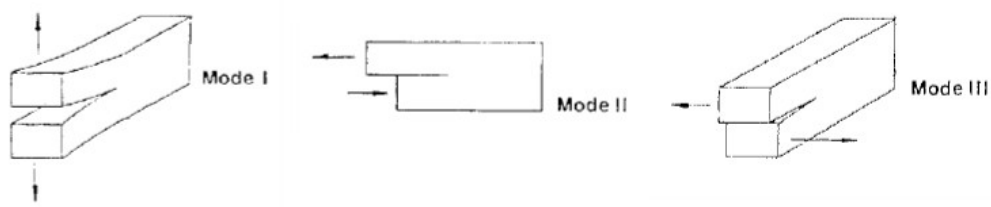

Figure 5: Principle modes of fracture [28].

2.1.3.2 Stresses in Adhesively Bonded Single Lap Joints (SLJ) and Mechanical Testing

As mentioned beforehand, the stress distribution in bonded joints are not quite uniform and can depend on many factors. Thus, for strength evaluation these factors should also be considered. For SLJs having the same adhesive-adherend material system, factors affecting the stress state are summarized below [21] [28] [29]:

- Production process of the joint (adherend surface treatment, preparation and application of the adhesive, environmental conditions during the production),
- Residual stresses occurring during the production (thermal stresses can occur due to different adherend thermal capacity and shrinkage of the adhesive),
- Thickness of the adherends and adhesive layer,
- Size of the overlap area,
- Storage conditions after production prior to testing,
- Testing conditions,
- Defects.

Stress state of a joint can be calculated by analytical and numerical methods. The strength of the joint can be predicted using various failure criteria based on continuum and fracture mechanics [30]. Various analytical and numerical models are developed specifically for SLJs. For the comparative study of these analytical models, Stein et al.'s work [31] can be referred. Not all analytical models are applicable for hybrid structures, as adherends must be of the same material in the models. Different mechanical tests are designed to determine the intrinsic properties of the adhesives [29].

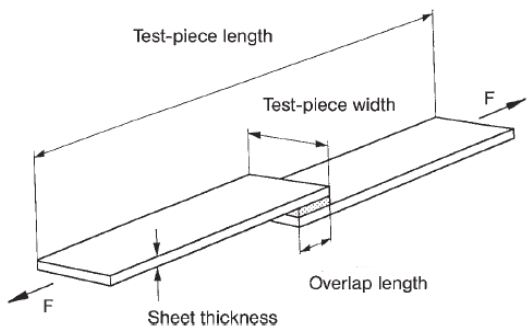

Figure 6. Single-lap joint test sample [20].

The strength of a bonded joint can be evaluated by tensile loading of SLJ until failure (Figure 6), resulting in shear stress in the overlap region. The obtained strength value is named lap shear strength or tensile shear strength.

The strength of the adhesive joint is calculated as follows (Eq. (1));

$$\tau_B = \frac{F_{fail}}{A} \quad (N/mm^2) \qquad where \qquad A = b \times l_o \tag{1}$$

where τ_B is tensile shear or adhesive strength, F_{fail} is maximum force at break, A is overlap area, b is the test sample width and l_o is overlap length. Eq. (1) is constructed on a simplified assumption, which is the idealized situation where the adherend is not strained by the applied force and there is no moment or bending [30]. Therefore, shear stress is assumed to be distributed evenly along the overlap length. However, the resulting strength value results from a more complex stress state, rather than pure shear stress caused by applied load affecting only on the adhesive layer (Figure 7).

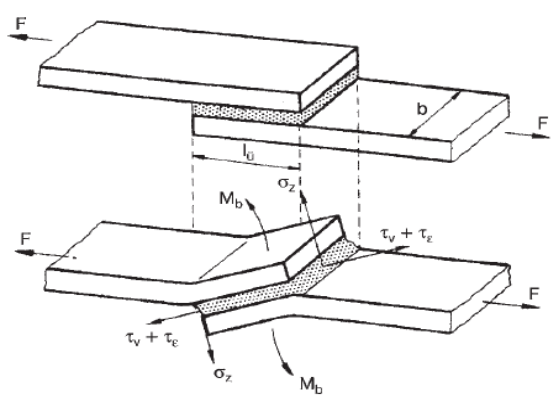

Figure 7. Stress state of a single lap joint under tensile load [20].

Actual stress state is explained by Habenicht [20] as follows:

- Eccentricity of the applied load causes bending of the adherends on the overlap ends resulting in the bending moment (M_b);
- The bending moment (M_b) results in transverse tensile stress or peel stress (σ_z) for the adhesive layer;

- The adherend extension in the overlap region results in tensile and shear stresses parallel to the adhesive layer(τ_e);

- The adherend displacement in the overlap region parallel to the adhesive layer results in shear stress (τ_v).

Figure 8 shows the shear stress distribution along the overlap length of the adhesive joint. In an idealized situation there is uniform stress distribution, although the stresses are largest at the end of the overlap length [21]. Therefore, failure is likely to begin at the end of the overlap and propagate into the adhesive layer [25].

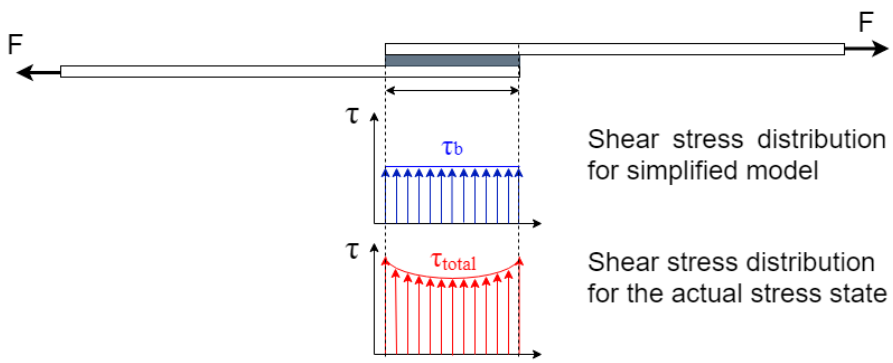

Figure 8. Shear stress distribution in the overlap region for single lap joints under tensile load.

2.1.4 Production of Bonded Joints

Production of the adhesive joints can be divided into two main process steps; steps for obtaining the adhesive forces (adhesion) and steps for obtaining the adhesive film strength (cohesion) [20]. The first process includes surface treatment and adhesive application, where as the second process includes the curing of the adhesive [20].

Before adhesive bonding, usually preparation of the adherend surface is required in order to optimize adhesion. This process, where cleaning, chemical and/or physical modification of the adherend surfaces take place, is known as surface treatment [32]. Inadequate surface treatment is considered the main reason for adhesive bond failure [28]. Therefore, the effect of surface treatment on joint strength is well-known and widely researched.

Depending on the adherend material, different steps can be involved in this process.

There are two different types of adhesive application methods for the hybrid structures; co-curing and secondary bonding [26][33][34]. The former is a single step process, where excess resin of the composite structure is used for the bonding process. Therefore, curing of the reinforced polymer and joining of the hybrid structure occur simultaneously. On the contrary, latter is a two step process, where the adhesive is applied after the curing process of the composite is complete. In some sources [19][35], the term '*co-curing'* is used for the adhesive-adherend system consisting of solely un-cured laminates. The term *'co-bonding'* is used, when only one of the adherends is an un-cured laminate. Throughout the thesis, co-curing is used for the joining of aluminium-CFRP hybrid structures.

Hybrid structures can be co-cured by various composite production methods; such as, resin transfer moulding (RTM), autoclave, and vacuum bag methods, etc..

For the experiments, metal surfaces were subjected to surface treatment with specific steps and the single-lap test samples were produced through vacuum infusion process (VIP). Therefore, only the details for the utilized methods for the test sample production are supplied in this chapter.

2.1.4.1 Surface Treatment

A surface treatment is a necessary step for optimizing surface properties and promoting adhesion mechanisms. Metal surfaces are usually covered with weak layers, which inhibit the adhesion mechanisms. The typical metal surface layers are shown in Figure 9, where the basic material represents the metal that is used.

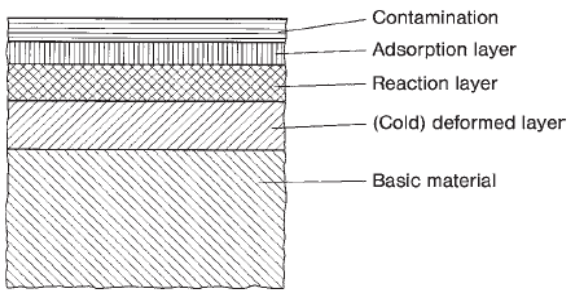

Figure 9. Surface layers on untreated metal [20].

The contamination layer can consist of organic or inorganic foreign particles like dirt, dust, oil, paint, etc.. The adsorption layer can consist of absorbed moisture and other molecules

from the ambient air. The reaction layer is formed during the manufacturing of the metal, where oxygen or moist in the ambient air is chemically reacted to the base material in this layer [20]. By applying an appropriate surface treatment these weak surface layers can be removed and modified to create an active surface for adhesive bonding.

The general outline for the surface treatment is shown in Figure 10. However, depending on the production and service conditions of the joint, as well as the adherend and adhesive material, some steps can be excluded or combined.

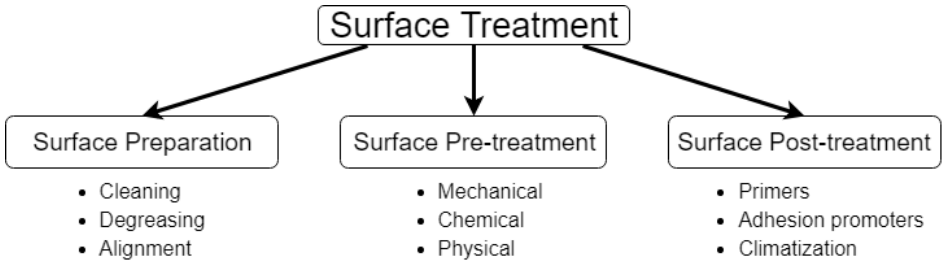

Figure 10. Steps for the surface treatment of adherends [20].

Surface preparation is applied to remove the contaminants on the surface. On the other hand, by surface pre-treatment, it is aim to modify the surface topography and/or chemistry to create an active surface. Surface post-treatment steps can be applied to maintain the altered surface of enhance bonding capabilities.

During the production process, aluminium plates were subjected to a type of mechanical treatment called grit blasting. Grit blasting is able to remove contamination, remove oxidized layer [36] and change the surface roughness of the metal [28] that has an influence on the strength of the joint.

The effect of various surface treatments, as well as solely the surface roughness on the adhesive joints' shear strength has been investigated widely [32][37][38][35][39][40][41][42][36][43][44][36][45]. It has been shown that there is an optimum surface roughness for maximum strength of adhesive joints, depending on the adherend and the adhesive material, the joint geometry and the production of the joint.

2.1.4.2 Vacuum Infusion Process (VIP) for Hybrid Structure Production

One of the co-curing methods for hybrid production can be done using VIP (also known as vacuum assisted resin infusion process-VARIP, and vacuum assited resin transfer moulding-VARTM). In the conventional VIP for the composite materials, the resin is impregnated through the reinforcement using vacuum. In this method, a single sided mould covered with a vacuum bag is used, in addition to some extra layers such as peel ply, flow mesh and breather [46]. These layers are used to ease the flow (flow mesh), ease de-moulding (peel ply), and remove excess resin (bleeder & breather). Depending on the mould size and the materials, the arrangement of the layers might change in VIP process. Spiral inlet tube (where resin is fed) and outlet tube configuration depends on the produced geometry. Also some of the layers, such as bleeder, or breather can be excluded.

For hybrid structure production, the mould is designed to supply complete contact between the reinforcement and the metal. When resin is infused under vacuum with complete wetting of the reinforcement, inherently adhesive will be applied as well [33]. Then the structure is left for curing under appropriate conditions.

The exemplary arrangement of the VIP for the co-curing of hybrid structure is depicted in Figure 11.

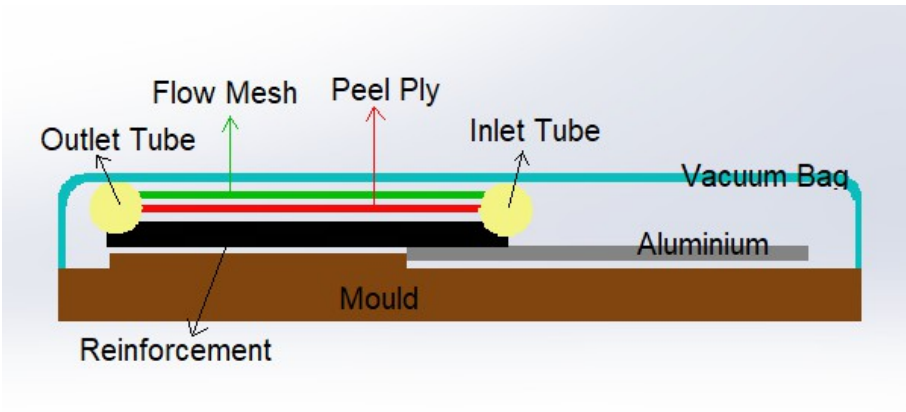

Figure 11. Illustration of vacuum infusion process mould configuration for hybrid structure.

2.1.5 Quality Assessment and Damage Monitoring of Bonded Joints

The quality of bonded joints is determined by the defects, mechanical performance and durability in service conditions [24]. It can be investigated using non-destructive testing techniques or destructive mechanical tests. In this section, the goal is to give an overview of NDT methods and their role in damage monitoring.

Non-destructive testing (also known as non-destructive inspection/evaluation (NDI)&(NDE)) is broadly defined as "*the examination, test or evaluation performed on any type of test object without changing or altering that object in any way, in order to determine the absence or presence of conditions or discontinuities that may have an affect on the usefulness or serviceability of that object*" [47].

NDT methods can be used to monitor structures in various stages of their life time; during the production phase and during the service life. NDT monitoring of a structure during the service time can give not only diagnostic information of the quality, but also prognostics regarding the damage evolution and residual life [48]. Therefore, this potential of NDT can be exploited to predict and prevent the failure of the joint, by monitoring the defects and correlating them to the joints performance.

NDT methods for the inspection of joints after bonding and during service are *Ultrasonic Methods, Thermal Methods, Spectroscopic Methods, Vibration Techniques, Acoustic Emission, X-ray Methods, Optical Holography Methods* [25]. However, only some of these methods can be used for condition monitoring of the bonded joints.

Ultrasonic NDT methods are considered most suitable for the adhesive joints [7]. These methods can show variations in terms of utilized wave type and mode, as well as, the incident angle of the wave. Guided waves ultrasonics are utilized in condition monitoring due to advantages such as; sensitivity to defects and mechanical properties, ability to propagate over long distances with little attenuation and possibility of remote wave generation and detection.

A specific type of guided wave, named shear horizontal guided wave, was used for monitoring the single-lap joint during the mechanical loading. Therefore, following section (section 2.2) is devoted to US-NDT basics and the relevant theoretical information in order to give an insight to the guided wave ultrasonic monitoring process.

2.2 NON DESTRUCTIVE TESTING (NDT) WITH ULTRASONICS

In US-NDT methods, physical phenomenon of sound wave propagation is exploited. The sound waves propagate in the medium through the periodic motion of particles (i.e. vibration of the particles) inside the medium. When the sound waves have a frequency above 20 kHz up to a few GHz, they are named ultrasound. The sound wave is a type of mechanical energy, which causes stresses in the media during propagation. Damage alters the mechanical properties of a joint; thus, US waves respond to such changes. The interaction of the US waves with boundaries or defects results in different characteristic behaviours, which depend on the wave type, mode and incident angle. This property is exploited for quality assessment and damage monitoring of the joints. Therefore, wave mode selection with optimal propagation characteristics is an important part of US-NDT [49].

Ultrasonic NDT methods that are used for the characterization of adhesive joints are *Normal Incidence Narrow-Band Pulsed Spectrometry, Ultrasonic Spectroscopy, Harmonic Imaging-Nonlinear Ultrasonic Techniques, Oblique Incidence Ultrasonic Technique, Shear Wave Resonance techniques and Guided Wave Ultrasonic Techniques.* During the experimentation guided wave ultrasonic technique was utilized. Therefore, details for this method are elaborated, in addition to the general overview of ultrasonic methods.

2.2.1 Basics Components of Ultrasonic Non-Destructive Testing Systems

Basic components for the US-NDT systems are the pulser/receiver/amplifier, cabling, transducers and an oscilloscope [47][50]. The pulser section generates electrical pulses, that are sent to the transducer. Then, the transducer excites the ultrasonic pulses in the test object by converting from the electrical pulses. After travelling in the test object, the pulse is captured by a receiving transducer. Depending on the inspection mode, the receiving transducer can be the same or a different transducer. The receiving transducer converts the ultrasonic pulse back to the electrical pulse. Finally the electrical pulse is sent back to the receiver section, amplified and sent to the oscilloscope to be displayed.

Transducers are used to convert mechanical energy to electrical energy and vice versa, either in order to excite a sound wave or to capture it. Depending on the needs, that might be imposed by the test objects geometry, material parameters, testing environment, etc.,

various types of transducers can be used. Different wave propagation modes can be excited by the appropriate transducer type and excitation frequency. If two transducers are used for sending and receiving the US waves, it is called pitch-catch inspection mode. If one transducer is used to both send and receive the waves, than it is called the pulse-echo inspection mode.

Results of the US inspection can be displayed as an 'A-scan', 'B-scan' or 'C-scan'. An A-scan displays received voltage amplitude versus time, where the amplitude of the voltage correlates to the received ultrasonic wave amplitude. B- and C-scans display a representative image of the scanned area. To create B- and C- scan images, information of the travelling time and amplitude of the echoed wave relative to the transducer unit is used [47]. B-scan displays a cross-sectional view of the test object, where the transducer unit moves along the inspected surface. A C-scan displays a planar view of the test object, which is at a particular depth [51].

2.2.2 Ultrasonic Waves Propagating in Homogeneous Isotropic Media

This section is devoted to the theory of ultrasonic waves in solid media, to give an understanding of possible wave interactions that might occur along the adhesive joints.

Ultrasonic waves can propagate in gas, fluid and solid media, however depending on the medium propagation modes differ. In gas and fluid media only compression waves (also known as longitudinal waves, pressure waves, primary waves) can propagate, whereas, in solids shear waves (also known as transversal waves, secondary waves) with different types of polarization can propagate as well. Gases and liquids restore only their volumes, after an application of an external force at low stress for short period of time. On the other hand, solids have the ability to restore their shapes as well. This ability is known as elasticity, and a medium showing this property is called an elastic medium. Ultrasonic waves propagating in an elastic medium are mechanical waves, i.e. elastic waves.

Elastic waves can be categorized either according to the direction of the particle displacement in the medium relative to the propagation direction of the wave or according to the spatial relation to the elastic medium. In accordance with the first classification, elastic waves can be divided into two categories, namely 'longitudinal' and 'shear' waves. According to second classification, they are categorized as 'bulk' and 'guided' waves. In

order to elaborate on those classifications the wave equation must be introduced. Equations for the wave propagation in solids are compiled from J.L Rose's book “Ultrasonic waves in solid media” [51] and Materials and Acoustics Handbook [52].

For an isotropic homogeneous non-dissipative medium, the equation of motion (Eq. (2)), the strain displacement equation (Eq. (3)) and the constitutive material equation (Eq. (4)) are presented in summation convention as following:

$$\sigma_{ij,j}+\rho f_i=\rho \ddot{u}_i \qquad where \qquad \sigma_{ij,j}=\frac{\partial \sigma_{ij}}{\partial x_j} \tag{2}$$

$$\varepsilon_{ij}=\frac{1}{2}(u_{i,j}+u_{j,i}) \tag{3}$$

$$\sigma_{ij}=\lambda \varepsilon_{kk}\delta_{ij}+2\mu\varepsilon_{ij} \qquad where \qquad \delta_{ij}=\begin{Bmatrix} 1 & if & i=j \\ 0 & if & i\neq j \end{Bmatrix} \tag{4}$$

where σ_{ij} is stress tensor, ε_{ij} is strain tensor, ρ is density, λ and μ are Lame constant, u_i is the displacement in the x_i direction, and δ_{ij} is Kronecker delta.

Substituting Eq. (3) and Eq. (4) into Eq. (2) eliminates the stress and strain terms. The resulting equation is also called Navier's equation of motion, which is shown in Eq. (5):

$$(\lambda+\mu)u_{j,ij}+\mu u_{i,jj}+\rho f_i=\rho \ddot{u}_i \quad where \quad u_{j,ij}=\frac{\partial^2 u_j}{\partial x_i \partial x_j} \quad , \quad u_{i,jj}= \tag{5}$$

The vector form of Eq. (5) is shown in Eq. (6) ;

$$(\lambda+\mu)\nabla\nabla\cdot\underline{u}+\mu\nabla^2\underline{u}=\rho\frac{\partial^2\underline{u}}{\partial t^2} \tag{6}$$

$$\nabla^2=\frac{\partial^2}{\partial x_1^2}+\frac{\partial^2}{\partial x_2^2}+\frac{\partial^2}{\partial x_2^2} \qquad \nabla=\frac{\partial}{\partial x_1}\times\underline{e_{x_1}}+\frac{\partial}{\partial x_2}\times\underline{e_{x_2}}+\frac{\partial}{\partial x_3}\times\underline{e_{x_3}} \tag{7}$$

Navier's equation of motion is a second order hyperbolic linear homogeneous partial differential equation. There are infinite number of solutions to the Navier's equation (Eq. (5) & (6)), all of which describes different wave propagation mode, depending on the physical boundary condition of the solid medium. In other words, boundary conditions depict the propagation mode of the wave. If an infinite medium is considered, then there

aren't any boundary conditions that need to be satisfied. So, the solutions describe the bulk waves. When the boundary conditions are defined, the solution that satisfies the boundary conditions, describes the guided waves.

2.2.2.1 Bulk Waves

In an infinite medium two types of propagation modes exist; longitudinal and shear waves. By solving Eq. (6), the wave equations for longitudinal and shear waves can be obtained.

By applying Helmholtz decomposition to the displacement vector, $\underline{u}$ is expressed as the sum of two different vectors (Eq. (8)). The first term is the divergence of scalar potential (φ), the second term is the curl of the vector potential ($\underline{H}$).

$$\underline{u}=\nabla\varphi+\nabla\times\underline{H} \qquad \nabla\cdot\underline{H}=0 \tag{8}$$

By substituting Eq. (8) into Navier's Eq. (equation (6)), and applying rotation & divergence vector operations, Eq. (9) is obtained:

$$\nabla\left[(\lambda+2\mu)\nabla^2\varphi-\rho\frac{\partial^2\varphi}{\partial t^2}\right]+\nabla\times\left[\mu\nabla^2\underline{H}-\rho\frac{\partial^2\underline{H}}{\partial t^2}\right]=0 \tag{9}$$

Eq. (9) is satisfied by two equations (Eq. (10) & (11)), which is the simplified representation of Navier's equation of motion (Eq. (6)).

$$\nabla^2\varphi=\frac{1}{c_L^2}\frac{\partial^2\varphi}{\partial t^2} \quad \textit{where} \quad c_L^2=\frac{\lambda+2\mu}{\rho} \tag{10}$$

$$\nabla^2\underline{H}=\frac{1}{c_T^2}\frac{\partial^2\underline{H}}{\partial t^2} \quad \textit{where} \quad c_T^2=\frac{\mu}{\rho} \tag{11}$$

If the curl of the vector potential is assumed to be zero, i.e. zero rotation of the vector field($\nabla\times\underline{H}=0$), than displacement is obtained for the longitudinal wave travelling with velocity c_L as in Eq. (12). Assuming zero rotation means only dilatational disturbance occurs during the longitudinal wave propagation, as depicted in Figure 12-b. In other words, particle displacement is parallel to the wave propagation direction.

$$\underline{u_L}=\nabla\varphi; \qquad \frac{\partial^2\underline{u_L}}{\partial t^2}-c_L^2\nabla^2\underline{u_L}=0 \tag{12}$$

If the divergence of the scalar potential is assumed to be zero ($\nabla\varphi=0$), than displacement is obtained for the shear wave travelling with velocity c_T Eq. (13). The particle displacement is perpendicular to the shear wave propagation direction, as shown in Figure 12-a.

$$\underline{u_T}=\nabla\times\underline{H}\,; \qquad \frac{\partial^2 \underline{u_T}}{\partial t^2}-c_T^2\nabla^2\underline{u_T}=0 \tag{13}$$

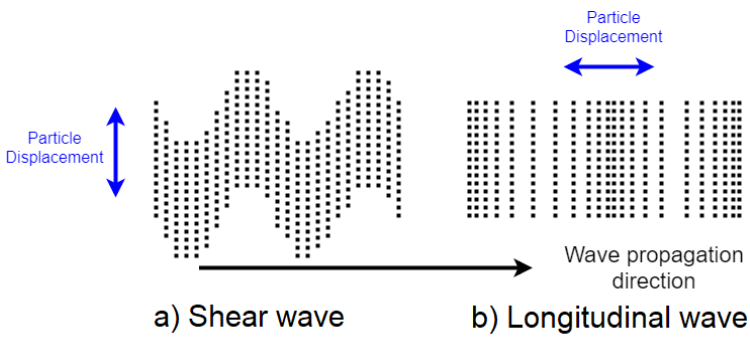

Figure 12. Shear and longitudinal wave propagation in solid media.

If a harmonic plane wave is propagating inside the homogeneous isotropic medium, a possible solution of the displacement vector is (Eq. (14))

$$\underline{u}(x_1, x_2, x_3, t)=\underline{A}\ \exp(i\ (\underline{k}\,\underline{x}-\omega t)) \quad where \quad k=2\pi/\boldsymbol{\lambda} \quad . \tag{14}$$

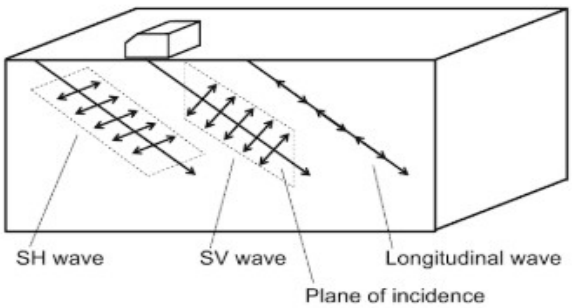

Figure 13. Particle displacement and wave propagation direction of the waves [66].

In Eq. (14), $\underline{k}$ is the wave number vector which is parallel to the propagation direction, $\boldsymbol{\lambda}$ is here wave length, $\underline{A}$ is constant vector which characterizes the particle displacement direction, known as 'polarization direction'. The displacement vector for shear waves has two components, each characterizing the polarization direction as in Figure 13.

- Reflection and Refraction of Bulk Waves

If an ultrasonic wave encounters a boundary between two media, some proportion of the energy is reflected and some proportion is refracted (i.e., transmitted to the second medium). The density and the elasticity of the medium are the factors that affects the proportion of the reflected and refracted energy. A physical property, called acoustic impedance (Eq. (15)), can be used to calculated the proportions of the energy.

$$Z = \rho \cdot c \tag{15}$$

When two homogeneous isotropic semi infinite solid media are in contact, several assumptions can be made for problem simplification. At the boundary, i.e. interface, particles of the two media have equal displacement on the direction normal to the boundary; and, no shear stress is exerted on the boundary due to particle displacement [52]. Under these assumptions, the reflection and transmission coefficients on the boundary at normal incident angle are calculated as follows (Eq. (16)):

$$R = \frac{Z_2 - Z_1}{Z_1 + Z_2} \quad and \quad T = \frac{2Z_2}{Z_1 + Z_2} \tag{16}$$

When non-zero incident longitudinal or shear vertical wave is incident on the boundary, mode conversion occurs. But when the horizontally polarized shear wave is incident, there cannot be conversion to any other mode [53].

- Phase and Group Velocity

The superposition of the group of waves with equal amplitude but slightly different frequencies results in a wave packet. Individual oscillations in the wave packet have different velocities, called 'phase velocity', while as a wave packet they travel with the same velocity, called *group velocity*. If group and phase velocity are equal to each other, the wave displays non-dispersive behaviour. Otherwise, it presents *dispersive behaviour*. This behaviour is elaborated on more in the next section.

2.2.2.2 Guided Waves – SH Guided Waves

As mentioned beforehand, guided waves are the solution to the Navier's equation (Eq. (5))in the finite domain with different boundary conditions. General forms of the boundary conditions are presented below:

$$\underline{u}(x,t)=u_0(x,t) \qquad \textit{surface displacement} \tag{17}$$

$$t_i=\sigma_{ji}n_j \qquad \textit{surface traction} \tag{18}$$

When displacement and traction boundary conditions are both defined on different surfaces, it is called a mixed boundary condition. Some of the well-known guided waves are Rayleigh, Lamb, Love, Stonely and Shear Horizontal (SH) waves. However, only the SH waves are detailed in this section.

SH guided waves can be considered as the superposition of bulk shear waves propagating in a plate, that are reflected from upper and lower surfaces. The plane of the particle displacement is parallel to the surface of the plate (Figure 14).

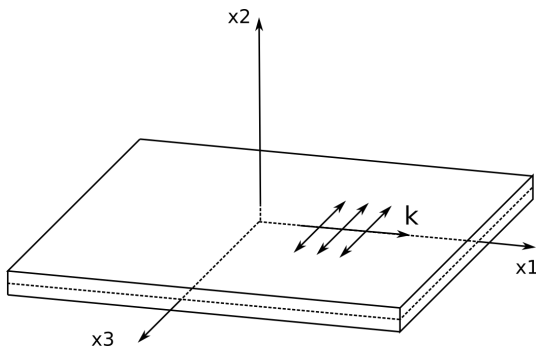

Figure 14. Propagation and particle displacement direction for SH wave [51]

There are several ways to find the solution to Eq. (5) for SH guided waves, such as the Helmholtz decomposition, partial wave analysis, and transverse resonance [51]. Here. they are derived from the displacement equations of motions.

Figure 14 shows SH guided wave propagating in a plate, where the propagating direction is on x_1 and the particle displacement is in direction x_3 , which means the bulk shear waves are polarized along x_3. The wave vectors, whose magnitude is wave number k and where the direction is in the wave propagation direction, lie on the x_1, x_2 plane. In addition they are inclined in a way that they satisfy the traction free boundary conditions on the surfaces

of the plate.

Since the particle displacement is on x_3, SH guided waves displacement vectors become:

$$u_1(x,t)=u_2(x,t)=0 \tag{19}$$

The solution to Navier's equation is assumed to have following form:

$$u_3(x_1,x_2,t)=f(x_2)\mathrm{e}^{i(kx_1-\omega t)} \quad where \quad k=2\frac{\pi}{\lambda}=\frac{\omega}{c_p} \tag{20}$$

where c_p is the phase velocity .

Since u_3 is independent of x_3 in Eq. (20) , the wavefront is infinitely extended along x_3, i.e. the particle displacement happens along the complete width of the plate. The actual physical displacement vector field is the real part of Eq. (20). Using the displacement vectors in Eq. (19), Navier's equation (Eq. (5)) becomes

$$\frac{\partial^2 u_3}{\partial x_1^2}+\frac{\partial^2 u_3}{\partial x_2^2}=\frac{1}{(c_T^2)}\frac{\partial^2 u_3}{\partial t^2} \tag{21}$$

Substituting the assumed solution (Eq. (20)) into simplified Navier's equation (Eq. (21)) gives equation 22, with the general solution presented in equation 23:

$$\frac{\partial^2 f(x_2)}{\partial x_2^2}+(\frac{\omega^2}{c_T^2}-k^2)f(x_2)=0 \tag{22}$$

and

$$f(x_2)=A\sin(qx_2)+B\cos(qx_2) \quad where \quad q=\sqrt{\frac{\omega^2}{c_T^2}-k^2} \quad . \tag{23}$$

The first term on the right hand side of the displacement field in Eq. (24) represents the antisymmetric mode, whereas the second term represents the symmetric mode of SH waves:

$$u_3(x_1,x_2,t)=[Asin(qx_2)+Bcos(qx_2)]\mathrm{e}^{i(kx_1-\omega t)} \quad . \tag{24}$$

Traction free boundary conditions on the surfaces are;

$$\sigma_{22}|_{x_2=\pm h}=\tau_{12}|_{x_2=\pm h}=\tau_{23}|_{x_2=\pm h}=0 \quad where \quad \tau_{23}=2\mu\varepsilon_{23}=\mu\frac{\partial u_3}{\partial x_2} \quad . \tag{25}$$

Calculation of τ_{23}, by using Eq. (24) and boundary conditions in Eq. (25) results in the dispersion equations in Eq. (26):

$$\sin(qh)=0 \quad symmetric \quad mode; \quad \cos(qh)=0 \quad antisymmetric \quad mode \tag{26}$$

where $qh=n\pi/2$ is solution for the dispersion equations.

Combining Eq. (20), (23) and (26) leads to a different form of dispersion equation (27), whose solution in terms of thickness and frequency product is given in Eq. (28) as follows:

$$\frac{\omega^2}{c_T^2}-\frac{\omega^2}{c_p^2}=\left(\frac{n\pi}{2h}\right)^2 \quad , \tag{27}$$

and

$$c_p=c_t/\sqrt{(1-(nc_t)^2/4(df)^2)} \qquad n=0,1,2,3\ldots \quad . \tag{28}$$

By inserting the definition of wave number, *k*, presented in Eq. (20) and differentiating the dispersion equation presented in Eq. (27), following dispersion equation for the group velocity is obtained (Eq. (29)):

$$\frac{d\omega}{dk}=\frac{k\,c_T^2}{\omega^2} \quad . \tag{29}$$

Substitution of Eq. (29) into Eq. (27) and simplifying leads to group velocity relation in terms of frequency and thickness product (Eq. (30)):

$$c_g=c_t\sqrt{(1-(nc_t)^2/4(df)^2)} \qquad n=0,1,2,3\ldots \quad . \tag{30}$$

A cut-off frequency is a limit, below which SH mode cannot be excited. It is calculated by assuming infinite phase velocities and zero group velocities. For n^{th} mode SH wave, the cut-off frequency is calculated as follows:

$$(f.d)_n=\frac{n\,c_T}{2} \quad where \quad n:mode, \quad d:thickness, \quad c_T:shear\ wave\ velocity \tag{31}$$

The group and phase velocity relations presented in Eq. (28), Eq. (30) and Eq. (31) are used to plot the dispersion diagrams for the aluminium alloy used in hybrid samples and calculate the SH wave propagation velocity for the experiments.

2.2.3 Electromagnetic Acoustic Transducers

As mentioned beforehand, there are various types of transducers (also named probe, search unit, test head) such as, Piezoelectric (PZT) Transducers and Electromagnetic Acoustic Transducers (EMAT). They are a vital equipment for the US-NDT applications to convert mechanical energy and electrical energy into each other. PZT transducers and EMATs use different physical principles to generate a US wave. Depending on the parameters to be measured and the wave modes to be propagated, different type of PZT transducers and EMATs can be used with different constructions [49]. During the experimentation shear horizontal guided waves were generated and captured using EMATs. Therefore, only principles for EMAT are detailed. The theory of EMAT is compiled from the Hirao and Ogi's book “EMATs for Science and Industry” [54].

EMATs have the advantage of making NDT possible without contact and usage of couplant medium over its counterparts, however with the restriction of being used on electrically conductive or ferromagnetic materials due to its working mechanism.

An EMAT consists of a high-frequency coil and permanent magnets or electromagnets, whose configuration can depend on the mode of the elastic wave to be generated or the geometry of the test object. Using the proper configuration for an EMAT, a bulk wave, longitudinal guided wave, axial polarized shear wave, shear horizontal wave or Rayleigh wave can be generated. When the coils in the EMAT are in close proximity to the test object, they produce an electromagnetic field that penetrates the test object. The interaction between the electromagnetic field in the material and biasing magnetic field causes deformation (elastic waves) on the test object.

Actually an EMAT exploits coupling mechanism between electromagnetic and elastic fields, by utilizing the Lorentz forces and/or Magnetostricton, as well as Magnetization forces, depending on the ferromagnetism of the test object. In case the test object is not ferromagnetic but conductive, the Lorentz Force mechanism excites the US waves in the test object.

EMATs that generate guided SH waves have a meander-line coil, whose period depicts the SH-wave frequency (Figure 15). These type of EMATs require a large biasing magnetic field, however when the magnetic field is applied in angled direction lower biasing magnetic fields can be used [54].

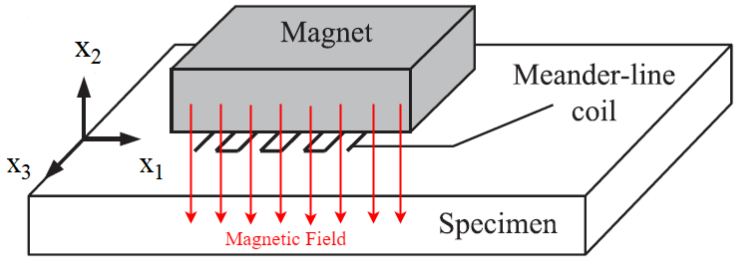

Figure 15. Illustration of EMAT with meander coil [16].

The wave generation is analysed in three steps; the calculation of the electromagnetic fields inside the material, calculation of the body forces caused by the interaction between the electromagnetic and electric fields, and the calculation of the acoustic fields caused by the body forces.

When a current passes through the coils, electrons in the conductive material are subjected to an electric field. Therefore the Coloumb force $-e\underline{E}$ is exerted on each electron. When there is a biasing magnetic field as well, than Lorentz force $e\underline{v}_e \times \underline{B}$ is additionally exerted.

The equation of motion for the electron is

$$m\dot{\underline{v}}_e = -e(\underline{E} + \underline{v}_e \times \underline{B}) - \frac{m\underline{v}_e}{\tau} \tag{32}$$

where m is electron mass, e is electron's charge, $\underline{v}_e$ is mean electron velocity, and τ is mean time of electron-ion collision. The first term on the right hand side represents the electromagnetic forces, i.e. Coulomb + Lorentz forces.

The momentum that electrons have is transferred to ions by collisions, therefore body forces are applied to ions formulated as follows;

$$\underline{f} = N Z_e(\underline{E} + \dot{\underline{u}} \times \underline{B}) + n_e \frac{m\underline{v}_e}{\tau} \quad , \tag{33}$$

where N is ion density, Z_e is ion charge, n_e is the electron density and $\underline{u}$ is ion displacement.

Since $n_e e = N Z_e$ and the electron velocity is much larger than the ion velocity, equation (33) reduces to:

$$\underline{f}=-n_e e\,\underline{v_e}\times\underline{B}=\underline{J_e}\times\underline{B}\equiv\underline{f_L} \quad where \quad \underline{J_e}=-n_e e\,\underline{v_e} \quad , \tag{34}$$

where J_e is the electron eddy current density. The force per unit volume on ions can be approximated to the Lorentz force that excites elastic wave in solids.

2.2.4 Measuring the Quality of an Adhesively Bonded Joint with Ultrasonic Waves

The A-scans display results of the interaction between the waves and the test object material as an electrical signal whose independent variable is time and dependent variable is amplitude of the signals voltage ($A=f(t)$). The signal might be subjected to the loss of information due to various types of noise. Therefore, in order to increase the accuracy of the results some digital signal processing (DSP) methods can be applied.

Various characteristic parameters of the signal, such as time of flight (ToF: required time for a wave packet to travel a specific distance), amplitude, frequency, wave velocity or phase shift can be used to evaluate the adhesive joints. The signal can be investigated in the time or in the frequency domain to extract these parameters. The goal is to correlate the parameters of the signal to the mechanical properties or to the structural damage quantitatively and qualitatively.

When there is damage in the joint, it affects the mass, integrity and stiffness of the joint; consequently, the physics of mechanical waves, i.e. ultrasonic waves, propagating through the joint [25]. These ultrasonic changes can manifest as mode conversion, dispersion, attenuation, scattering or superposition of the waves [55].

For damage assessment, the signal obtained from a defect free joint can be taken as a reference, and compared to the investigated joint [55][56]. When there is a defect, it will change the proportions of the reflected and transmitted energy of the incident wave. The reflected energy is larger, when the difference of acoustic impedance is higher. Therefore, defects containing air or any other low density substance, will increase the reflected energy from the boundary [57]. The amplitude of the signal is representing the amplitude of the wave. It can be used to evaluate the reflection and transmission, thus, the defects within the joint. The time of flight (ToF), which is the travelling time of the wave, can be used to locate the defects [58].

Finding the mechanical properties of the joint is realized by solving an inverse problem,

that consists of the following steps [52]:

- measuring the quantities of ultrasonic parameters,
- using a model to simulate the measured ultrasonic quantities by optimizing the investigated mechanical parameters.

As mentioned in section 2.1, mechanical properties are affected by numerous parameters. Therefore, in order to obtain an accurate model, these factors should be considered and assumption should be made accordingly.

Capabilities of the current ultrasonic technologies on bonded joint quality assessment are summarized in the next section by focusing on the adhesively bonded hybrid structures and the shear horizontal guided wave ultrasonic methods.

2.3 STATE OF THE ART

Choi and Kim (2006) [13] investigated the single-lap adhesive joint consisting of two aluminium plates with same thicknesses using SH_0 mode waves and compared the experimental observations with the one-dimensional transmission line model. They have calculated the reflection and transmission coefficients on the joint boundary. Assumptions for the experiments were; negligible adhesive thickness, bonding with no defects and normal incident of the waves to the plate edges. In the model, it was assumed that there were only two impedance boundaries at the edges of the joint, which are parallel to the plate edges. Under the assumptions, the model suggests that the reflection and transmission coefficients are functions of the joint width and the wavelength. It was concluded that the suggested model only supported the experiments for low frequency (less than 110 kHz) SH_0 waves.

Le Crom and Castaings (2010) used SH waves to infer shear stiffness of an adhesive joint consisting of aluminium plate and a composite patch [8]. They compared the ultrasonic results with the one-dimensional semi analytical finite element (SAFE) model. SH_0 mode was excited at the aluminium plate, and propagated pass through the joint at different curing stages of the adhesive. During the propagation through the uncured joint, SH_1 mode was observed. After passing the joint, SH_1 waves were converted back to SH_0 mode. However, after curing was complete no mode conversion was observed. Using SAFE

model, dispersion curves and SH waves propagating through the joint were calculated. Boundary conditions were assumed to be varying, which implemented in the SAFE model as a combination of shear-springs (i.e., springs that only have shear stiffness). Stress is assumed to be continuous at the boundary (i.e., interface), with the uniform density of shear springs having constant shear stiffness. On the other hand, variable interface conditions, which can be caused by the defects, are represented by the displacement difference of the materials around the boundary (i.e., adherend and adhesive). Results of the experiments and SAFE model have shown that SH_0 and SH_1 modes are sensitive to rather large changes in the adhesives cohesive properties. Therefore, these modes could be used to monitor effects of ageing on shear stiffness of the adhesive bonds.

K. Arun et al. (2011) investigated bond quality of the single lap adhesive joints consisting of two aluminium plates by comparing the ultrasonic data with finite element (FE) analysis [14]. During the US measurements, SH_0 waves were excited and captured at the opposite sides of the joints. First, excitation of the waves by EMATs were modelled. Then, particle displacements caused by EMAT excitation were calculated. Three different interface conditions were investigated, one was assumed to be defect free, while others had some intentionally introduced defects. In addition to the US signals that propagated through the joint, the signals that echoed at the joint were observed both experimentally and numerically. The decrease in the amplitude of the signals that are interacting with the bond was observed for the good interface conditions. It was concluded that the direct signal from the joints is more sensitive to cohesive properties of the adhesive, while the echoed signal is more sensitive to the interfacial properties.

Peres et al. (2011) investigated two types of single lap adhesive joints consisting of two aluminium plates and two CFRP materials with same adherend geometries[15]. Shear horizontal waves were generated and captured from the opposite sides of the joint. Different interface conditions, such as different curing stages, pollution of the bonding area and the different surface treatments of the adherends, were observed. When compared to the reference signals, which were obtained from the 'good' bonded adhesive joints, the signal variations caused by different states of interfaces were captured. The amplitude of the signal exhibited increase during the curing, as the bonding was established. Yet, no changes due to different surface treatments were observed during the experiments. The interface variations were modelled as combination of shear and transverse springs for

numerical analysis. Although, the empirical results couldn't be reproduced by simulations, sensitivity of the SH_0 modes to interfacial states were confirmed.

In 2014, Castaings used SH waves for investigation of single-lap adhesive joints, consisting of two aluminium plates with same thicknesses, but different bond qualities [7]. US results have shown good reproducibility and sensitivity of SH waves to different interface conditions. The inverse problem was solved numerically in the frequency domain. The stiffness of the boundary between adherend and adhesive was modelled similarly to the previous work of Peres et al. [15] that is explained above. Besides, they have added absorbing regions in simulations, in order to suppress unwanted reflections from the edges of the adherends. Calculated signals by the numerical model complied with the observed US signals; therefore, the shear modulus of the adhesive and shear stiffness of the interface were quantified.

Quirin et al. (2016) used SH waves for quality evaluation of adhesion on aluminium and polymer boundaries in small structures [59]. SH waves reflected from the bonded area were investigated. US results have shown good repeatability and sensitivity of SH_0 waves to dimensional changes in the bonded area. The amplitude decrease in the reflected wave from the joined edge was related to the increased bond quality.

Herrmann et al. (2016) used SH waves for the adhesively bonded aluminium-CFRP hybrid structure characterization [60]. The ultrasonic signals were compared to the reference signals. The damped signals reflected from the joint were considered to be an indication of a good bonding.

Ding et al. (2016) analytically determined the reflection and transmission coefficients of the SH_0 wave incident to the adhesive joints' imperfect interfaces [11]. In the analytical model, non-linear effects and attenuation of the waves were ignored; adhesive and adherends were considered isotropic. The mechanical parameters were calculated numerically, where different interface states were characterized with combination of different shear stiffness coefficients. The proposed theoretical model shows that different interface quality, wave frequency and the adhesive thickness have an effect on the reflection and the transmission coefficients.

In 2019, Schwartz et al. used SH waves generated by using EMAT for characterizing the bonding in a complex aluminium-CFRP hybrid structure [61]. A pitch-catch mode was

used for examining the hybrid structures. The effect of defects on the US characteristics were investigated by comparing to a reference US signal. By examining the ToF of the peaks, it was indicated that the position of defects can be detected. Through the decrease in amplitude of the peaks, the qualitative characterization of the bonding state of the joint was shown. Moreover, the delamination of the hybrid structures, which occurred during the mechanical test, could be detected.

In the current state of technology for non-destructive testing of adhesive joints, some ultrasonic techniques are able to detect some defects within the joints and have the potential to measure their strength [24]. However, the detection of the *kissing bonds (also known as the weak bond)* remains an issue [62]. The ultrasonic SH guided waves techniques are preferred due to various advantages such as, SH wave sensitivity to the cohesion and adhesion in the joint, remote accessibility to the joint and easy generation due to EMAT technology. In the presented literature, it has been show that the SH guided waves have the potential to assess the quality of the bonded joints.

3. EXPERIMENTAL DETAILS

Hybrid test pieces, with single lap joint (SLJ) configuration, were produced using the vacuum infusion process (VIP). By using the VIP production method, bonding between aluminium and CFRP was established via co-curing. The DIN EN 2243-1 standard for single lap shear test method for structural adhesives between metal adherends was taken as a guideline for the test sample preparation. However, restrictions exposed by the available equipment and the premises of the thesis led to deviation from the test sample dimensions depicted by the DIN standard (Figure 16).

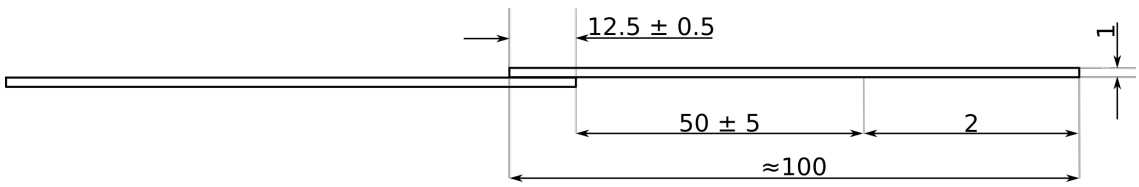

Figure 16. Single lap joint test sample geometry described in DIN EN 2243-1.

The main purpose of the experimentation is to use shear horizontal ultrasonic (SH-US) guided waves generated by electromagnetic acoustic transducers (EMATs) for damage monitoring under various service conditions. Therefore, adjustments of the specimen dimensions were made to fulfill this purpose.

The DIN standard describes a single lap shear test for adhesive shear strength determination between the *metal adherends,* while in this thesis hybrid aluminium-CFRP hybrid structures were tested. Since the EMATs cannot be used directly on CFRP, (see Section 2.2.3) only the aluminium portion of the test sample is available for placing the transducers without any aiding medium.

For hybrid SLJ test piece production, 2 mm thick aluminium alloy-AA6082 adherend was used. In order to decide on the most suitable EMAT and test piece configuration for damage monitoring, various factors were considered. First, the EMATs were chosen by considering the suitable probe frequency. Two types of EMATs were available, the one with 4 mm trace length and approximately 0.8 MHz probe frequency and the one with 3 mm trace length with approximately 1 MHz probe frequency [63]. Then, the suitable length of the aluminium part was sought in order to obtain a distinct wave packet which contains the information only from the bonded area using the available ultrasonic equipment.

As mentioned beforehand in theory (Section 2.2.2.2), propagation velocity of the sound wave in the solid medium depends on the thickness and frequency. Also, the symmetric mode SH_0 wave has the advantage of the non-dispersive propagation behaviour. Therefore, the generation of any antisymmetric and higher order symmetric mode SH wave was avoided. Figure 17 illustrates the dispersion diagrams for the aluminium alloy AA6082, generated using Eq. (28) & Eq. (30). The shear wave velocity, c_T, of 3.122 mm/µs is calculated using material parameters of AA6082 as described in Eq. (11). The reference lines in Figure 17 are given at 0.75±0.5 MHz and 1 MHz at 2 mm material thickness.

According to the figure, both EMATs seem to excite SH_1 mode. Indeed, using Eq. (31) the cut-off frequency of 0.78 MHz is obtained for the SH_1. Hence, both EMATs will excite SH_1 for the given thickness of 2 mm. The SH_1 propagation velocity at 0.8 MHz frequency (0.69 mm/µs) is lower compared to propagation velocity (1.95 mm/µs) at 1 MHz. Having lower SH_1 propagation velocity, waves need longer propagation time inside the test sample; thus, the interference with the SH_0 waves of interest can be avoided. Hence, EMAT with 0.8 MHZ probe frequency was chosen to be used in the experiments.

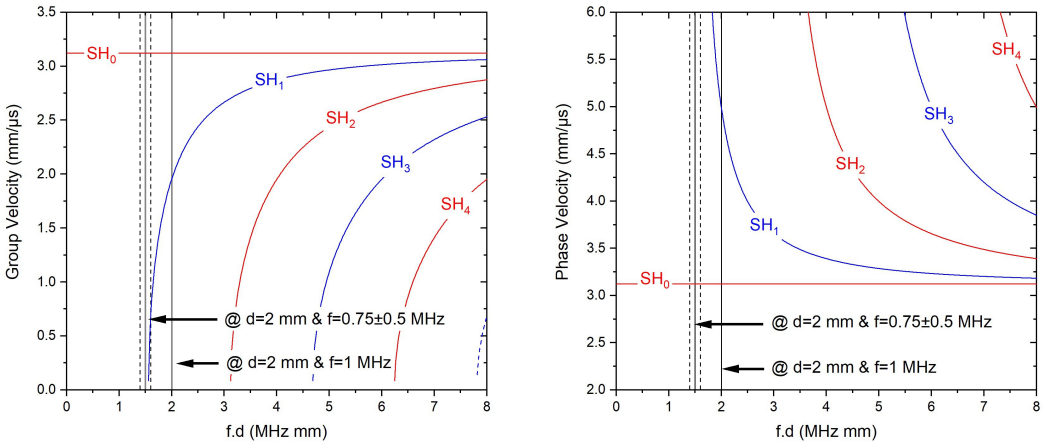

Figure 17. Dispersion diagrams for aluminium alloy AA6082

The hybrid samples were examined using pitch-catch configuration. Since, the SH waves can only be excited on the aluminium part of test pieces, available space for placing EMATs was limited. Moreover, in order to investigate the bonding condition of the overlap area, distinct wave packet reflected from the bonded edge, which is not subjected to interference, was tried to obtain.

The 0.8 MHz EMATs have 26.23 mm width, 36.5 mm length, and 30 mm height. Possible transducer-test piece configuration were tried on aluminium samples with different lengths. The width of the generated wave packets by chosen EMAT and the amplifier paralysis at the beginning of the A-scans (Figure 19), distinct wave packets couldn't be obtained for the 100 mm long aluminium.

Considering the 12.5 mm overlap length, the dimensions of the EMAT heads and the grip length of the universal test machine cross heads, it was decided to have following configuration illustrated in Figure 18.

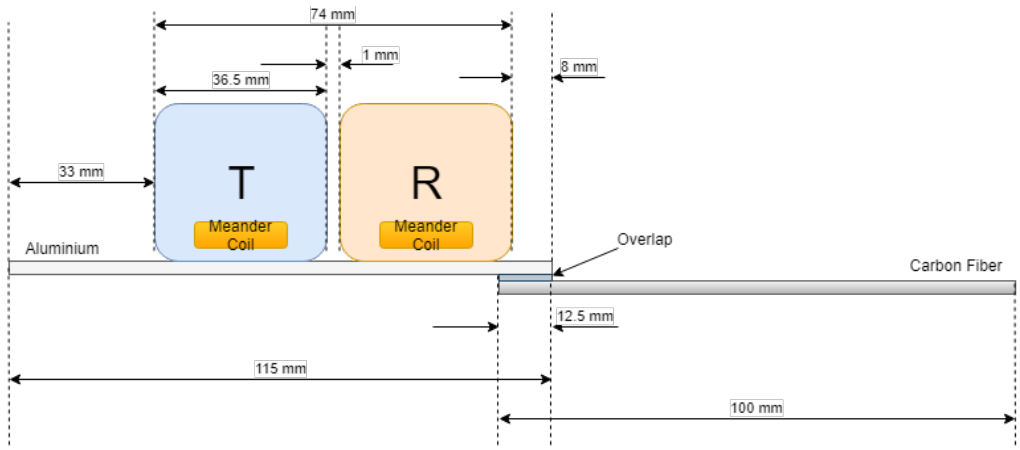

Figure 18. Position of the transducers relative to the test sample

An exemplary A-scan is associated with the configuration presented in Figure 18 is illustrated as follows (Figure 19):

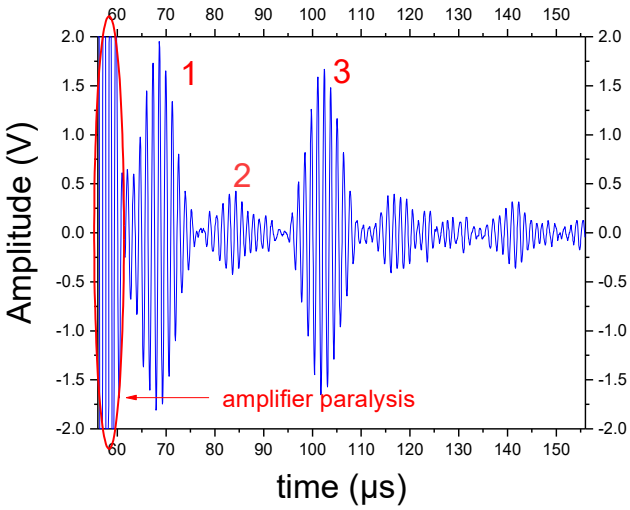

Figure 19. A-scan with dead-time at the beginning of the captured waveform (stress free TP1-1 sample)

3.1 PRODUCTION OF THE TEST SAMPLES

The vacuum infusion process (VIP) was used for the production of hybrid test samples. Therefore, bonding of the joints were established by co-curing. Before VIP, the aluminium parts were subjected to a surface treatment, where DIN EN 13887 was taken as a guideline.

The VIP was held after the surface treatment of the aluminium parts. The aluminium plates were used for sample production, from which three hybrid test samples were cut after the

bonding process was complete. Three sets of hybrid test samples were produced. All the samples had the same carbon fibre reinforcement layer configurations, however two different types of resin were used as a matrix.

After the bonding process was completed (i.e., resin was cured), hybrid single lap structures were subjected to heat treatment as recommended in the respective data sheets (see Appendix A). Finally, each single lap hybrid structure was cut into three pieces to be used in the experiments. The general scheme of sample production is illustrated in Figure 20.

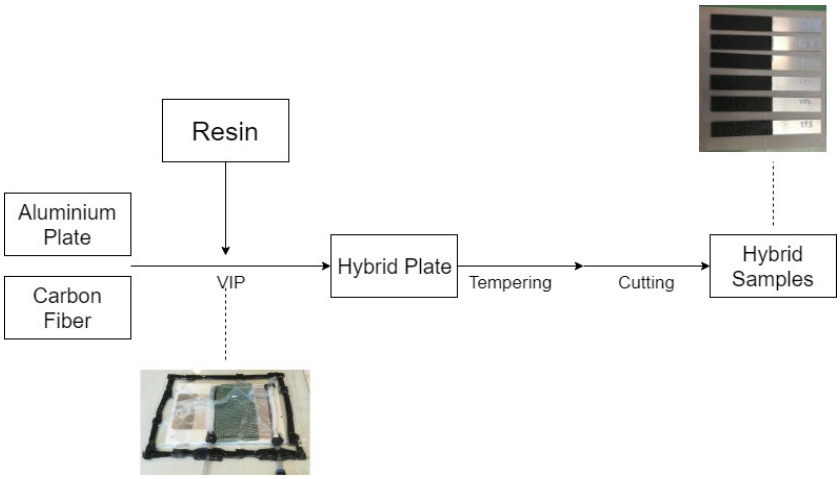

Figure 20. Schematic for the hybrid test sample production process.

3.1.1 Preparation of Aluminium Plates

Aluminium Alloy AA6082 was cut into dimensions 115 mm length x 100 mm width x 2 mm thick plates using wire erosion. Before applying any surface treatment, one aluminium plate was grit blasted using different Corundum (aluminium oxide) grit sizes ranging from FEPA[1] 30 to 220. The reason for this was to determine the proper grit size in order to promote proper bonding for the aluminium adhesive interface. The surface roughness parameters were measured using a profilometer. Three different measurements were taken along different regions on the sample and averaged. The average of the surface roughness parameters are presented in Table 1 .

1 Federation of European Producers of Abrasives (FEPA) has standardized grit sizes according to their dimensions [64].

Grit Size (µm)	R_a (µm)	R_z (µm)	R_{max} (µm)	FEPA Grit
Untreated	0.175	1.468	2.038	Untreated
600	7.484	58.036	61.530	FEPA 30
300	4.923	34.652	39.920	FEPA 54
212	3.724	26.634	30.808	FEPA 70
180	3.057	22.565	24.939	FEPA 80
125	2.289	18.002	20.812	FEPA 100
75	1.939	15.001	16.672	FEPA 150
53	1.058	7.394	8.422	FEPA 220

Table 1: Surface Roughness Parameters (Ra: Arithmetic mean roughness value Rz: mean roughness depth Rmax: maximum roughness depth)

The suggested grit size in DIN EN 13887 is between 45 µm and 106 µm, in this case grit size of 75 µm (FEPA150) was used. The aluminium plates were first degreased using acetone. Then, the surfaces of the plates were covered to only expose the bonding area for grit blasting. Finally, the surface was cleaned again from the remaining corundum, and was ready for the bonding. The detailed steps for the surface preparation of the aluminium plates is presented in Appendix B.

3.1.2 Preparation of Hybrid Samples

Two layers of plain 1x1 weave and two layers of +45/-45/0 triaxial carbon fabrics were cut into 140 mm x 160 mm rectangles for each set of test samples. Stacking sequence was $[0/90/(+45/-45/0)]_s$ (resin flow direction is considered 0°). Two types of resin were used; Elium 150 thermoplastic resin and HP-E3000 Epoxy-Hardener system. Except the surface area that was spared for bonding, the aluminium plates were covered with release agent in order to impede unwanted bonding.

After the aluminium plate was placed in the mould, carbon reinforcements were laid. On top of the carbon reinforcement, one layer of peel ply, one layer of breather and one layer of flow mesh was placed. Following the placement of the inlet and outlet tubing, the vacuum bag was sealed by using sealant tape (Figure 21). When the vacuum was established, the mould was dehumidified for a while in order to establish reproducible results. In the mean time, resin was mixed on hot plate stirrer and set for the infusion process. Then, the inlet tube was released for resin impregnation. Succeeding the complete wetting of the reinforcement, the mould was left for curing. Finally, the hybrid structures

were tempered; afterwards, cut into 25 mm width test samples by table cutting wheel. The technical details of the complete production process is supplied in Appendix B.

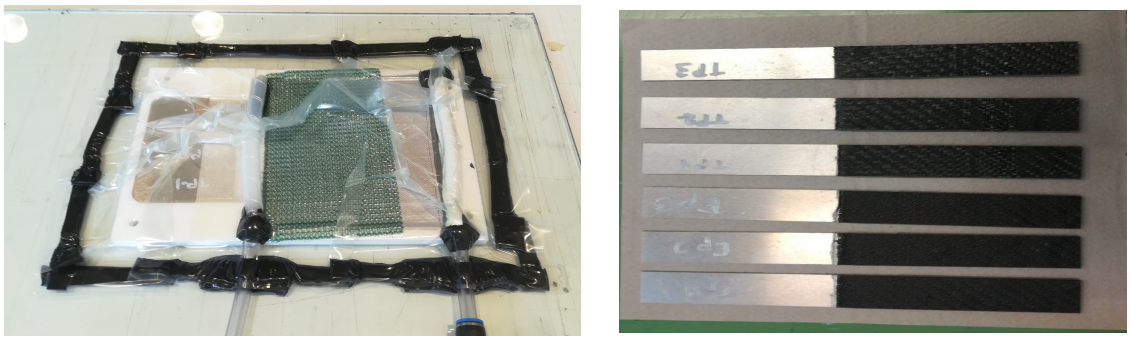

Figure 21. Sealed mould before resin impregnation (right) and cut Ep# & TP1-# test pieces.

Before it was mentioned that three sets of hybrid samples were produced. They were distinguished according to the matrix they have; TP1-#, TP2-#, Ep#. The hash sign is reserved for the number of the samples that are cut from the each production set. During the curing of the first set (TP1-#), vacuum was lost. Therefore, the samples were not cured under vacuum. However, these samples were still used for the experiment (Figure 21). The possible effects of this production mishap is discussed later.

3.2 EQUIPMENT FOR THE EXPERIMENT

The test samples were monitored by the ultrasonic system, while they were subjected to quasi-static and dynamic load by the universal test machine (Instron 8500). The mechanical response of the samples during loading were captured using the Labview software. the diagram of the ultrasonic system is shown in Figure 22. The signal generator produces low power electrical signals, which are then fed in to power amplifier for amplification. The generated signals had 0.75 MHz test frequency, and the pulse rate was 50 Hz and 80 Hz depending on the software that is used to capture the US data. In other words, 50 or 80 pulses were generated per second and each pulse had 0.75 MHz test frequency. The signals are sent to transmitter, and due to coupling of electric and elastic fields, ultrasonic waves (elastic waves) are generated within the aluminium part of the sample. After propagation in the sample, ultrasonic waves are captured by the receiver via the reverse Lorentz force mechanism and converted to the electric pulses again. After

amplification, the signals are captured by the oscilloscope (PicoScope 2206B), and displayed on the computer using a software as an A-scan representation. The softwares used for US data acquisition were PicoScope 6 and Labview. Technical details of the US systems are supplied in Appendix C.

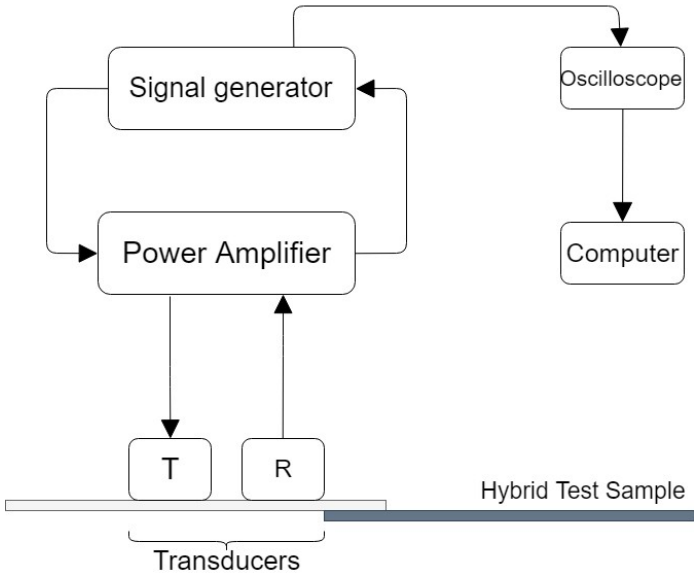

Figure 22. Schematic representation of the ultrasonic system

Figure 22 doesn't represents the actual position of the samples and transducers. The samples were vertically positioned inside the tensile test machine. Since metallic parts of the test samples are not ferrous, transducers can not be fixed on the sample without any mounting. Therefore, a special tool was designed for fixing the transducers on the sample. The transducers had to be in contact with the sample during the mechanical loading while applying minimum stresses on the sample, in addition to staying at a constant position (see Figure 18) relative to each other and the sample. The tool for holding the transducers is presented in Figure 23. The technical details and mounting instruction can be found in Appendix C & D.

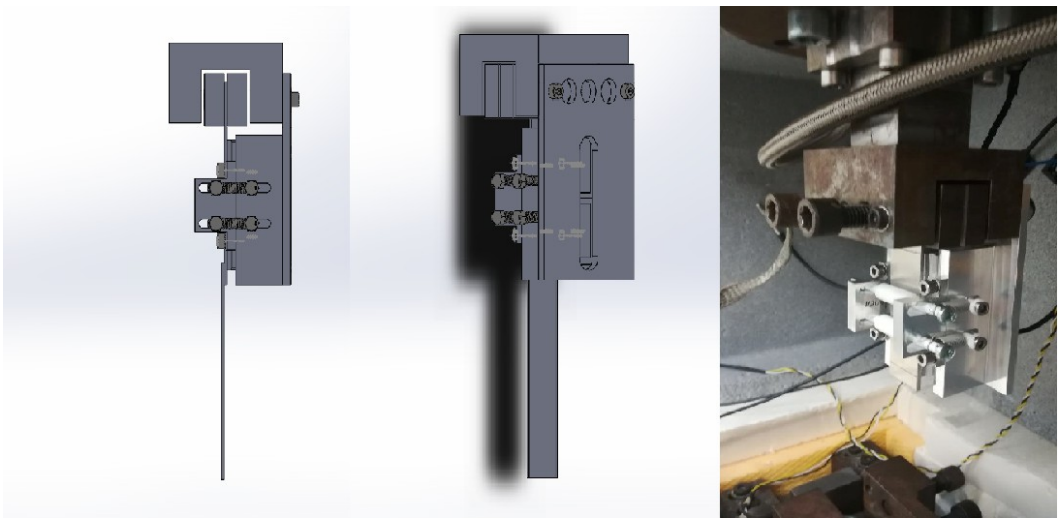

Figure 23. Tool for holding transducers

3.3 EXPERIMENTAL PROCEDURE & ANALYSIS

The single-lap joint samples were subjected to mechanical loading applied by a universal test machine. In order to eliminate the influence of the environmental conditions, an isolation chamber was used. The temperature inside the chamber was kept constant at 23 °C. Two electromagnetic acoustic transducers (EMATs) with 0.8 MHz probe frequency were used to generate and receive the SH waves in a pitch-catch mode. The SH waves were excited at a 0.75 MHz test frequency. However, the waves are generated over a range of frequencies rather than a single frequency, where the group velocity represents the velocity of the wave packets.

As presented beforehand in the dispersion diagrams (Figure 17), the test frequency is close to the cut-off frequency of SH_1 mode. Considering the frequency range of 0.75±0.5 MHz, the possible SH_1 velocities range from 0.3 to 0.69 mm/µs. Therefore, the SH_1 waves might have been excited as well. However, since the SH_1 mode has lower velocity, it was not expected to interfere with the wave packets of interest within the given dimensions of aluminium part of the hybrid test pieces.

In Figure 24, the A-scans and power spectre of two aluminium test pieces that have the same width and thickness, but different lengths are presented. During the US measurements for the presented figure, the wave excitation parameters and the distance between the EMATs were same.

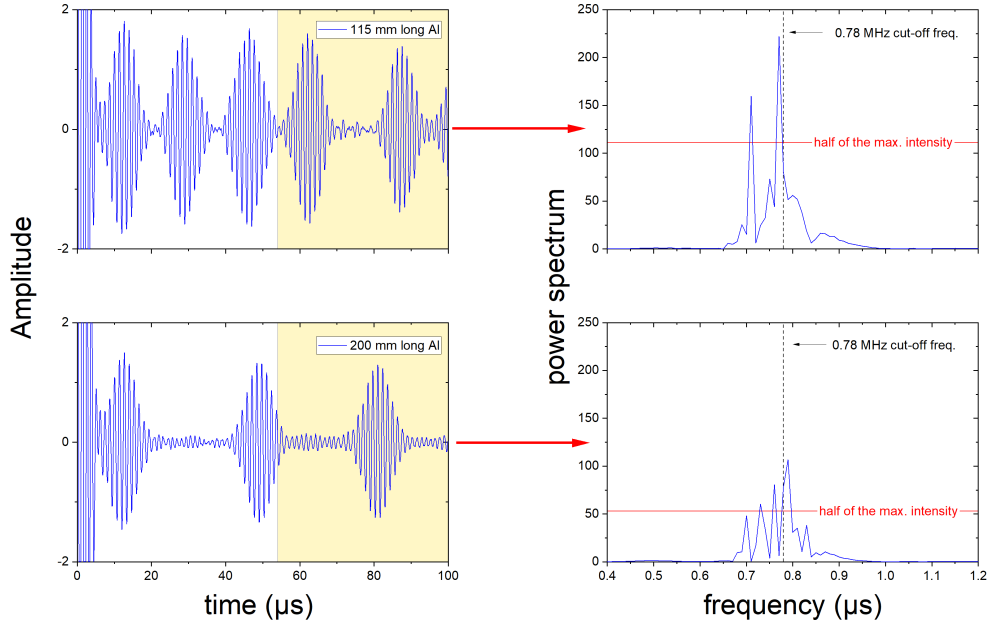

Figure 24. A-scan and frequency spectrum of 115 mm and 200 mm long aluminium. The coloured portion in A-scans represents the possible SH1 mode

The possible places, which SH_1 waves with maximum group velocity of 0.69 mm/µs can be observed is marked in A-scans. The power spectra of the A-scans are presented with the reference lines on SH_1 cut-off frequency and the half intensity of the peak frequency. For 115 mm long aluminium, the peak frequency is less than cut-off frequency. Therefore, no SH_1 is observed. On the other hand, for 200 mm long aluminium test piece, the peak frequency is slightly larger than the cut-off frequency. Therefore, it is possible to observe SH_1 modes. In between wave packets, low amplitude additional signals can be seen in A-scan of 200 mm aluminium piece. However, additional signal in the marked range cannot be directly related to SH_1 mode as the amplitude is very low and comparable to the additional signal observed in between first and the second wave packet.

As mentioned beforehand, the first three wave packets are investigated for US characterisation. Thus, although the excitation of additional SH_1 is possible, it is not expected to interfere with the wave packets of interest within the hybrid samples.

3.3.1 Preliminary Measurements

In order to set a reference for the experimental result interpretation, some preliminary experiments were held. As mentioned before, there were two different sets of data acquired from the different systems, the ultrasonic system and the tensile test system. In order to ensure functioning of the two systems simultaneously, the data acquisition capabilities of the ultrasonic system was measured.

The optimum sampling rate, the number of captured waveforms per second and the total number of the stored waveforms were determined. The total number of stored waveforms was the decisive factor for the data acquisition limits. The duration of the mechanical loading was planned according to the limitations of the US system. Afterwards, the initial state of the test samples by comparing to an unbonded reference 115 mm long aluminium test piece (Al-115) was investigated using the US system.

First, Al-115 is analysed using different methods to capture ToF, amplitude and area. Al-115 has the same dimensions as in hybrid samples. It is examined to set a reference for the initial state of the wave packet that is reflected from the overlap area in hybrid samples. Next, a 200 mm long aluminium test piece (Al-200) was loaded within the elastic limits to investigate the influence of aluminiums stress-state on the ultrasonic signal. Different methods are compared only for aluminium test pieces, and narrowed down to one method. For the rest of the investigation the chosen method is used for ToF, amplitude and area determination.

The A-scans of the stress free test samples and the bond free aluminium were measured using the same configuration that is presented in Figure 18. In all measurements, the relative positions of the EMATs to each other and the aluminium part of the test pieces were kept constant. The EMATs were connected by a plate to ensure constant 1 mm distance relative to each other and placed on the sample on the same position by hand as it was during the mechanical loading (Figure 25).

In Figure 26, the wave propagation paths, associated with the measurement configuration presented in Figure 18, are illustrated. The first wave packet (WP1) is travelling directly from the transmitter to the receiver, which is a path with the shortest distance. The second wave packet (WP2) is reflected from the bonded edge, which contains the integrated information of the bonded area. The third wave packet (WP3) is reflected from the bond free edge. The samples were fixed to the universal test machine by this end. Therefore, the

third wave packet associated to the wave that was reflected from a clamped/gripped edge to the cross-heads of the test machine.

Figure 25. Depiction of initial state ultrasonic measurement of the test pieces.

The middle point of the EMATs are used for calculating the path lengths travelled by the wave packets (see Figure 26). For theoretical time of flight calculations, the propagation velocity of the SH_0 wave is taken as 3.122 mm/µs. The travelled distance are taken as 37.5 mm, 90 mm and 140 mm for WP1, WP2 and WP3, respectively. The sampling rate for the US system is taken as the standard deviation for the theoretical ToF values.

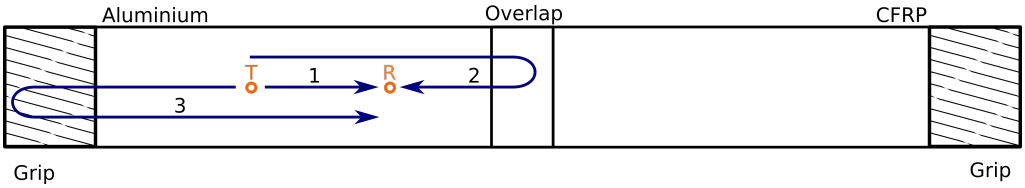

Figure 26. Propagation paths for the first three wave packets

3.3.1.1 Initial state of Al-115

The A-scan of Al-115 was measured five times, with a sampling rate of 20.83 MHz, in order to assess the reproducibility of the results. One of the A-scans obtained form the US measurements is presented in Figure 27.

At the beginning of the A-scan, an electrical component which is termed as dead time or amplifier paralysis is observed [7][65]. Therefore, the WP1 is partly buried in this electrical component.

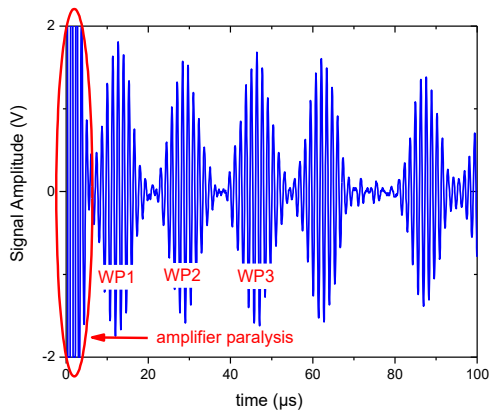

Figure 27: A-scan for Al-115 sample.

For the analysis, ToF and the amplitude values of wave packets were determined using different methods. These methods were the maxima method, the zero-crossing method and the enveloping method. In addition, these values were calculated using the absolute of the signal as well.

In the maxima method, the ToF and the amplitude values were calculated from the global maxima point in the relative wave packets (see Figure 28). This method gives direct information from the raw data.

In the zero-crossing method, only ToF values were determined from the points where signal has a zero amplitude between the maxima and the minima. Since, there weren't any sampling points with zero amplitude, two sampling points closest to the x-axis were used to determine the zero-crossing point. Linear regression was applied to the points, that were positioned on the positive and negative side of the x-axis.

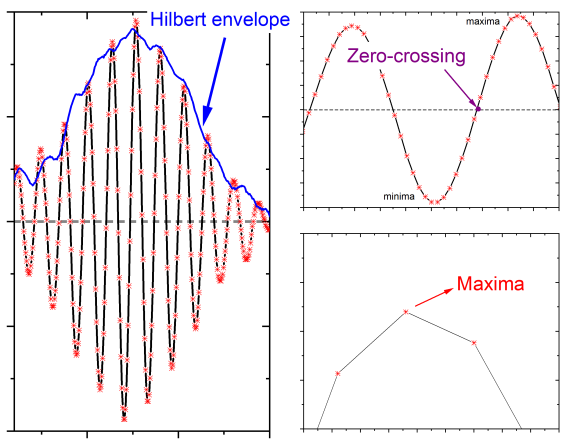

Figure 28. Illustration of the methods that are used for ToF, amplitude and area determination of the wave packets.

In the enveloping method, the signal was enveloped using Hilbert transform. Hilbert transform of a signal, *f(t)*, is defined as (Eq. (35))

$$s(t)=f(t)+i\,h(t) \tag{35}$$

where *s(t)* is analytical signal and *h(t)* is the Hilbert transform of a signal. Analytical signal is the envelope of the real signal. The maxima of the Hilbert envelope is used for ToF and amplitude estimations. The area under the curve is calculated only up to half of the amplitude. The reason is to avoid changes that might be caused by the interference of the wave packets.

For investigating the repeatability of the measurements, mean (μ) and standard deviation (σ) of the ultrasonic parameters were calculated as follows

$$\mu=\frac{1}{N}\sum_{i=0}^{N-1}x_i \quad and \quad \sigma=\sqrt{\frac{1}{N-1}\sum_{i=0}^{N-1}(x_i-\mu)^2} \quad where \quad N=5 \quad . \tag{36}$$

Additionally, normalized amplitude values were calculated in order to increase the accuracy of the comparisons. The amplitude values are normalized by dividing the signal amplitude to the WP1 amplitude. The effects caused by varying contact between the transducers and the samples were eliminated by normalizing the amplitude values.

The analysis of the US and mechanical results are done using Matlab R2018a and the results are plotted using Origin 2018b softwares.

3.3.1.2 Tensile Test

The Al-200 test specimen with 25 mm width, 200 mm length and 2 mm thickness was monitored while being subjected to quasi-static tension within the elastic limits. The sensitivity of the ultrasonic waves to the stress state of the aluminium specimen is investigated. The aim is to detect possible changes in the US characteristics such as ToF, amplitude and area caused by the stress state of the aluminium. So during the monitoring of the hybrid test pieces under mechanical loading, the changes caused by stressing the specimen and the changes caused by integrity of the bonded area can be differentiated.

Al-200 was measured during stress free state, clamped on one edge and during the tensile test, while the distance between transducers were kept constant. In Al-200, three distinct wave packets were observed within 100 μs time span of A-scan, which are corresponded to

wave paths shown in Figure 29. Although WP1 path length was kept constant, WP2 and WP3 varied. But the distance travelled by WP3 was always larger than WP2.

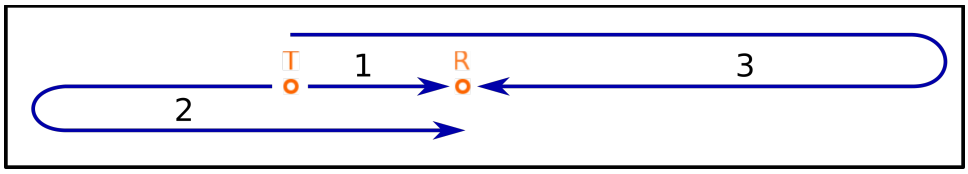

Figure 29. Wave paths for Al-200. The third wave path is longer than the second wave path. The first wave path is always the shortest.

The US characterization of Al-200 is done using the methods described in initial state of Al-115. After comparison of the methods, the most suitable one is used during the monitoring of the hybrid samples.

3.3.1.3 Initial state of Hybrid Test Pieces

The ToF and amplitude values of the first three wave packets are calculated for the hybrid test specimens. After the calculation of the mentioned parameters, results for each hybrid test sample were compared to aluminium test piece. The aim of this comparison was to observe changes caused by the bonding and to have a reference signal for the mechanical experiments. Each measurement was repeated five times and reproducibility of the results were investigated as explained beforehand using Eq. (36).

3.3.2 Condition monitoring

3.3.2.1 Quasi-static Test

The TP1-1 sample was pulled at 2 mm/min rate until failure occured. During the testing, DIN EN 2243-1 describing the single lap shear test method designated for structural adhesives, was taken as a guideline. The shear strength of the adhesive joint was calculated as stated in Eq. (1). The data acquisition from the ultrasonic system was started before the mechanical loading. Therefore, the acquisition time of both systems was adjusted accordingly. The US system captured ten A-scans (also referred to as waveforms) every second via Picoscope 6 software with 31.25 MHz sampling rate.

3.3.2.2 Incremental Step Test

The TP1-2 sample was subjected to a sinusoidal cyclic load at 5 Hz frequency at increasing

load steps. In each step, only 1000 cycles were used due to the limitations of the data storing capability of the Picoscope 6 software that was used for capturing US data. The mechanical loading was force controlled, where driving mean force (F_m) and amplitude (F_a) parameters were correlated to the failing load obtained from the quasi-static test of TP1-1 sample. The maximum load (F_{max}) varied starting from 40% to 90% of the adhesives failing load (see Eq. (37)):

$$F_{max} = nF_{fail} \qquad n: 0.4 \;\; to \;\; 0.9 \tag{37}$$

Mean force (F_m) and force amplitude (F_a) were calculated using the stress ratio (R) of 0.1 as shown in Eq. (38):

$$F_m = \frac{F_{max} + F_{min}}{2} \;, \quad F_a = \frac{F_{max} + F_{min}}{2} \;, \quad R = \frac{F_{min}}{F_{max}} \quad where \quad R = 0.1 \tag{38}$$

The stiffness of each cycle is calculated by dividing the difference between force maximum and minimum to the difference between position maximum and minimum (Eq. (39)):

$$k = (F - max - F_{min}) / (d_{max} - d_{min}) \tag{39}$$

In Figure 30, all the force relations for cyclic load is illustrated. The change of the amplitude and ToF values during the dynamic test were examined. In each step, data acquisition from the ultrasonic system had started before the mechanical system; therefore, the acquisition time of both systems is adjusted. Every second, the US-system captured about 18 waveforms.

TP1-2 sample was monitored during the incremental step test. Each step consists of 1000 cycles with 5 Hz frequency. The force was increased from 40% to 90% of the maximum strength obtained from the quasi-static test of TP1-1 sample. The test was force controlled, therefore the sinusoidal variations of the load was constant. By applying various loads, it was aimed to introduce small changes and defects in the joint to examine the detection capabilities of the US-system of these changes.

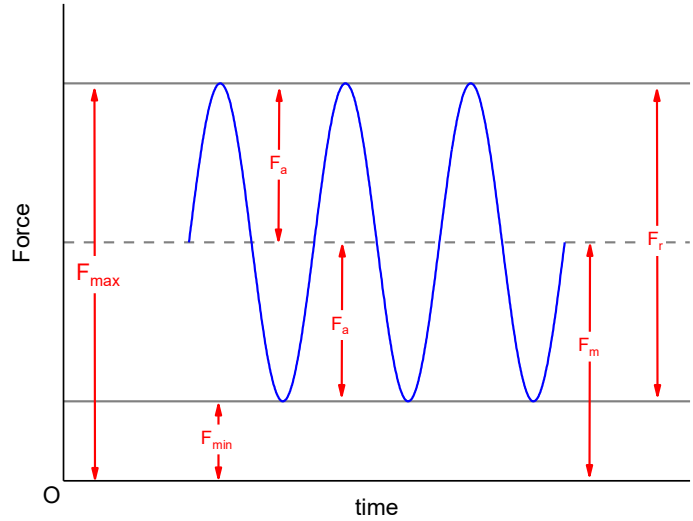

Figure 30. Dynamic force-time relations. F_{max}: maximum force, F_{min}: minimum force, F_a: force amplitude, F_m: mean force, F_r: range of stress

3.3.2.3 Dynamic Test

The TP1-3 sample was subjected to sinusoidal cyclic load at 5 Hz frequency and approximately 70% of the adhesive failing load obtained from the quasi-static test. The test was force controlled, whose parameters (F_{max}, F_m, F_a) were calculated as explained for the load incremental step test. During the experiment, US data was captured using Labview software with 125 MHz sampling rate. However, in order to speed up the ToF and amplitude calculations, sampling points at 25 MHz were used.

Only limited amount of hybrid samples were available for monitoring under mechanical loading. Therefore, the statistical accuracy of the results cannot be assessed in this work. However, the goal of conducted experiments is to determine the applicability of US-SH waves for damage monitoring, rather than the characterisation of the strength of the adhesive joint.

As mentioned beforehand, different softwares were used for different measurements. Also, during different measurements, different sampling rates were used to test the limits of US-system. Some US system parameters are presented for all three experiment in Table 2.

Mechanical Test	Initial State Measurements	Al-200 Tensile Test	TP1-1 Quasi-static Test	TP1-2 Load Incremental Step Test	TP1-3 Dynamic Test
Sampling Rate	20.83 MHz	125 MHz	31.25 MHz	31.25 MHz	125 MHz
Sampling Period	48 ns	8 ns	32 ns	32 ns	8 ns
Sample Number	2,083	10,000	3,125	3,125	10,000
Time Shift	55.943 µs	56 µs	58.309 µs	56.278 µs	56 µs
Software	PicoScope 6	Labview	PicoScope 6	PicoScope 6	Labview

Table 2. Sampling information of the US system during the mechanical experiments

4. RESULTS & DISCUSSION

In this section, first the results for the preliminary US measurements are presented. Initial state of the hybrid test pieces are characterized in relation to the reference Al-115 specimen. The possible effect of the stress-state on the US parameters is examined and the most suitable method for ToF and amplitude estimation is presented. Later, the results of damage monitoring are presented and discussed in relation to initial state of the hybrid samples.

4.1 PRELIMINARY MEASUREMENTS

First, ToF and amplitude estimation methods are presented and suitability of damage monitoring is discussed. The methods are assessed using Al-115 and Al-200 US measurements.

Then, the ultrasonic characteristics of hybrid test pieces prior to mechanical loading are presented. It is aimed to determine the effect of bonding on the wave packets and set reference values for the ultrasonic characteristics such as ToF and amplitude. These reference values are referred to as initial state and used to interpret changes in the ultrasonic characteristics during the mechanical loading.

4.1.1 Comparison of Ultrasonic Parameter Estimation Methods

4.1.1.1 US Characterization of Al-115

In Table 3, the ToF values for the first three wave packets in Al-115 are presented. It can be seen that the measured ToF values deviate from the theoretical values for each

estimation method. Besides, WP1 and WP3 have always larger mean value compared to the theoretical ToF, while WP2 values do not exhibit consistent behaviour compared to the theoretical ToF.

The possible reason for the difference between theoretical and measured ToFs can be due to imprecise positioning of EMATs relative to each other and to the test piece.

When the ToF standard deviations are compared, WP2 and WP3 exhibit larger deviations than WP1. During the measurements, the distance between EMATs, i.e. the path travelled by WP1, was kept constant. On the other hand, connected EMATs were removed from the sample and replaced again on the same position in the beginning of every measurement. Therefore, the EMAT position relative to the test piece might have been slightly different in each measurement. Hence, having larger standard deviations for WP2 and WP3 than WP1 is a plausible result.

Parameter	Time of Flight (μs)					
# of Wave Packet	WP1		WP2		WP3	
Statistics	μ	σ	μ	σ	μ	σ
Theoretical	12.012	0.048	28.828	0.048	44.843	0.048
Maxima	12.653	0.026	28.426	0.221	46.358	0.218
Maxima-abs	12.528	0.269	28.685	0.299	46.099	0.502
Hilbert	12.470	0.079	28.973	0.534	46.195	0.641
Hilbert-abs	12.470	0.291	28.925	0.717	46.080	0.529
Zero-crossing	12.347	0.020	28.102	0.223	46.039	0.220

Table 3. Time of flight values for the first (WP1) and second (WP2). Al-115 reference test sample measured 5 times.

Among the presented methods, the zero-crossing methods seem to give improved results in terms of standard deviation. However, it is comparable to the results obtained from the raw data, i.e. information obtained from the maxima. Especially, for WP1 the standard deviations for these methods are comparable to the sampling period of the US system. However, amplitude and area values should also be considered before any conclusion.

As shown in Table 4, the amplitude values for WP2 and WP3 are lower than WP1. Since SH waves are know to propagate along long distances with little attenuation, this decrease cannot be linked to attenuation. In addition, WP3 amplitude is slightly larger than the WP2, although the path travelled by WP3 is longer. Therefore, attenuation During the

measurements EMAT heads are closely placed. Since the EMATs are known to be sensitive to surrounding electromagnetic noise [16], the amplitude variation could be a result of electromagnetic interference between the EMAT heads.

Parameter:	Amplitude (V)					
# of Wave Packet:	WP1		WP2		WP3	
Statistics:	μ	σ	μ	σ	μ	σ
M:	1.835	0.114	1.580	0.014	1.596	0.109
M-abs:	1.841	0.101	1.593	0.034	1.618	0.097
Hilbert:	1.861	0.107	1.608	0.025	1.633	0.103
Hilbert-abs	1.841	0.099	1.595	0.035	1.622	0.093

Table 4. Amplitude values for the first (WP1) and second (WP2). Al reference test sample measured 5 times.

When the area of the wave packets is examined, larger standard deviations can be seen. Especially, area estimation with Hilbert method for absolute signal seems to give less accurate results.

Parameter:	Area (V*μs)					
# of Wave Packet:	WP1		WP2		WP3	
Statistics:	μ	σ	μ	σ	μ	σ
Hilbert:	86.424	2.582	80.574	5.373	86.424	2.582
Hilbert-abs	97.766	4.265	67.435	9.519	97.766	4.265

Table 5. Area of the first (WP1) and second (WP2). Al reference test sample measured 5 times.

When all the ToF values are considered, only the zero-crossing method indicates a slight improvement of the estimations. On the other hand, the amplitude values do not indicate any significant improvement in accuracy. Therefore, the discussion of the methods are continued for the tensile test of Al-200.

4.1.1.2 Ultrasonic Monitoring of Al-200 during Tensile Test

Figure 31 illustrates the A-scans of Al-200 in various conditions. In stress free state three wave packets have comparable amplitudes, with additional signal in between the wave packets (Figure 31-a). The additional signal could be due to generation of SH_1 mode waves, as the signal generation frequency is close to cut-off frequency of the SH_1 mode.

In Figure 31-b, when Al-200 is clamped on the edge where WP3 reflects, decrease and shift in the amplitude is observed. The amplitude decrease can be interpreted as energy

transmission to the grips of the universal test machine. The time shift, i.e. ToF increase, could be the result of multiple reflections within the grip heads. On the other hand, in literature, it has been shown that increase in applied tensile stress results in increase of ToF [66][67]. Although in this case grips only exert contact stress, the possible effects of increased local stress state on the ToF should also be considered.

The A-scan measured during the tensile test, where both edges are clamped, is shown in Figure 31-c. Therefore, similar changes in amplitude and ToF of WP2 is expected as in WP3. During the measurements, only 80 µs of time span was recorded; therefore, WP3 cannot be observed. In addition, an overall decrease in the amplitude is observed. This can be linked to changing contact between the EMATs and the test piece. Thus, normalized amplitude values are also used for comparison to mechanical data.

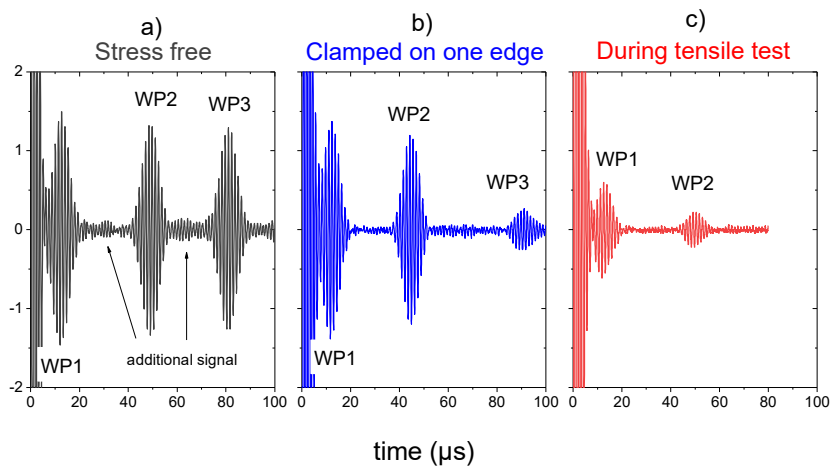

Figure 31. A-scans for Al-200 specimen during various stress states

In Figure 32, the comparison of ToF estimation methods during the tensile test is presented. Here, the absolute signal investigation is excluded. The maxima of the peaks are examined in two different manners. First, for each A-scan the maxima of the wave packets are captured. Second, the maxima of the first captured A-scan is taken as reference, than the maximum values of this reference peak is considered for ToF and amplitude values (referred to as P-maxima). The same procedure is also applied for the the zero-crossing method. Since Hilbert method is enveloping the signal, as mentioned in section 3.3.1, it was excluded from the reference peak analysis.

When reference peaks are used for the estimation of ToF, the standard deviation is much lower compared to the other methods. The reason for this difference is, the maxima of the wave packet changes between consecutive peaks, even though there is change of neither the stress state nor the position of the EMATs relative to the sample.

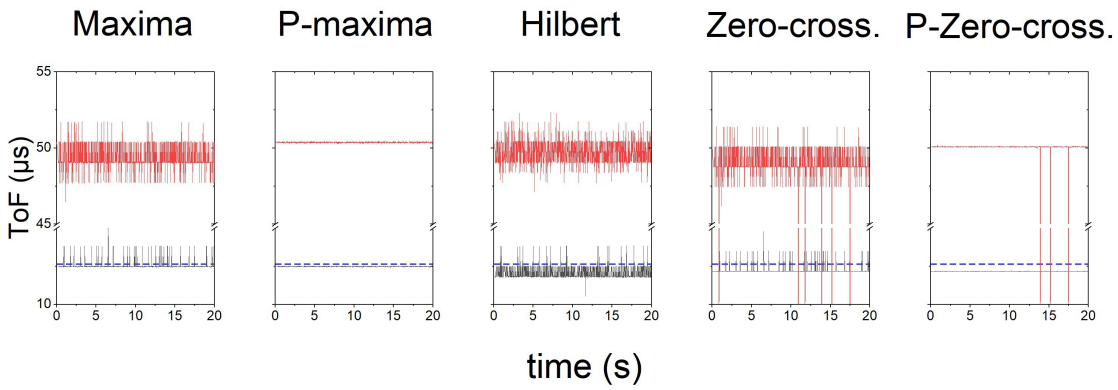

Figure 32. Comparison of ToF values calculated using various methods during the course of Al-200 tensile test. Absolute signal measurements are excluded. (Gray curves: WP1, Red curves: WP2)

The same behaviour can be observed, when the absolute signal is also investigated. In Figure 33, it is shown that when the reference peak is used for ToF estimations (P-maxima-abs.) the variation of the estimations is lower.

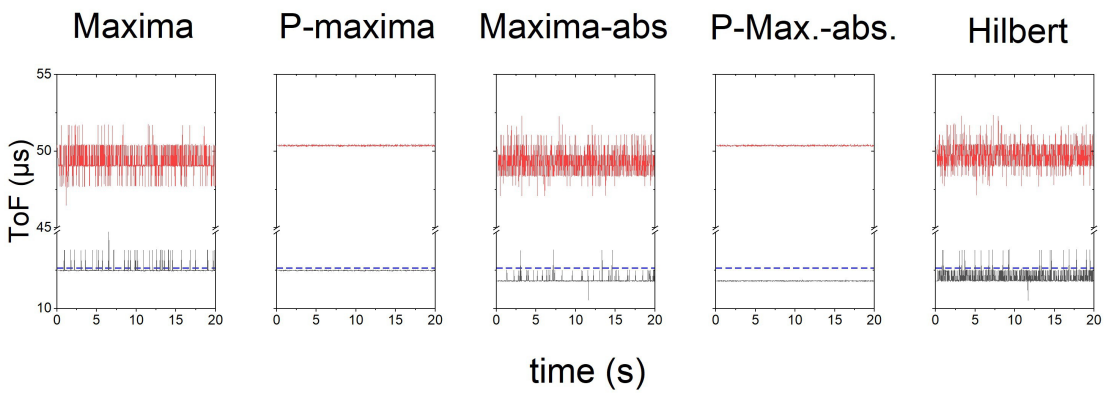

Figure 33. Comparison of ToF values calculated using various methods during the course of Al-200 tensile test. (Gray curves: WP1, Red curves: WP2)

In the zero-crossing method, sometimes singularities are observed due to the calculation method for the ToF. In this method, two points closest to zero amplitude are used for linear regression to determine zero-crossing points of the wave packets. When one of the points is too close to zero amplitude, ill condition occurs and it results in an infinite value.

In Figure 34, the mechanical results are presented along with the US parameters. The US parameters are calculated by using the first A-scan as a reference and calculating the maxima of the reference peak (P-Maxima method). The Al-200 test piece was stressed up to 150 MPa. The results indicate that the stress state of the aluminium has no effect on the US parameters within the elastic limit. Therefore, during the damage monitoring of the hybrid samples, the change in US parameters, due to stress state of the aluminium part, is not expected.

The analysis of the US parameters estimation methods cannot be concluded with the current results. However, it is shown that using solely the raw US data for the amplitude and ToF estimation can be misleading. Therefore, during the mechanical loading of the hybrid samples, reference peak is used for US parameter estimations.

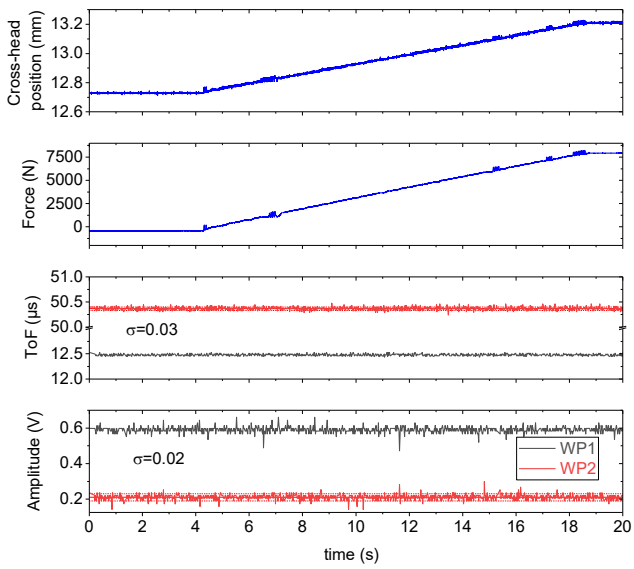

Figure 34. Comparison of US and mechanical data during the tensile test

4.1.2 Initial State

The initial state of the hybrid samples are determined by averaging five different US measurements using Eq. (36). The results are compared to the Al-115 test piece to determine the effect of bonding to ultrasonic characteristics.

4.1.2.1 Ep samples

The A-scans of the Ep samples along with the Al-115 are presented in Figure 35. At first glance. the wave packets that are reflected from the bonded edge can be differentiated. Due to the interaction with the joint, the amplitude of the WP2 is damped.

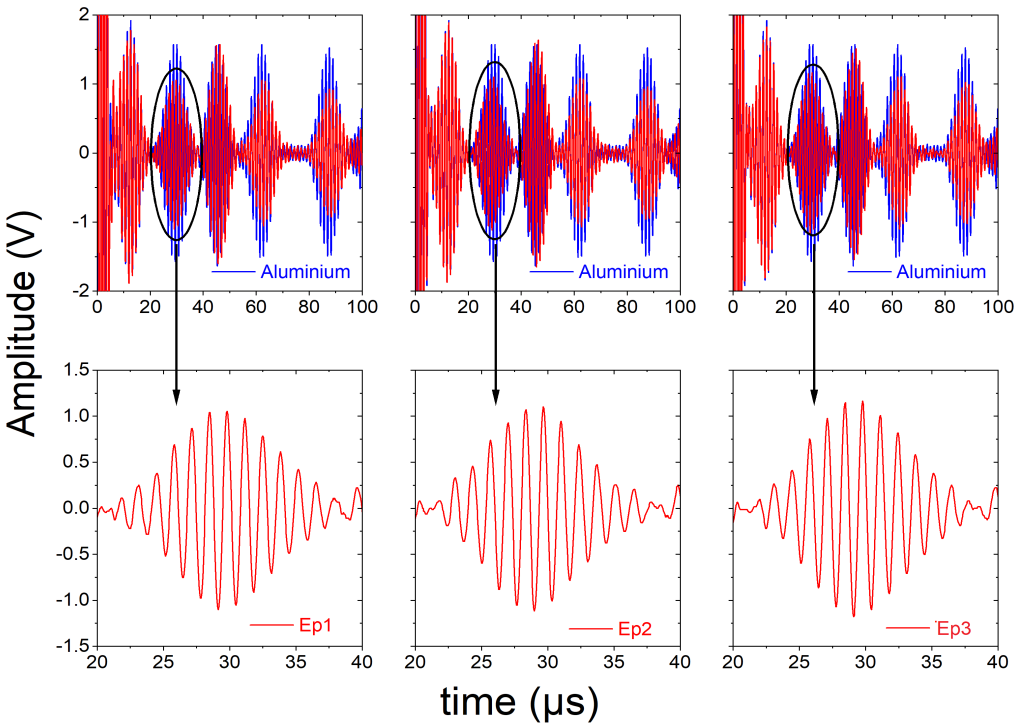

Figure 35. A-scans for Ep samples. Second wave packet (WP2), which is interacting with the joint is magnified.

In Table 6 and Figure 36, the ToF and amplitude values for WP1 and WP2 of Ep and Al-115 samples are presented. The results are estimated from the maxima of the wave packets. The ToF and amplitude mean values of WP1 remain within the standard deviation when compared to Al-115. The ToF mean values of WP2 are slightly larger, but this could be the due to variation of the EMATs position relative to the test pieces rather than an influence of

the bonding. On the other hand, the decrease in amplitude of WP2 is more pronounced, which indicates the transmission of the mechanical energy from aluminium to CFRP. In other words, some portion of the SH waves are transmitted to CFRP.

Parameter:	Amplitude (V)				Time of Flight (µs)			
# of Wave Packet:	WP1		WP2		WP1		WP2	
Statistics:	µ	σ	µ	σ	µ	σ	µ	σ
Al-115:	1.835	0.114	1.580	0.014	12.653	0.026	28.426	0.221
Ep1:	1.775	0.129	1.035	0.060	12.653	0.026	29.002	0.593
Ep2:	1.800	0.121	1.035	0.058	12.662	0.021	29.702	0.086
Ep3:	1.841	0.045	1.199	0.034	12.379	0.004	29.168	0.694

Table 6. Mean and standard deviation of ToF and amplitudes for Ep samples and Al-115. The results are averaged from 5 different measurements

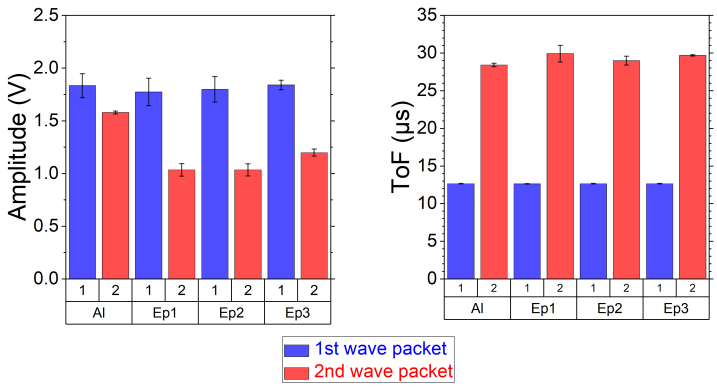

Figure 36. Graphical depiction of mean and standard deviation of ToF and amplitude for Ep samples and Al-115. The results are averaged from 5 different measurements.

4.1.2.2 TP2 Samples

The A-scans of the TP2 samples with Al-115 are presented in Figure 37. Similar to the Ep samples, the amplitude of the wave packets reflected from the bonded edge are damped.

The reproducibility of the ultrasonic parameters is presented in Table 7 and Figure 38. When ToF and amplitude values are examined, the results of WP1 for each sample indicate good accuracy and precision. In addition, the interaction of WP2 with the joint is clearly indicated by the lower amplitude values compared to Al-115.

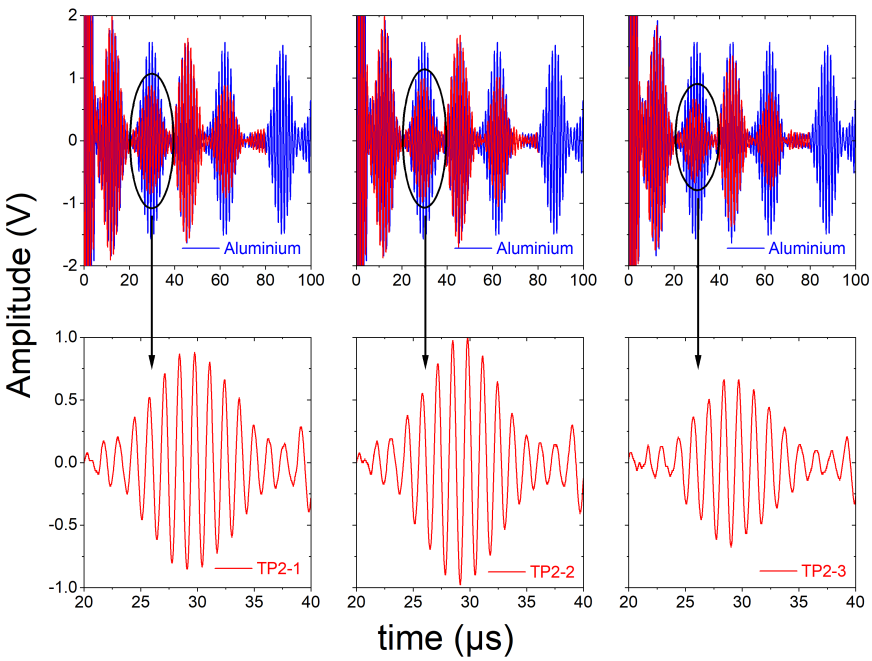

Figure 37. A-scans for TP2 samples. Second wave packet (WP2), which is interacting with the joint is magnified.

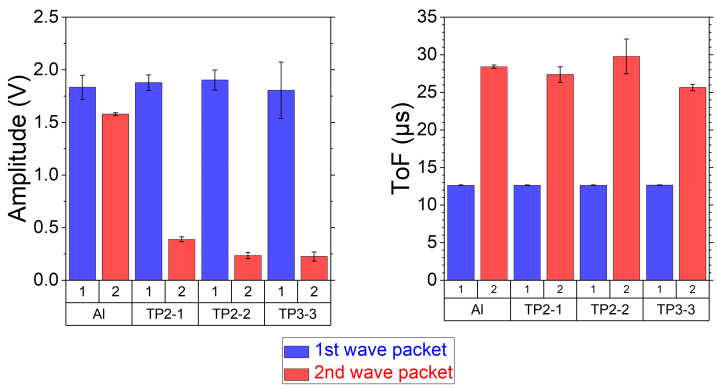

Figure 38. Graphical depiction of mean and standard deviation of ToF and amplitude for TP2 samples and Al-115. The results are averaged from 5 different measurements.

Parameter:	Amplitude (V)				Time of Flight (µs)			
# of Wave Packet:	WP1		WP2		WP1		WP2	
Statistics:	µ	σ	µ	σ	µ	σ	µ	σ
Al-115:	1.835	0.114	1.580	0.014	12.653	0.026	28.426	0.221
TP2-1:	1.959	0.014	0.888	0.029	12.387	0.012	29.597	0.600
TP2-2:	1.975	0.018	0.961	0.029	12.379	0.012	28.635	0.523
TP2-3:	1.880	0.029	0.712	0.034	12.379	0.004	29.168	0.694

Table 7. Mean and standard deviation of ToF and amplitudes for TP2 samples and Al-115. The results are averaged from 5 different measurements

4.1.2.3 TP1 Samples

The A-scans of the TP1 samples along with Al-115 are presented in Figure 39. The wave packets, which are reflected from the bonded edge, can be differentiated, as they are highly damped compared to the Al-115. Unlike the presented hybrid structures beforehand, the shape of the WP2 is not symmetric.

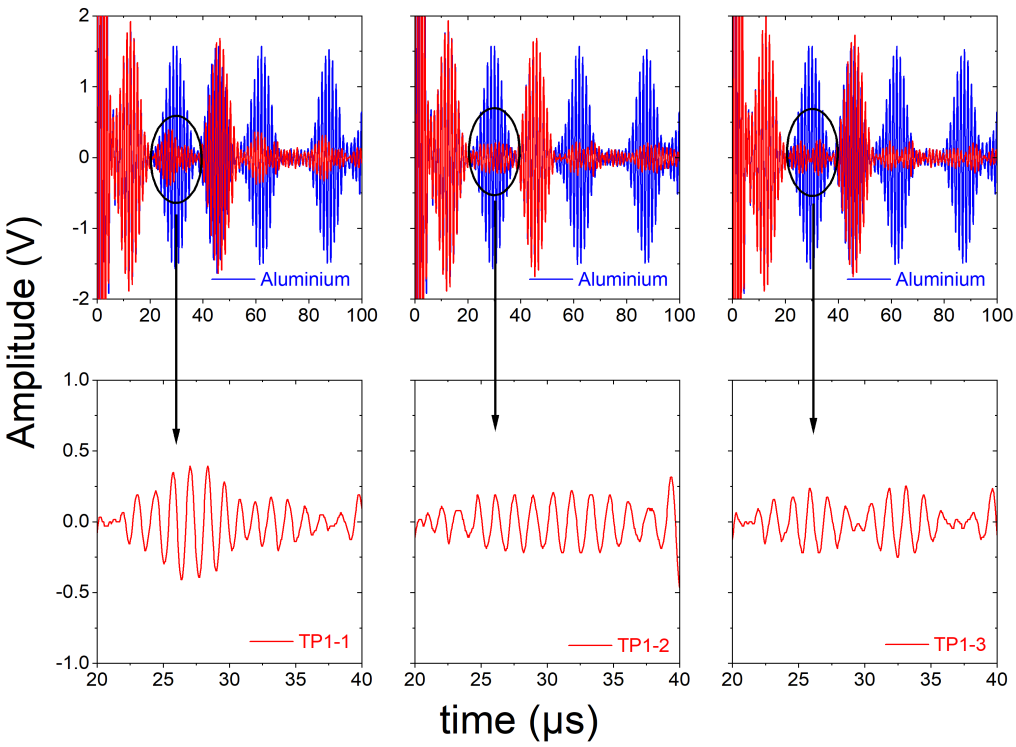

Figure 39. A-scans for TP2 samples. Second wave packet (WP2), which is interacting with the joint is magnified.

The reproducibility results are presented in Table 8 and Figure 40. The ToF and amplitude values of WP1 is captured accurately in all TP1 samples. For WP2, the amplitudes have lower standard deviation, while the ToF exhibits less precision.

Parameter:	Amplitude (V)				Time of Flight (µs)			
# of Wave Packet:	1st Wave Packet		2nd Wave Packet		1st Wave Packet		2nd Wave Packet	
Statistics:	µ	σ	µ	σ	µ	σ	µ	σ
Al-115:	1.835	0.114	1.580	0.014	12.653	0.026	28.426	0.221
TP1-1:	1.879	0.073	0.390	0.023	12.653	0.026	27.389	1.039
TP1-2:	1.904	0.094	0.249	0.032	12.653	0.026	32.102	1.812
TP1-3:	1.807	0.267	0.233	0.038	12.672	0.034	28.848	4.102

Table 8. Mean and standard deviation of ToF and amplitudes for TP1 samples and Al-115. The results are averaged from 5 different measurements

Usually, decrease in the amplitude of the wave packets are attributed to the transmission of the energy in bonded joints; hence, good bonding between adherends [4][14][59][61]. In this case, due to the geometry of the samples, this conclusion might be a misconception. The decrease in amplitude could be due to superposition of the WP2 with additional signal echoed somewhere within the overlap. The shape of the wave packets, which consists of two peaks complies with this assumption. In addition, larger deviations of ToF show that this value is sensitive to the slight changes.

The travelling distance of WP2 is relatively short and the width of the wave packets is rather wide. During the propagation, WP2 can be partially reflected from somewhere in the beginning of the overlap area. Thus, WP2 can be subjected to a destructive interference with the echoed wave packet.

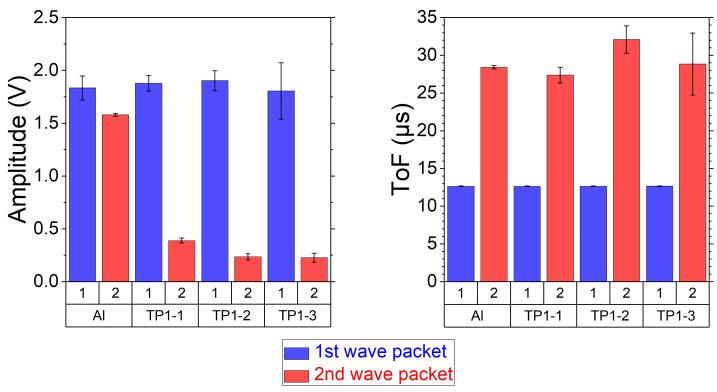

Figure 40. Graphical depiction of mean and standard deviation of ToF and amplitude for TP1 samples and Al-115. The results are averaged from 5 different measurements.

In Figure 41, the normalized amplitude values of WP2 for all sample types are presented. The amplitudes are normalized by dividing to the amplitude of WP1. The hybrid samples with the same material system (TP1 and TP2) have different values. The reason can be

linked to different bonding quality of the samples. Although the TP2 and Ep samples have rather symmetric shape for WP2, the normalized amplitude variation within each sample set can also be a result of the superposition of the waves.

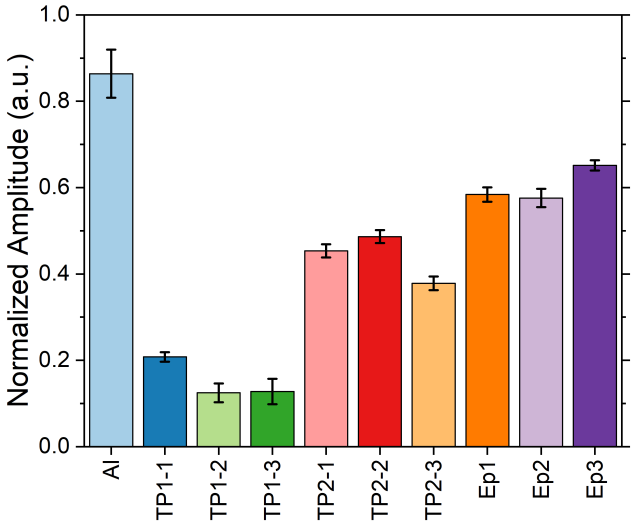

Figure 41. Normalized amplitude values for second wave packets for all test pieces.

4.1.3 TP1-1 Quasi-static Test

In Figure 42, the A-scans for the TP1-1 sample are presented. The Figure 42-c and -d represent the stress free state of TP1-1 and Al-115, while the others represent the TP1-1 sample placed in the universal test machine, just before the mechanical loading and after the failure. As mentioned before, the WP3 reflects from the clamped edge, thus, the amplitude is damped significantly. In addition to damping in the amplitude, also the shift of the wave packet is observed.

Furthermore, the shape of WP2, which is reflected from the bonded edge, has changed as presented in Figure 42-a. When compared to initial state of the TP1-1, the shape of WP2 is more symmetric. After the failure of the sample, WP2 amplitude becomes comparable to the WP1. The overall decrease of the signal amplitude is observed when TP1-1 is placed in the universal test machine. This is associated to the changing contact between the EMATs and the test piece.

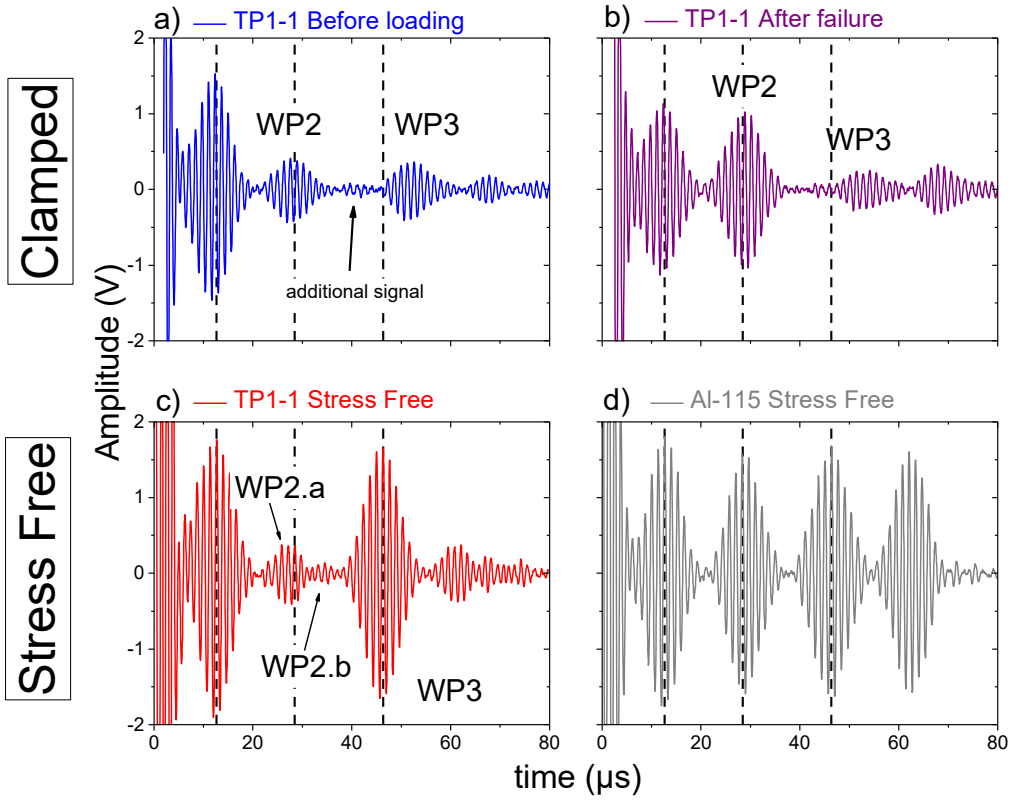

Figure 42. TP1-1 sample and Al-115 A-scans at various states. Reference lines are placed at Al-115 ToF for WP1, WP2, and WP3.

The Figure 43 shows the mechanical data during the course of the quasi-static single lap shear test of TP1-1. The sample failed at approximately 3.1 kN force, which correlates to the adhesive joint strength value of 9.92 MPa. This value is calculated using Eq. (1) as described in the DIN EN 2243-1 standard. The force and displacement behaviour indicates brittle failure.

In Figure 44, the change of ToF and amplitude values are shown during the quasi-static test, where the reference amplitude values are correlated to the mean and standard deviation of TP1-1 at the initial state. The amplitude values for both wave packets exhibit similar changes during the mechanical loading. As it is shown for the Al-200 tensile test results, the stress state of the aluminium has no affect on the amplitude and ToF values. Therefore, the change of the amplitude concerning WP1 can be a result of changing contact between the transducers and the test piece. In order to verify this presumption normalized amplitude values are calculated and compared to the mechanical results (Figure 45).

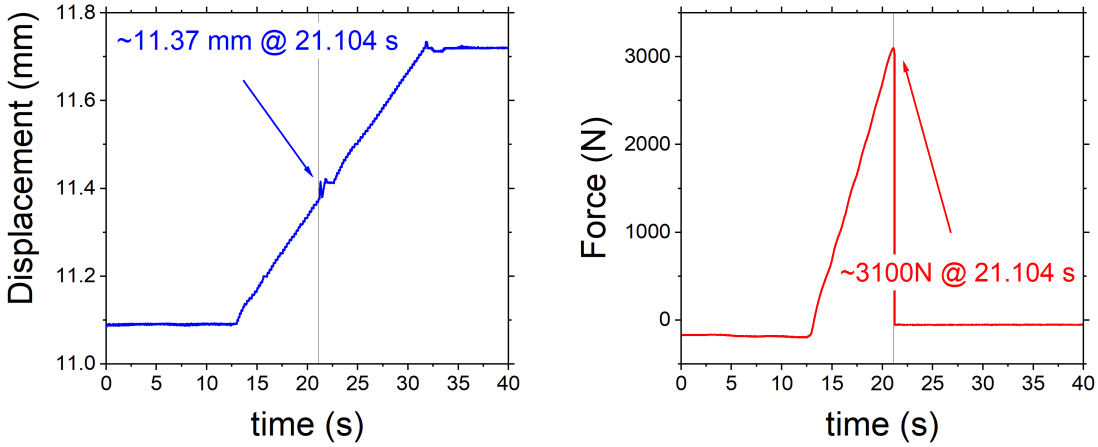

Figure 43. Force and cross-head displacement during the quasi-static test. Test is position controlled with v = 2mm/min.

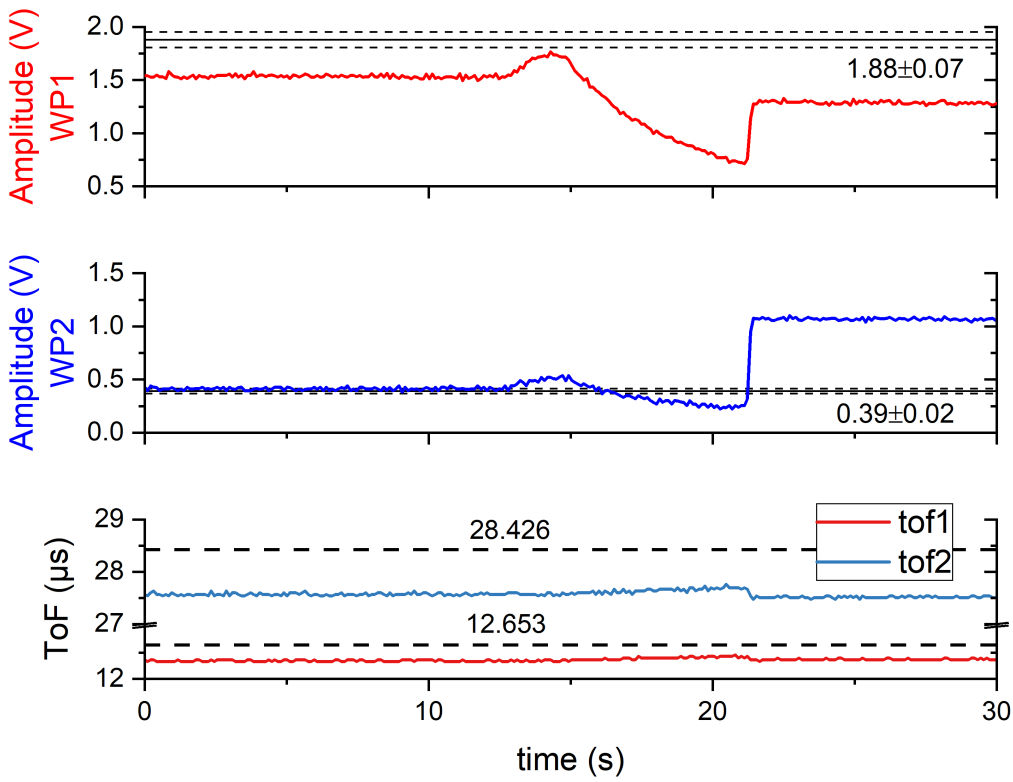

Figure 44: Amplitude and ToF change during the quasi-static test of TP1-1

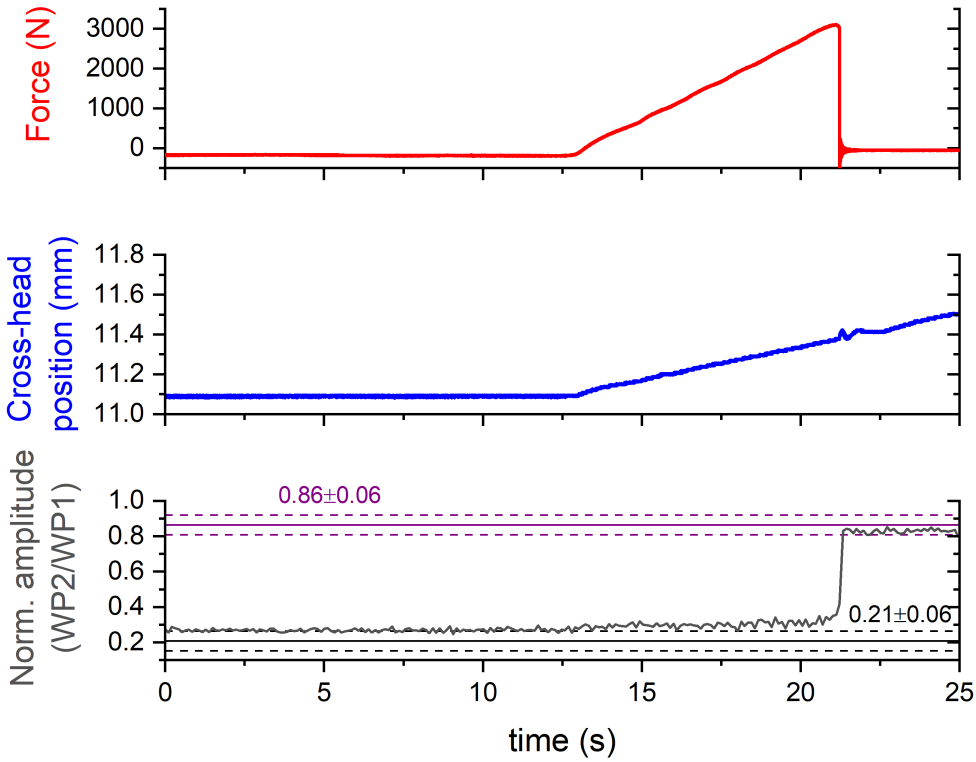

Figure 45. Mechanical data with normalized amplitude for the second wave packet. Reference values indicate the initial state of the TP1-1 (black lines) and the Al-115 (purple line) samples.

As Figure 45 indicates, the normalized amplitude do not exhibit a pronounced change until the failure. At the beginning, the normalized amplitude value is within the normalized amplitude range of TP1-1 initial state. The amplitude value changes abruptly only at the moment of failure. This sudden change of the normalized amplitude complies with the brittle failure of the test piece. Moreover, it can be seen that the normalized value recovers to the normalized amplitude of Al-115 after failure.

4.1.4 TP1-2 Incremental Step Test

In Table 9, the maximum force (F_{max}), mean force (F_m) and force amplitude (F_a) for the incremental step test is presented. Each step is referred by the percentage of the failing load obtained from the TP1-1 quasi-static test. The test parameters and the acquired results show slight variations up to approximately 80 N. This could be due to low sensitivity of the universal test machine to such low force variations.

Test Parameters				Experimental Results			
Steps	F_m (N)	F_a (N)	F_{max} (N)	F_m (N)	F_a (N)	F_{max} (N)	Steps
40%	660	540	1200	593	540	1139	40%
50%	825	675	1500	755	679	1447	50%
60%	990	810	1800	920	811	1740	60%
70%	1155	945	2100	1084	949	2045	70%
80%	1320	1080	2400	1248	1084	2341	80%
90%	1485	1215	2700	1411	1219	2645	90%

Table 9. Mechanical parameters of the incremental step test of TP1-2 test specimen.

An exemplary cyclic load and displacement at the 70% step is presented in Figure 46. Due to low sensitivity, the position curve exhibits small ripples, which results in a time difference between the force and position maxima. In other words, the maximum force is not always associated to the maximum displacement. Therefore, during the displacement calculations, the position acquired at maximum and minimum force was taken into consideration, instead of maximum and minimum of the cyclic displacement.

In Figure 47, the results obtained from the raw data are presented. The maximum displacements increases each step with increasing load, as a result of increased straining. Additionally, within each step there are disruptions, which might be correlated to occurring defects under dynamic load. However, these variations within each step are so small that they can be a result of lower sensitivity of the mechanical systems.

When the variations of stiffness are examined, excluding the 90% step, variations within each step are likely the result of the lower sensitivity of the mechanical systems to small changes. On the other hand, at the 90% step larger variations in the position results in pronounced decrease in stiffness.

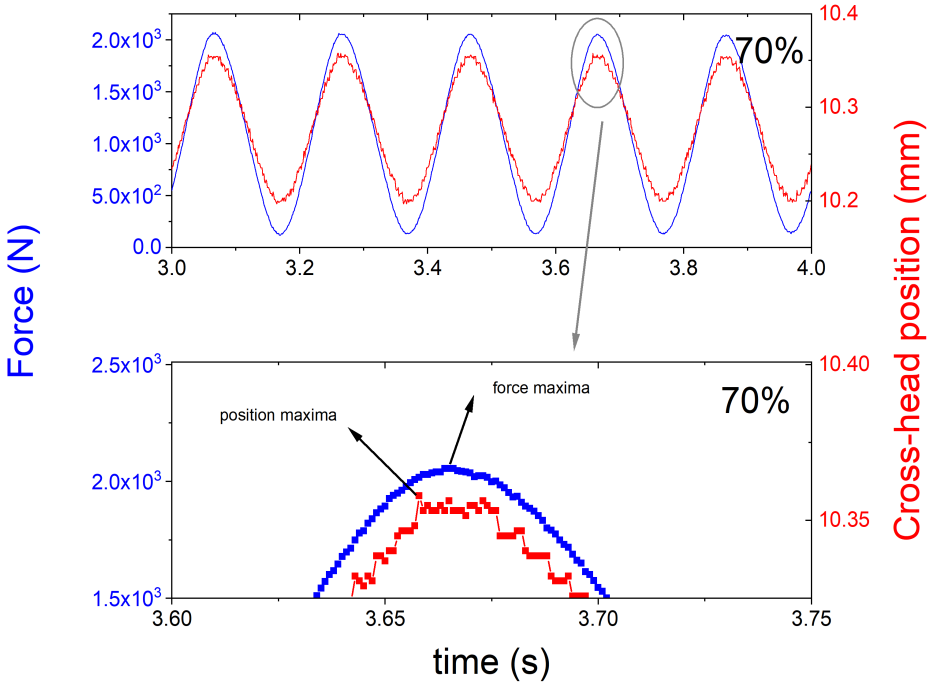

Figure 46. Force and position variation during one second at 70% step.

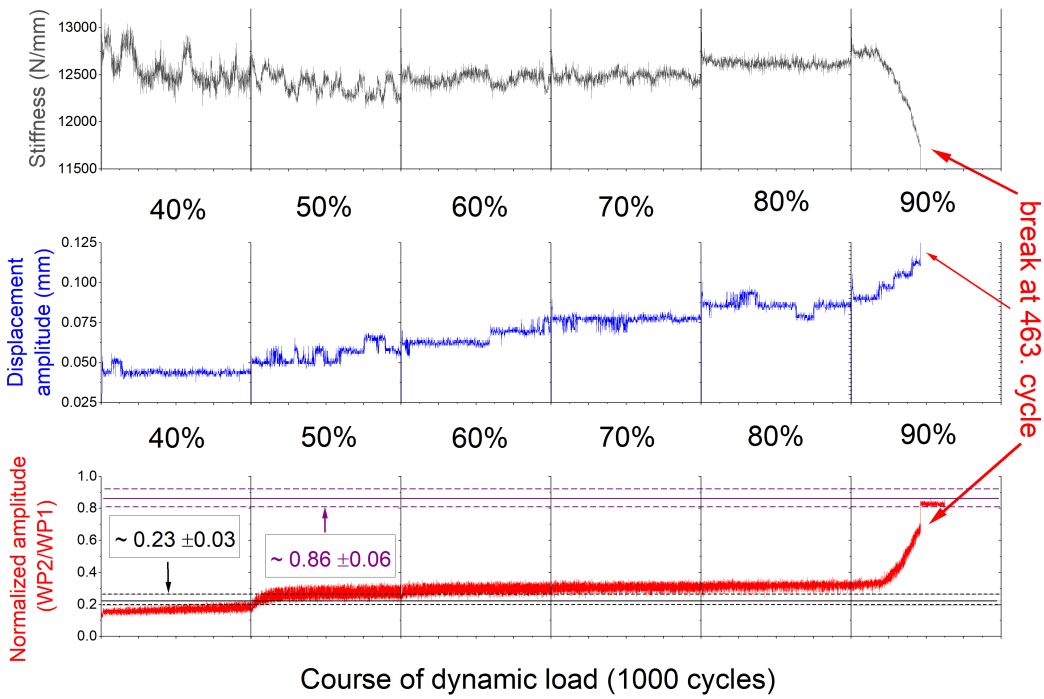

Figure 47. Raw mechanical data of the force controlled incremental step test. Reference lines are given for the initial state of TP1-2 (black lines) and Al-115 (purple lines) test piece.

In Figure 48, the US data obtained during the incremental step test is presented. With increasing F_a, the amplitude of WP1 exhibits an increasing amplitude range, while the amplitude variation for WP2 is less pronounced. It is shown that the amplitude values of the wave packets propagating in aluminium are not affected by the stress-state within the elastic region (see Section 4.1.1.2). Therefore, the increased amplitude range of the WP1 is linked to change of contact between the EMATs and the TP1-2 test sample.

On the other hand, the ToF values of WP1 and WP2 do not exhibit any change. The ToF of WP1 is expected to stay constant, as it is not affected by the stress-state of aluminium and does not interact with the bonded area. In order to elaborate more on ToF of WP2, the normalized A-scans, which are captured at the beginning of each step, are presented in Figure 49.

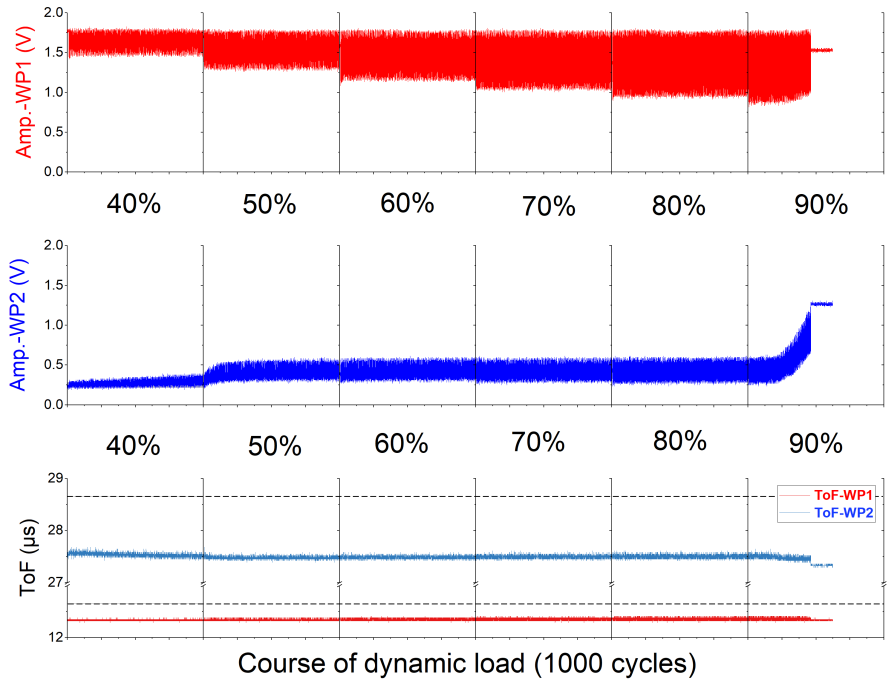

Figure 48. Ultrasonic data during the load incremental step test. (WP1: 1st wave packet, WP2: second wave packet.)

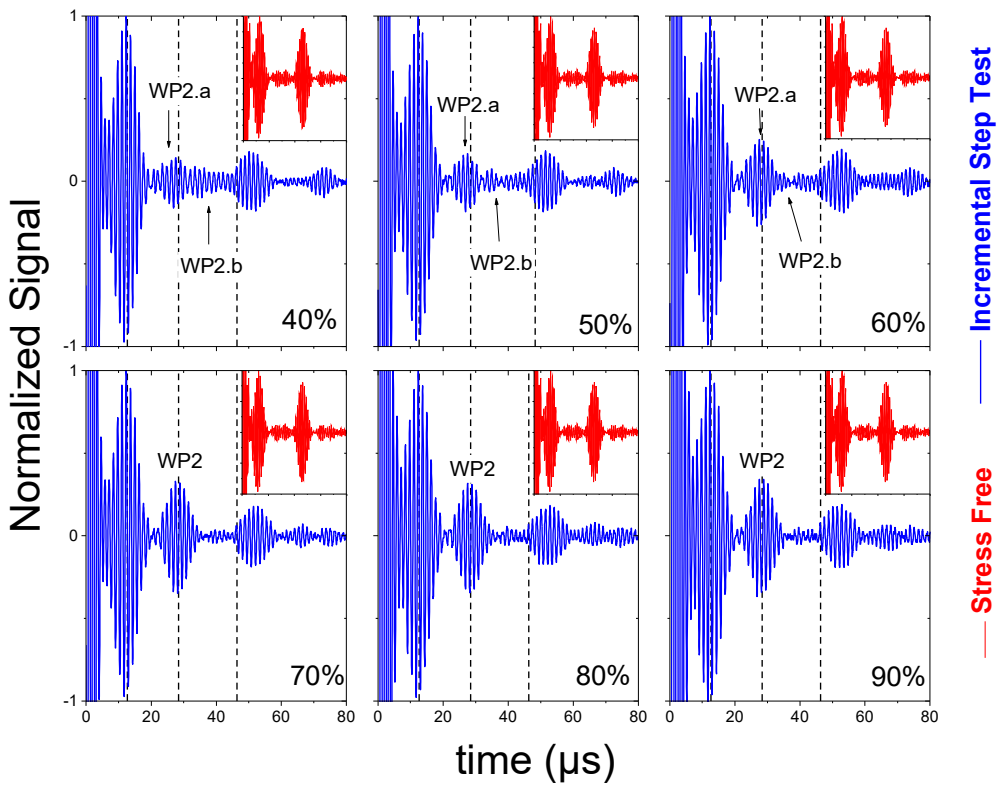

Figure 49. A-scans of TP1-2 at the beginning of each step

As mentioned beforehand in the discussion about the initial state of TP1-2, WP2 consists of two peaks. After a certain point, the shape of WP2 changes and exhibits a single peak. This behaviour can be associated to the changing integrity of the bonded area. As presented in Figure 50, after failure occurs, the shape of WP2 recovers and becomes similar to the WP2 of Al-115.

In Figure 51, the displacement amplitude is presented along with the normalized amplitude and ToF of WP2. The normalized amplitude at the 90% step exhibits a steep change up to failure. This change can be interpreted as an indicator of damage propagation. At the failure event, the normalized amplitude values become equal to the normalized amplitude of WP2 of Al-115.

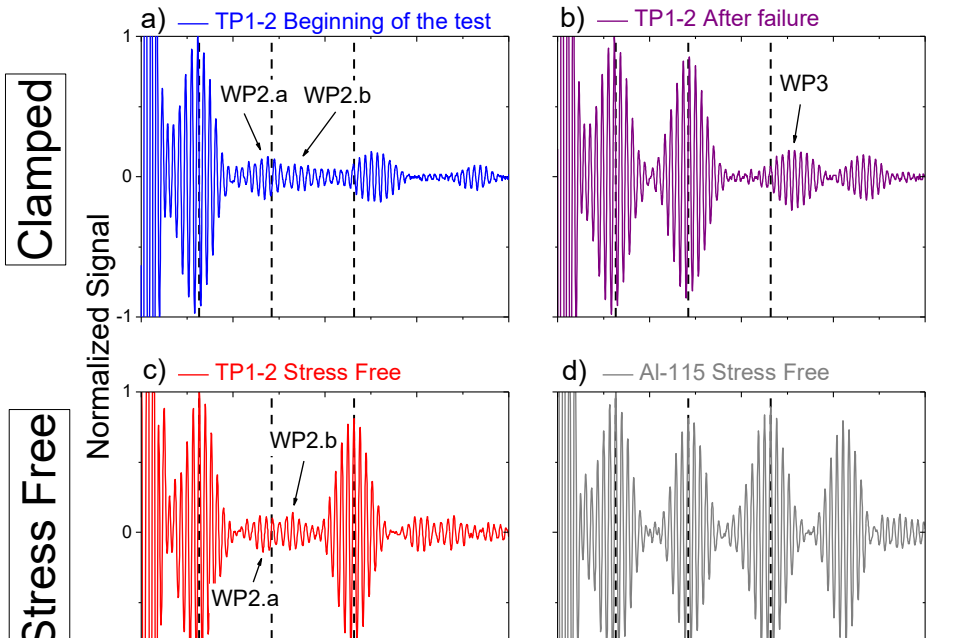

Figure 50. Comparison of A-scans of stress free Al and different states of TP1-2

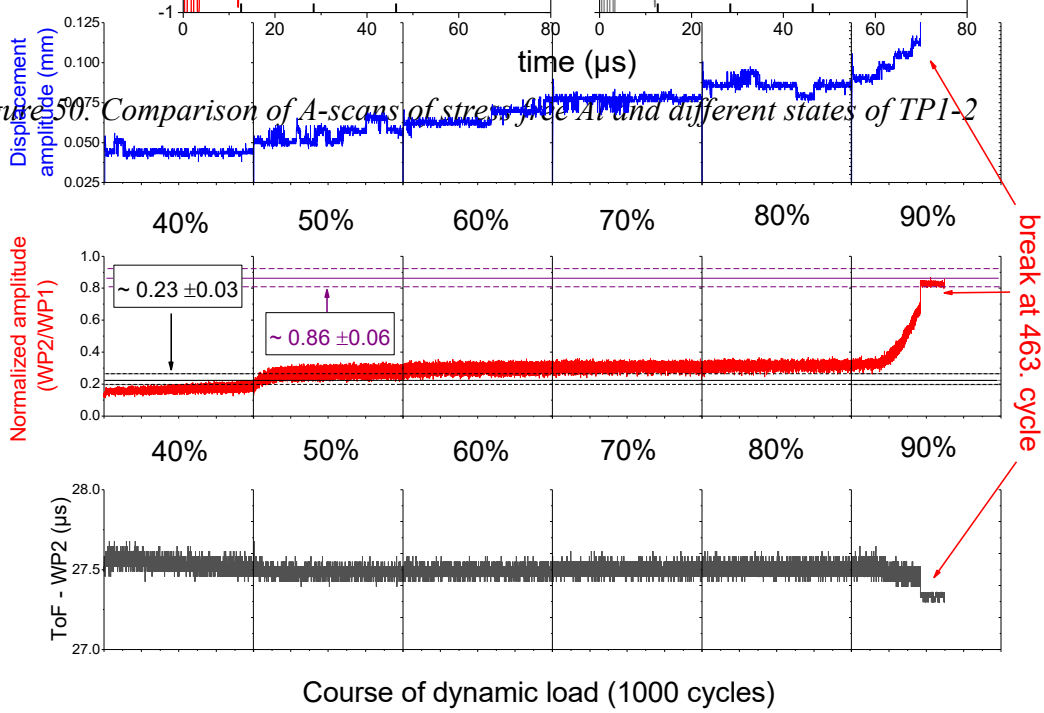

Figure 51. Comparison of displacement amplitude and WP2 ultrasonic properties. Reference lines are given for Al-115 (upper-purple) and TP1-2 initial state (lower-black).

4.1.5 TP1-3 Dynamic Test

The TP1-3 dynamic test was conducted at maximum force, which is correlated to approximately 70% of the failing load obtained from the TP1-1 quasi-static test. In Figure 52, the maximum force, maximum cross-head position and stiffness of each cycle are presented, while in Table 10, the test parameters and experimental results are shown. The maximum force variations are considered to be a result of the low sensitivity of the universal test machine.

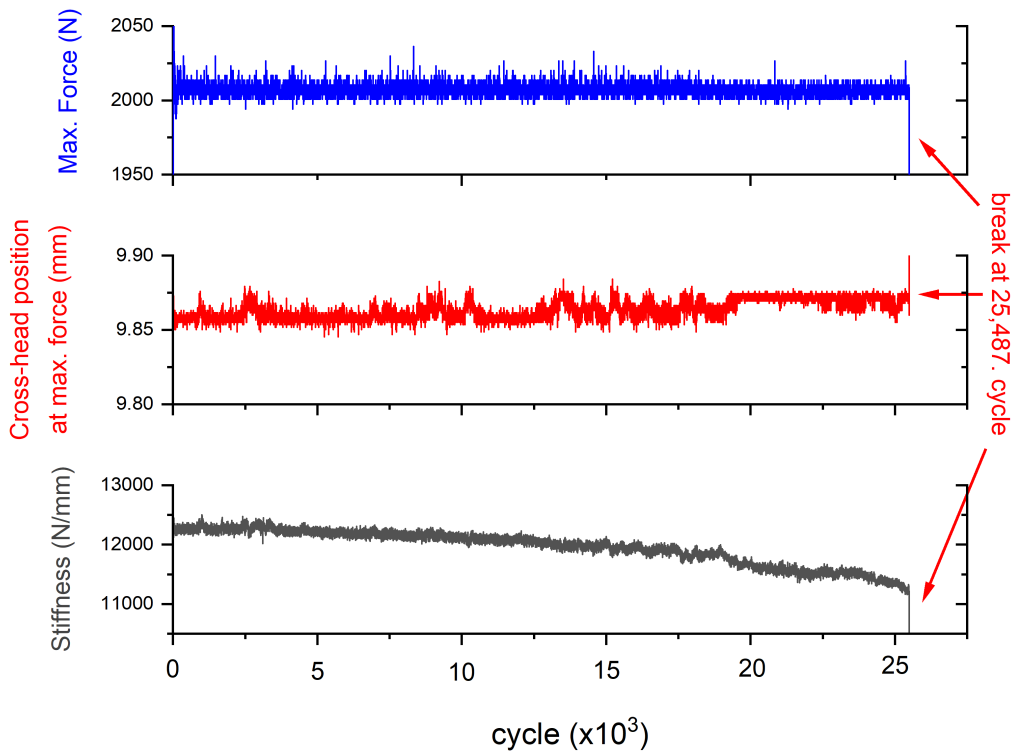

Figure 52. Maximum force, cross-head position and stiffness of TP1-3 during dynamic test.

TP1-3 Dynamic Test			
Steps	F_m (N)	F_a (N)	F_{max} (N)
Exp. Parameters:	1115	945	2060
Exp. Results:	1059	948	2006

Table 10. Comparison of force relations obtained from experimental results for TP1-3 dynamic test.

During the course of the dynamic test, a gradual decrease in stiffness is observed. Although, the maximum position of the cross head does not exhibit a pronounced change, after 20,000 cycle, TP1-3 seem to be more strained under cyclic load.

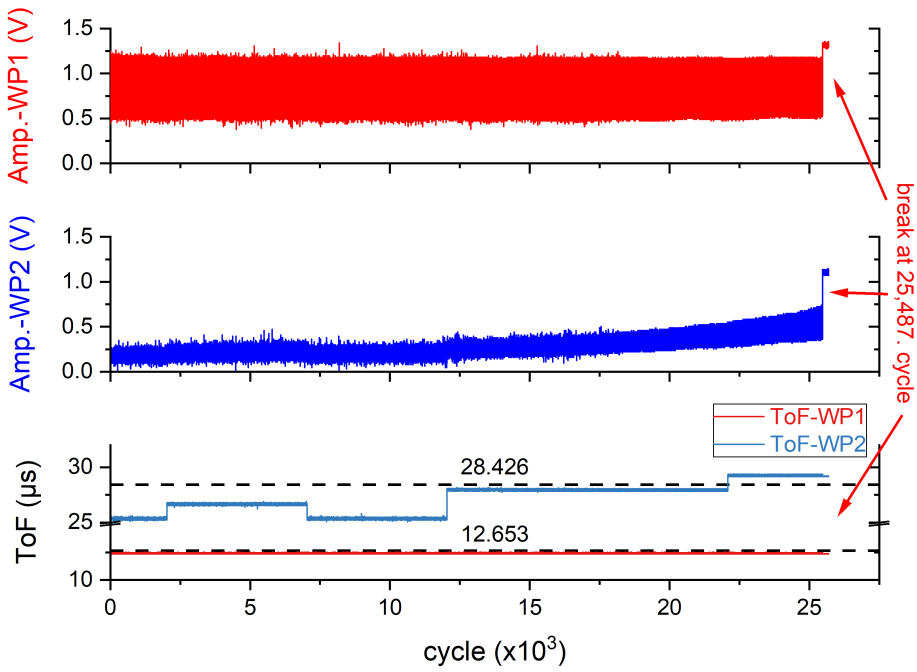

Figure 53. Amplitude and ToF change of WP1 and WP2 during the course of TP1-3 dynamic test.

When the US results are examined, amplitude variations of WP1 are observed, similar to the incremental step test of TP1-2. This is linked to the contact change between the EMATs and test piece during cyclic loading (see Figure 53). On the other hand, a gradual increment in the amplitude of WP2 is observed, starting around the 15,000th cycle. The ToF values of WP1 remain constant throughout the experiment, while a step-wise variation for ToF values of WP2 is observed. In order to explain this variation, the A-scans should be examined first. As illustrated in Figure 55, WP2 has an irregular shape unlike WP1. As mentioned while discussing the initial state of the TP1-3 sample, the standard deviation of the ToF values of WP2 exhibit higher standard deviations compared to the amplitude values. This can be explained by the determination method of ToF and amplitude. When determining the ToF and amplitude values, maxima within a certain region is checked. The global maxima seems to interchange between WP2.a and WP2.b, which results in such a characteristic ToF change for WP2. Yet, an overall increase in ToF of WP2 compared to the begining of the experiment is observed. Also, when the A-scans are examined, after a

certain limit the shape of the waves becomes similar to the shape of WP1. In Figure 55, the ToF change of WP2 is presented with reference lines obtained from the reproducability calculations for the initial state of TP1-3. Although, there is a certain increment in the ToF values during the test, ToF still remains within the standard deviation. On the other hand, the normalized amplitude exhibits a gradual increase while the stiffness decreases. This behaviour can be linked to the damage propagation. Furthermore, the failure event can be clearly detected through a sudden change of amplitude of WP2. This change can be observed in the normalized A-scans (see Figure 56) as well. The shape of WP2 changes right after failure and becomes similar to the shape of Al-115.

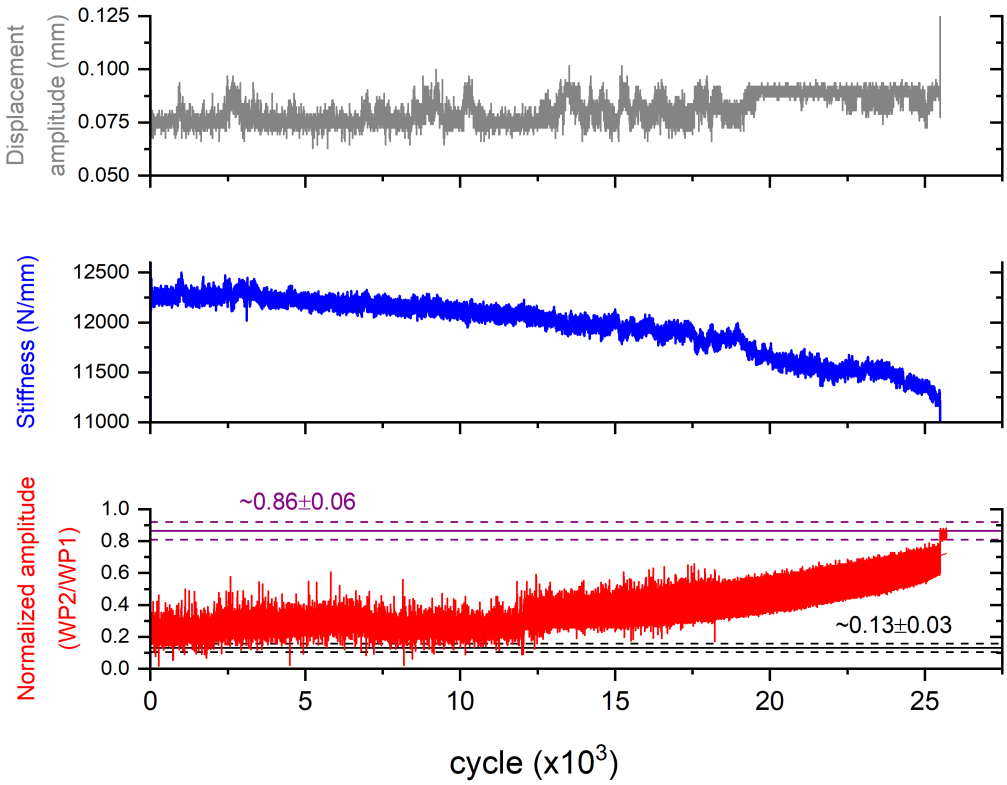

Figure 54. Some mechanical and ultrasonic characteristics during TP1-3 dynamic load.

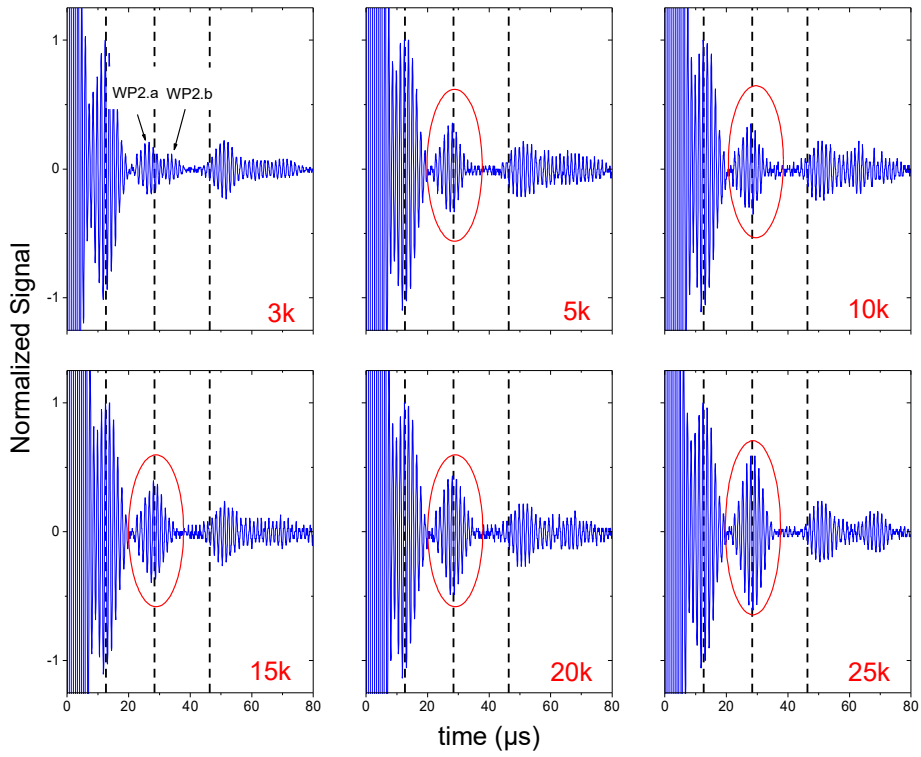

Figure 55. A-scans representing the various cycles throughout TP1-3 dynamic experiment.

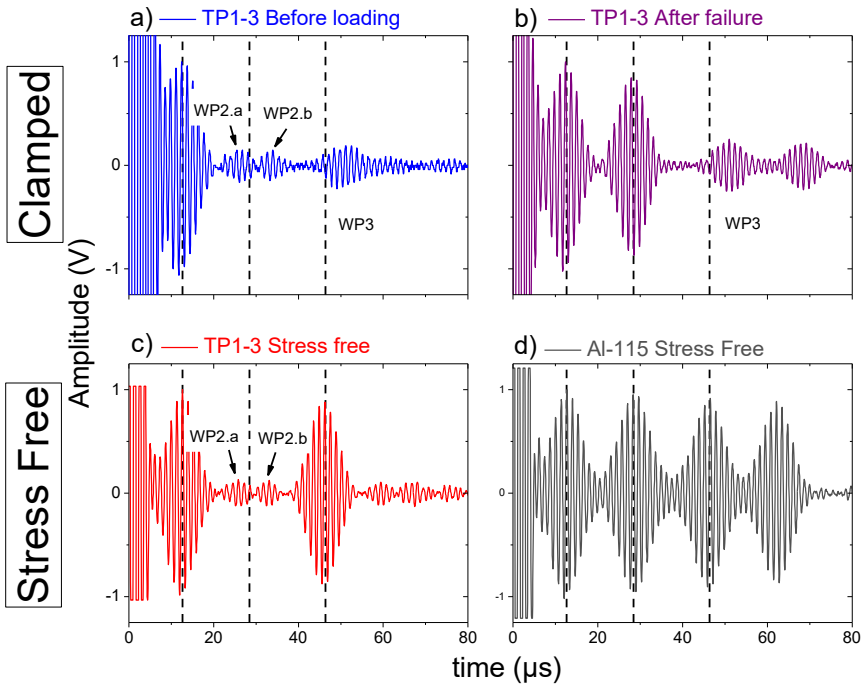

Figure 56. A-scan comparison of TP1-3 and Al-115 at different states. Reference lines represent WP1, WP2, WP3 ToF for Al-115.

5. CONCLUSION & OUTLOOK

The focus of this thesis is to investigate the applicability of the shear horizontal guided wave ultrasonic technique for damage monitoring of a bonded joint in Al-CFRP hybrid structures during the service life. Various literature sources related to this subject were explored and an experimental procedure was realized to fulfill this purpose. The vast majority of the SH wave related literature investigated bonding areas between adherends with similar material. The studies related to bonded hybrid structures mostly focused on the characterization of the existing defects within the joint or the determination of the strength of the joints. So far, research concerning the SH ultrasonic guided wave condition monitoring of the hybrid structures during the cyclic loading has not been conducted.

In this study, first the initial state of joints is investigated by comparing them to reference ultrasonic waveforms. It is shown that the interaction of the wave packets with the bonded area results in changes of the ultrasonic characteristics such as the amplitude and time of flight. This result complies with the previous related literature [7][14]. On the other hand, due to the specific geometry of the investigated hybrid structures, the correlation between the amplitude decrease and the bonding quality couldn't be established. The A-scans of some hybrid samples point in the direction of a possible superposition of wave packets. This could possibly lead to a loss of information for the assessment of amplitude and time of flight due to destructive interference, for similar hybrid structure geometries and transducer system combinations.

During the quasi-static testing, the ultrasonic characteristics of the waveforms only vary within the standard deviation range. At the failure event, an abrupt change in the amplitude value can be observed. This sudden change of the ultrasonic waveform complies with the brittle failure behaviour, which is also supported by the mechanical test results.

The load incremental step test results show that after a certain limit, possible formation of defects within the bonded area causes significant changes in the ultrasonic waveforms. The changes in the amplitude of the wave packets interacting with the bonded area are observed to be closely related to the mechanical changes of the hybrid structure. The change in amplitude can be attributed to the damage propagation in the joint.

The ultrasonic results of the dynamic test also supports the possible relation between the amplitude of the interacting wave packet and the integrity of the bonded area. The

observed gradual change in amplitude of the related wave packet up to failure exhibits similarity to the decrease in stiffness of the joint. This fact could be exploited in future work to predict the failure of the joint.

The amplitude variation of the wave packets that are reflected from the bonded edge are shown to be sensitive to the changes of the bonding in the hybrid structures. This behaviour is expected, as suggested in various literature [15]. However, the ultrasonic changes during the cyclic mechanical loading has not been investigated yet.

Unlike the amplitude analysis, the change in time of flight during mechanical loading cannot be directly correlated to the integrity of the bond. The possible destructive interference caused by the reflections within the bonded area, prevent the accurate detection of the time of flight.

The experiments were conducted on a limited number of samples. Although, it is shown that the amplitude analysis can detect the changes of the bonding integrity after a certain threshold, this should be verified by investigating a broader sample size. By investigating more test specimens under cyclic loading, the possible correlation between the ultrasonic and mechanical behaviour can be confirmed and an empirical model can be realized. Moreover, the life-cycle relations to the ultrasonic characteristics can be explored to predict failure of the bonded hybrid structures.

In conclusion, the shear horizontal guided ultrasonic waves are shown to be suitable for the damage monitoring of hybrid structures. The failure event of the bonded hybrid structures can be detected through the relative change in amplitude of the wave packet interacting with the joint. Furthermore, this behaviour has the potential to be used in predicting the failure of the bonded joint in hybrid structures.

Bibliography

1: S. Yang, L. gu, R. F. Gibson, "Nondestructive detection of weak joints in adhesively bonded composite structures", *Composite Structures*, vol. 51, pp. 63-71, 2001
2: B. Ehrhart, B. Valeske, C. Bockenheimer, "Non-destructive evaluation (NDE) of aerospace composites: methods for testing adhesively bonded composites" in *Non-Destructive Evaluation (NDE) of Polymer Matrix Composites*, Woodhead Publishing Ltd., 2013
3: A. Praminik et al., "Joining of carbon fibre reinforced polymer (CFRP) composites and aluminium alloys – A review", *Composites Part A: Applied Science and Manufacturing*, vol. 101, pp. 1-29, 2017
4: M. Schwarz, J. Summa, S. Quirin, H. G. Herrmann, "New Approaches in Nondestructive Characterisation of Defects in Metal - CFRP Hybrids", *Materials Science Forum*, vol. 825-826, pp. 976-982, 2015
5: T.E.A. Riberio, R.D.S.G. Campilho, L.F.M. da Silva, L. Goglio, "Damage analysis of composite–aluminium adhesively-bonded single-lap joints", *Composite Structures*, vol. 136, pp. 25-33, 2016
6: J.C. Berg, "Semi-empirical strategies for predicting adhesion" in *Adhesion Science and Engineering*, : Elsevier Science B. V., 2002
7: M. Castaings, "SH ultrasonic guided waves for the evaluation of interfacial adhesion", *Ultrasonics*, vol. 54, pp. 1760-1775, 2014
8: B. Le Crom, M. Castaings, "Shear horizontal guided wave modes to infer the shear stiffness of adhesive bond layers", *The Journal of the Acoustical Society of America*, vol. 127, pp. 2220-2230, 2010
9: X. He, "A review of finite element analysis of adhesively bonded joints", *International Journal of Adhesion and Adhesives*, vol. 31, pp. 248-264, 2011
10: P.Cawley, C.C.H. Guyott, "Non-destructive Inspection of Adhesively Bonded Joints", *The Journal of Adhesion*, vol. 21, pp. 279-290, 1987
11: J. Ding, B. Wu, C. He, "Reflection and transmission coefficients of the SH0 mode in the adhesive structures with imperfect interface", *Ultrasonics*, vol. 70, pp. 248-257, 2016
12: M. Bruneau, C. Potel, "Materials and Acoustics Handbook", London, ISTE ltd., 2009
13: M. S. Choi, S. J. Kim, *Reflection and transmission of normal incidence SH0 waves at a lap joint*: Proceedings of the Korean Society for Nondestructive Testing Spring Meeting 2006, 2006
14: K. Arun et al., *An EMAT Based Shear Horizontal (SH) Wave Technique for Adhesive Bond Inspection*: AIP Conference Proceedings, 2012
15: P. Peres, et al., *New experimental investigations of adhesive bonds with ultrasonic SH guided waves*: 18th International Conference on Composite Materials, 2011
16: S. Wang, Z. Li, P. Li, X. Liu, G. Zhai, "Numerical and experimental evaluation of the receiving performance of meander-line coil EMATs", *Nondestructive Testing and Evaluation*, vol. 29, pp. , 2014
17: T. L. Yogesh, N.Arunkumar, "Failure Mode and Analysis of the Bonded/bolted Joints between a Hybrid Fibre Reinforced Polymer and Aluminium Alloy", *Journal of Advanced Materials and Processing*, vol. 3, pp. 49-60, 2015
18: L. F. M. da Silva, A. Öchsner, R. D. Adams, "Introduction to Adhesive Bonding Technology" in *Handbook of Adhesive Techonlogy*, Berlin Heidelberg: Springer-Verlag, 2011
19: B. Ehrhart, B. Valeske, C. Bockenheimer, "Non-destructive evaluation (NDE) of aerospace composites: methods for testing adhesively bonded composites" in *Non-Destructive Evaluation*

20: G. Habenicht, " Applied adhesive bonding: a practical guide for flawless results", Weinheim, Wiley-VCH, 2009
21: L. F. M. da Silva, "Design Rules and Methods to Improve Joint Strength" in *Handbook of Adhesive Techonlogy*, Berlin Heidelberg: Springer-Verlag, 2011,
22: L. J. Hart-Smith, "Adhesively Bonded Joints in Aircraft Structures" in *Handbook of Adhesive Techonlogy*, Berlin Heidelberg: Springer-Verlag, 2011
23: D. E. Peckham, Theories of Fundamental Adhesion,
24: Ehrhart, B., et al, "Methods for the quality assessment of adhesive bonded CFRP structures-A resume" in " NDE of Polymer Matrix Composites", Woodhead Publishing, 2013
25: R. D. Adams, Nondestructive Testing, 2011
26: K. C. Shin, J. O. Lim, J. J. Lee, "The manufacturing process of co-cured single and double lap joints and evaluation of the load bearing capacities of co-cured joints", *Journal of Materials Processing Technology*, vol. 138 , 2003
27: N. Rajic, "NDE of aerospace composites: flaw characterization" in *Non-Destructive Evaluation (NDE) of Polymer Matrix Composites*, : Woodhead Publishing Ltd.
28: John Comyn, "Adhesion Science", vol. 101, pp. 1-17, 1997
29: L. F. M. da Silva, "Failure Strength Tests" in *Handbook of Adhesive Techonlogy*, Berlin Heidelberg: Springer-Verlag, 2011
30: L. Tong, Q. Luo, "Analytical Approach to Joint Design" in *Handbook of Adhesive Techonlogy*, Berlin Heidelberg: Springer-Verlag, 2011
31: N. Stein, J. Felger, W. Becker, "Analytical model for functionally graded adhesive single lap joints: A comparative study", , vol. , 2017
32: S. Ebnesajjad, Surface Treatment of Materials for Adhesive Bonding, Elsevier Inc., 2014
33: A. Streitferdt, N. Rudolph, I. Taha, "Co-curing of CFRP-Steel Hbrid Joints Using the Vacuum Assisted Resin Infusion Process" , 2017
34: Han-Gi Son et. al, "Fatigue behaviour of metal pin-reinforced composite single-lap joints in a hygrothermal environment", *Composite Structures* , vol. 108, pp. , 2014
35: S. Budhe, A. Ghumatkar, N. Birajdar, M. D. Benea, Effect of surface roughness using different adherend materials on the adhesive bond strength, 2015
36: K. Leena, et. al, "Effect of surface pre-treatment on surface characteristics and adhesive bond strength of aluminium alloy", *International Journal of Adhesion & Adhesives*, vol. 70,2016
37: G. Lucchetta, F. Marinello, P.F. Bariani, "Aluminum sheet surface roughness correlation with adhesion in polymer metal hybrid overmolding", 2011
38: R. P Chumble, D. H. Darekar, "Influence of Surface Roughness of Adherend on Strength of Adhesive Joint", *International Journal of Engineering Development and Research*, vol. , 2017
39: T. Kleffel, D. Drummer, "Investigating the suitability of roughness parameters to assess the bond strength of polymer-hybrid structures with mechanical adhesion", *Composites* , vol. 117, 2017
40: M. H. Khan, et al., "Effect of oxidation and szrfcae roughness on the shear strength of single-lap-joint adhesively bonded metal specimens by tension loading", *Applied Adhesion Science*, vol. 4:21, pp. , 2016
41: A. F. Harris, A. Beevers, "The effects of grit-blasting on surface properties for adhesion", *International Journal of Adhesion & Adhesives*, vol. 19, 1999
42: Y. Boutar, et al., "Effect of surface treatment on the shear strength of aluminium adhesive single-lap joints for autootive applications", *International Journal of Adhesion & Adhesives*, vol. 67, 2016

43: A. Rudawska, et. al, "The effect of sanblasting on surface properties for the adhesion", *International Journal of Adhesion & Adhesives*, vol. 70, 2016
44: G. W. Critchlow, D. M. Brewis, "Review of Surface Pretreatments for Aluminium Alloys", *Int. J. Adhesion and Adhesives*, vol. 16,1996
45: S. G. Prolono, A. Urena, "Effect of surface pre-treatment on the adhesive strength of epoxy-aluminium joints", *International Journal of Adhesion & Adhesives*, vol. 29, 2009
46: K. -T. Hsiao, D. Heider, "Vacuum assisted resin transfer moulding (VARTM) in polymer matrix composites" in *Manufacturing Techniques for Polymer Matrix Composites (PMCs)*, : Woodhead Publishing Ltd.,
47: C. J. Hellier, "Handbook of Nondestructive Evaluation", Lightning Source UK Ltd., 2017
48: Balageas, D., "Introduction to Structural Health Monitoring", 2006
49: M. Veidt, C. K. Liew, "NDE of aerospace composites: structural health monitoring of aerospace structures using guided wave ultrasonics" in " NDE of Polymer Matrix Composites", Woodhead Publishing, 2013
50: L. W. Schmerr Jr. , "Fundamental Models and Measurements for Ultrasonic Nondestructive Evaluation Systems" in " Ultrasonic and Advanced Methods for Nondestrutive Characterization", World Scientific, 2007
51: Joseph L. Rose, Ultrasonic Waves in Solid Media, Cambridge University Press, 1999
52: , Materials and Acoustics Handbook, STE Ltd., 2009
53: K. J. Langenberg, R. Marklein, K. Mayer, Theoretische Grundlagen der zerstörungfreien Materialprüfung mit Ultraschall, Oldenburg Verlag München, 2009
54: M. Hirao, O. Hirotsugu, EMATs for science and industry, Springer, 2011
55: Z. Su, L. Ye, Identification of Damage Using Lamb Waves, , Springer, 2009
56: H. Sohn, S. B. Kim, S. D. Kim, "Guided wave based nondestructive testing: A reference-free pattern recognition approach", , vol. , pp. , 2007
57:R. D. Adams, P. Cawley, C. C. H. Giyott, "Non-destructive Inspection of Adhesively Bonded Joints", *The Journal of Adhesion*, vol. 21:3-4, pp. , 1987
58: R.D. Adams, B. W. Drinkwater, "Nondestrcutive testing of adheisvely- bonded joints", *NDT&E International*, vol. 2, pp. , 1997
59: S. Quirin, S. Neuhaus, H. G. Herrmann, "Testing ultrasonic SH waves to estimate the quality of adhesive bonds in small hybrid structures", , vol. , pp. , 2016
60: H. G. Herrmann, M. Schwarz, J. Summa, *New Approaches in Nondestructive Characterisation of the Interface in Metal-CFRP Hybrid Structures*: 19th World Conference on Non-Destructive Testing 2016, 2016
61: M. Schwarz, M. Schwarz, S. Herter, H. G. Herrmann, Nondestructive testing of a Complex Aluminium-CFRP Hybrid Structure with EMAT and Thermography, 2019
62: J. Moysan, et al., *Innovating for Structural Adhesive Bonding Evaluation and Analysis with Ultrasounds: A Summary*: 19th World COnference on NonDestructive Testing , 2016
63: S. Neuhaus, "Geführte SH-Ultraschallwellen an mit Polymeren gefügten Blechen", 2015
64: Federation of European Producers of Abrasives-Grit Sizes
65: S. Dixon, C. Edwards, S. B. Palmer, The analysis of adhesive bonds using electromagnetic acoustic transducers, 1994
66: G Hübschen, "Ultrasonic Techniques for materials characterization" in *Metarial Characterization Using Nondestructive Evaluation Methods*, : Elsevier, 2016, pp.
67: R. Murayama, "Non-Contact Stress Measurement during Tensile Testing Using an Emat for SH0-Plate Wave and Lamb Wave", , vol. , pp. , 2011

APPENDIX A DATA SHEETS FOR THE RESINS

ELIUM® 150

Technical Datasheet

LIQUID THERMOPLASTIC RESIN FOR CARBON-REINFORCED COMPOSITE

The **ELIUM® 150** is a low viscosity liquid, thermoplastic resin for **infusion** and **RTM** processes.
Through the use of the same low pressure processes and equipments used today to produce thermoset composite parts, these formulations lead to the production of thermoplastic composites reinforced by continuous glass, carbon or natural fibers. The resulting thermoplastic composite parts show mechanical properties similar to those of parts made of epoxy resins while presenting the major advantages of being post-thermoformable and recyclable and of offering new possibilities for composite/composite or composite/metal assemblies.

APPLICATIONS AND USE

ELIUM® 150 resin can be used to fabricate aesthetic or structural composites reinforced by glass, carbon, or other continuous fibers.
This resin can be used for RTM (Resin Transfer Molding), VARI (Vacuum Assisted Resin Infusion) and other closed mold processes.

TYPICAL LIQUID RESIN PROPERTIES

Property(1) at 25 °C	
Viscosity Brookfield LVF #2, 60 rpm	100 mPa.s

(1) Properties are typical values based on material tested in our laboratories. Typical values should not be construed as a guaranteed analysis of any specific lot or as specification items.

TYPICAL CURING CHARACTERISTICS

The **ELIUM®** resins are 2K based formulations that undergo radical polymerization to produce thermoplastic composite matrices. The polymerization is initiated by Peroxide compounds. Typical open time and peak time with 2,4% of water-free BPO at 50% active content are:

Reactivity(2) (200 grams)	Infusion open time	Injection open time	Peak time
15 °C	30 min.	35 min.	50 min.
20 °C	25 min.	30 min.	40 min.
25 °C	20 min.	25 min.	33 min.

(2) If a lower reactivity infusion resin is needed, we recommend to use the Elium® 180. Please contact your Arkema representative for more information.

The demolding can take place 5-10 minutes after reaching the peak exotherm.
Open time is the amount of time during which the viscosity of the resin is low enough to inject the resin. Temperature and peroxide ratio will affect the open and peak times. The recommended peroxide ratio is from 1,5% (slow reactivity) to 3% (higher reactivity). Out of this range the resin will not polymerize properly.
Room temperature polymerization leads to high conversion rate, so post-curing is generally not needed. If maximum mechanical properties are desired, post-curing at 80 °C for 4 hours is beneficial. Vinyl ester or epoxy molds with a glass transition of 100-120 °C are recommended.

ELIUM® BY ARKEMA

ELIUM® 150

INFUSION PROCESSING	Processing by infusion can be carried out at a vacuum ranging from 100 mbar to 500 mbar, due to the good fiber impregnation behavior of the resin. Before introducing the peroxide into the resin, firmly close the container and shake vigorously. If using Luperox® AFR40, skip the shaking step. Resin and peroxide must be mixed carefully for two minutes, to reach a homogeneous color and no particles, especially at the bottom and on the sides of the mixing pot. It is recommended to position a perforated plastic film or a cap on top of the pot during infusion, to reduce the smell in the workshop and prevent curing inhibition caused by air. The low viscosity of Elium® 150 allows a quick and complete fiber wetting with infusion distance up to 500 mm. Processing by infusion can be carried out at a vacuum pressure ranging from 100 mbar to 500 mbar, due to the good fiber impregnation behavior of the resin. The flow mesh length and break length between the resin inlet(s) and vacuum tube(s) have to be dimensioned to allow a full impregnation of the laminate in 10-15 minutes at 25 °C, with an additional 5-10 cm of break material before the vacuum tube, to avoid resin entering into the vacuum tubes. Following impregnation speeds can be used to dimension flow mesh and brake lengths: - resin impregnation speed into a laminate with flow mesh: 10 cm/min on average (15 cm for the first minute) - resin impregnation speed into a laminate without flow mesh: 1 cm/min in average The remaining resin in the pot will generally foaming and change color during the peak exotherm. If this resin is be used in combination with a pump system (for mixing and/or infusing), the machine has to be cleaned daily with acetone for the resin circuit and with water for the peroxide circuit.
INJECTION PROCESSING	Light RTM processing of Elium® 150 can be done under similar conditions than standard polyester resins. Specific injection machines are required to pump the Luperox® EZ FLO, so standard machines designed for MEKP should not be used. Contact your representative to have the details on the machine type. The machine has to be cleaned daily with acetone for the resin circuit and with water for the peroxide circuit.
TYPICAL MECHANICAL PROPERTIES	

Properties of a 4 mm unfilled resin casting	Value	ISO method
Rockwell Hardness (M)	100	2039
Shore D Hardness	85-90	868
Tensile Strength	76 MPa	527
Tensile Modulus	3.300 MPa	527
Tensile Deformation	6 %	527
Flexural Strength	130 MPa	178
Flexural Modulus	3.250 MPa	178
Compression Strength	130 MPa	684
Specific Gravity	1,19	1183
Heat Deflection Temperature	109 °C	75/A
Maximum Continuous Temperature Service	85 °C	-
Water Uptake (8 days)	0,5%	62
Coefficient of Linear Expansion	0,065 mm/m/°C	2155-1
Fracture Toughness Stress Intensity, K_{Ic}	1,2 MPa.m$^{0.5}$	13586

Properties of a carbon UD reinforced part(3)	Value	ISO method
Tensile Strength (0°)	2.350 MPa	527
Tensile Modulus (0°)	125 GPa	527
Strain at break	1,8%	527

Arkema
89 boulevard National
F-92257 La Garenne-Colombes Cedex – France
Tel.: +33 (0)1 78 66 23 00
Fax: +33 (0)1 78 66 23 97
elium-composites.com

ARKEMA
INNOVATIVE CHEMISTRY

ELIUM® 150

Tensile Strength (90°)	59 MPa	527
Tensile Modulus (90°)	8 GPa	527
Interfacial Stress	59 MPa	527
Tg after wet ageing (90°C, 90%RH, 7 days)	90-95 °C	int.
Tg-peak (tan δ)	120-125 °C	int.

Properties of a carbon NCF reinforced part(4)	Value	ISO method
Tensile Strength	1.280 MPa	527
Tensile Modulus	59 GPa	527
Tensile Strength +/- 45°	118 MPa	527
Tensile Modulus +/- 45°	3,6 GPa	527
Flexural Strength	870 MPa	14125
Flexural Modulus	65 GPa	14125
Compressive Strength	480 MPa	14126
Compressive Modulus	54 GPa	14126

(3) Molded with a UD carbon fabric from T700SC 12K fiber, fiber volume content: 60%
(4) Molded with a NCF 0-90° carbon fabric from T700SC 12K fiber, fiber volume content: 53%

THERMOFORMING

Fiber-reinforced Elium® parts can be thermoformed with heat and pressure. The use of a water-free peroxide for the Elium® polymerization is recommended when composite parts need to be thermoformed. This process requires the heating of the consolidated part at 180-200 °C for a few minutes, and the compression at a pressure between 5 and 20 bars depending on the reinforcement type and the thickness of the part.

ADHESIVE ASSEMBLY

Fiber-reinforced composites made with **ELIUM®** resins can be assembled with adhesives. The **SAF® 30** adhesive, from AEC Polymers, is recommended for structural bonding. A cohesive rupture is obtained with tensile lap shear strength at 17,5 MPa, according to the EN-1465. This adhesive is also recommended to bond metals, with lap-shear strength ranging from 18 to 21 MPa (aluminum 1050A, 6060 and 6061, stainless steel, steel).

CERTIFICATES and APPROVALS

The manufacturing, quality control and distribution of products, by Altuglas International, comply with one or more of the following programs or standard: Responsible care, ISO9001, ISO14001, ISO/TS16949, OSHAS18001.

STANDARD PACKAGES

These resins are supplied in non-returnable drums with net weight of 200 kg.

STORAGE

The shelf life of the resin in original sealed container is 6 months at a temperature not higher than 25 °C.

For further information we advise you to read carefully the current Safety Data Sheet.

ARKEMA Société anonyme au capital de 630 296 520 euros – 445 074 558 RCS Nanterre
- Dircom 01/02/2013 – Dircom - Crédits photos : Arkema, MVC C

Arkema
89 boulevard National
F-92257 La Garenne-Colombes Cedex – France
Tel.: +33 (0)1 78 66 23 00
Fax: +33 (0)1 78 66 23 97
elium-composites.com

ARKEMA INNOVATIVE CHEMISTRY

ELIUM® 150

See MSDS for Health & Safety Considerations

Date: May 2015

ARKEMA Société anonyme au capital de 630 296 920 euros - 445 074 685 RCS Nanterre
- Dircom 01/02/2013 – Dircom - Crédits photos : Arkema, MVC C

Arkema
89 boulevard National
F-92257 La Garenne-Colombes Cedex – France
Tel.: +33 (0)1 78 66 23 00
Fax: +33 (0)1 78 66 23 97
elium-composites.com

ARKEMA
INNOVATIVE CHEMISTRY

Epoxi-System HP-E3000GL

- Härter HP-E15GL / HP-E200GL / HP-E300GL -

Basis der Serie **HP-E3000GL** bildet ein ungefülltes Epoxidharz, welches mit unterschiedlichen Härtern individuell für den jeweiligen Verwendungszweck eingestellt werden kann.

Ein besonderes Merkmal des Systems ist der hohe Anfangs-Tg bei Härtung unter Raumtemperatur.

Die Verwendung des Härters **HP-E200GL** erhöht die maximale Glasübergangstemperatur (Tg MAX) auf 107°C. Gleichzeitig besitzt dieses System eine hohe Transparenz, sodass es sich besonders für Sichtcarbon-Bauteile eignet.

Das gesamte System besitzt eine Zulassung vom Germanischen Lloyd für den Bau von Booten und Windkraftanlagen.
(Approval No.: WP 1320014 HH, gültig bis 31.08.2016)

Eigenschaften:

- sehr niedrige Viskosität, dadurch sehr gute Tränkungseigenschaften
- Topfzeiten zwischen 15 (Härter **HP-E15GL**) und 300 Minuten (Härter **HP-E300GL**) frei einstellbar
- Glasübergangstemperaturen (Tg MAX) bis 107 °C (Härter **HP-E200GL**)
- hohe statische und dynamische Festigkeiten

Einsatzgebiete:

- Vakuuminfusionsverfahren (IMC/MTI, RI, VARI, SCRIMP®,…)
- Druckinjektionsverfahren (RTM, RIM,…)
- Faserwickeln
- Handlaminieren
- optische Anwendungen, wie z. B. Carbonsichtteile (Härter **HP-E200GL**)

Verarbeitungsdaten *-Harz-* :

		HARZ
Artikelbezeichnung		***HP-E3000GL***
Farbgebung		farblos
Farbzahl	[Gardner]	< 1
Mischungsverhältnis *(Gewicht)*	[Teile]	100 : 30 *(Härter s. folgende Seite)*
Topfzeit[1] *(bei 20°C)*	**[Minuten]**	**15 - 300**
Topfzeit[1] *(bei 25°C)*	[Minuten]	10 - 180
Verarbeitungstemperatur (optimal)	[°C]	20 - 25
Verarbeitungstemperatur (minimal)	[°C]	10

HP-Textiles GmbH ~ Otto-Hahn-Str. 22 ~ D-48480 Schapen
www.hp-textiles.com info@hp-textiles.com
Tel.: +49 (0) 5905-94 598 70 Fax: +49 (0) 5905-94 598 74

Verarbeitungsdaten -*Härter*- :

		HÄRTER		
		fast	*temp*	*slow*
Hauptmerkmale		- kurze Topfzeit - für niedrige Verarbeitungs-temperaturen	- höhere Tg - farblos (Carbonsichtteile)	- lange Topfzeit - für Infusion / Injektion
Artikelbezeichnung		***HP-E15GL***	***HP-E200GL***	***HP-E300GL***
Farbgebung		farblos bis leicht gelblich		
Farbzahl	[Gardner]	< 5	< 1	< 1
Farbgebung		gelblich	farblos, klar	farblos, klar
Mischungsverhältnis *(Gewicht)*	[Teile]	100 : 30 *(Harz s. oben)*		
Topfzeit[1] *(bei 20°C)*	**[Minuten]**	**15**	**200**	**300**
Topfzeit[1] *(bei 25°C)*	[Minuten]	10	150	180
Verarbeitungstemperatur (optimal)	[°C]	20-25	20-30	20-30
Verarbeitungstemperatur (minimal)	[°C]	10	15	15

optimaler Härtezyklus **HP-E15GL, HP-E300GL, HP-E200GL**	[h bei °C]	5h/60°C und 6h/80°C
für erhöhte Temperaturbeständigkeit *(Tg Max z.B. **HP-E200GL**)*	[h bei °C]	zusätzlich 2h/120°C

Spezifikationen:

Definierte und quantifizierte Merkmale unterliegen ständiger Kontrolle.

		Harz	**Härter**			
			fast	*temp*	*slow*	
Artikelbezeichnung		***HP-E3000GL***	***HP-E15GL***	***HP-E200GL***	***HP-E300GL***	
Dichte (20°C)	[g/cm³]	1.14 - 1.16	0.94 – 0.98	0.92 - 0.96	0.94 - 0.98	*PM.01.002*
Viskosität (25°C)	[mPa s]	600 - 800	20 - 30	40 - 60	8 - 13	*PM.01.003*
(NH)-Equivalent	[g/EQ]		50 - 55	50 - 55	50 - 55	*berechnet*
Epoxid-Equivalent	[g/EQ]	170 - 180				*berechnet*

Die Härter sind untereinander in jedem Verhältnis kombinierbar, um so die Topfzeit, bzw. Wärmestandfestigkeit flexibel einstellen zu können.

HP-Textiles GmbH ~ Otto-Hahn-Str. 22 ~ D-48480 Schapen
www.hp-textiles.com info@hp-textiles.com
Tel.: +49 (0) 5905-94 598 70 Fax: +49 (0) 5905-94 598 74

Mechanische Daten unter Verwendung der jeweiligen Härter:

		fast	temp	slow	Methode	Anford. GL
Artikelbezeichnung		*HP-E15GL*	*HP-E200GL*	*HP-E300GL*		
Dichte	[g/cm³]	1,16	1,16	1,16	DIN EN ISO 1183-A	keine
Zugfestigkeit	[MPa]	72	82	69	DIN EN ISO 527	≥ 55
Zug-E-Modul	[MPa]	2800	2.830	2.950	DIN EN ISO 527	≥ 2.700
Bruchdehnung	[%]	5,1	6,9	7,8	DIN EN ISO 527	≥ 2,5
Biegefestigkeit	[MPa]	102	106	106	DIN EN ISO 178	≥ 100
Biege-E-Modul	[MPa]	2800	2850	2750	DIN EN ISO 178	keine
Wärmeformbeständigkeit	[°C]	79	83	82	DIN EN ISO 75-2	≥ 70
Härte	[Shore D]	83	83	83	nach Temperung	keine
Wasseraufnahme 168h bei 23°C	[mg]	18	22	40	DIN EN ISO 175	≤ 50
Glasübergangstemperatur Tg MAX	[°C]	91	107	92	HP04.08	keine

Physikalische Daten ermittelt am ungefüllten Probekörper bei 20°C.
Härtung erfolgte 5h bei 60°C + 6h bei 80°C. Für „Tg MAX“ zusätzlich 2h bei 120°C.

Topfzeiten:

[1] Die Ermittlung der Topfzeit erfolgt nach interner Methode (HP04.06).
Hierbei werden 100g angemischtes Harzsystem in eine Alu-Schale eingewogen und die Becherbodentemperatur gemessen. Die Topfzeit ist der Zeitwert bei erreichen der 40°C Marke.

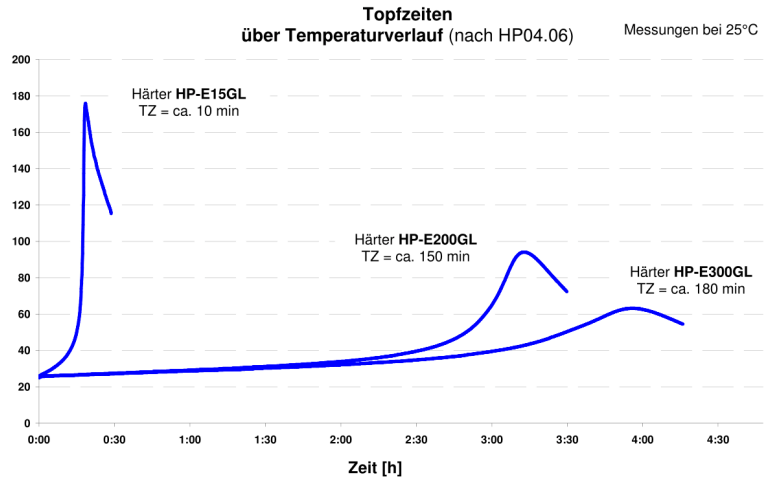

Bemerkung: Höhere Temperaturen oder größere Ansätze verkürzen die Topfzeiten deutlich!

HP-Textiles GmbH ~ Otto-Hahn-Str. 22 ~ D-48480 Schapen
www.hp-textiles.com info@hp-textiles.com
Tel.: +49 (0) 5905-94 598 70 Fax: +49 (0) 5905-94 598 74

Hinweise zur Zulassung:

Die Zulassung umfasst ausschließlich den zugelassenen Werkstoff.
Eine generelle Verwendbarkeit dieses Werkstoffes (auch in Verbindung mit anderen Werkstoffen) ist davon unabhängig durch den Hersteller oder den Anwender in geeigneter Form nachzuweisen.

Sicherheitshinweise:

Die Sicherheitshinweise sind den jeweiligen Gebinden zu entnehmen.
Nicht in die Hände von Kindern gelangen lassen. Einatmen von Dämpfen und Produktkontakt mit der Haut vermeiden. Geeignete Schutzhandschuhe und Schutzbrille tragen. Bei Anwendung nicht essen oder rauchen.
Während der Aushärtung wird Energie abgegeben, daher zur Vermeidung von Hitzestaus für ausreichende Wärmeabführung sorgen. Mengen der Einzelansätze auf den jeweiligen Arbeitsschritt abstimmen.
Das Epoxi-System ist kristallisationsarm.
Bei sehr niedrigen Temperaturen kann es dennoch zur Kristallisation des Härters kommen. Der Vorgang ist reversibel, z.B. durch Erwärmen im Wasserbad auf 40°C. Dabei auf vollständiges Aufschmelzen achten.
Lagerung und Verarbeitung des Systems unter Luftzutritt kann zur Carbamatbildung (Weißfärbung) führen.

Anwendungshinweise:

Wir empfehlen Vorversuche zur Prüfung auf Tauglichkeit für den jeweiligen Anwendungsfall.
Vor der Verarbeitung sollte das angemischte Harz ruhen und anschließend im Exsikkator unter Vakuum und leichtem Rühren ausreichend lange bei maximal 20°C entlüftet werden.

Zum Erreichen optimaler Bauteileigenschaften wird eine Temperung empfohlen.

Optimale Temperzyklen: 5h bei 60°C + 6h bei 80°C
Für erhöhte Temperaturbeständigkeit (*„Tg Max“ HP-E200GL)* zusätzlich 2h bei 120°C

Arbeitsmittelreinigung:

Nicht ausgehärtete Produktreste können mit Aceton oder Verdünner XB von Werkzeugen abgelöst werden. Arbeitsgeräte müssen nach dem Auswaschen mit dem Lösungsmittel gründlich ausgelüftet werden, um ein Eintragen des Reinigers in Folgemischungen zu vermeiden.
Ausgehärtetes Material kann nur mechanisch, z.B. durch Abschleifen entfernt werden.

Lagerung:

Schraubverschluss von Produktresten befreien. Deckel nicht vertauschen. Angebrochene Gebinde fest verschließen. Kühl und trocken lagern. Haltbarkeit bei optimaler Lagerung mindestens 12 Monate.

Liefergebinde:

Kunststoffbehälter mit Sicherheitsverschluss in unterschiedlichen Liefermengen
Größere Gebinde (z.B. Fassware, Container) nach Absprache.

Entsorgung:

Nicht in die Kanalisation, in Gewässer oder ins Erdreich gelangen lassen. Nicht ausgehärtete Produktreste sind Sonderabfall. Das ausgehärtete System ist Baustellenabfall / Hausmüll.

Weiterführende Informationen:

Weitere anwendungsspezifische Informationen können angefordert oder auf unserer Internetseite unter Produktinfo abgerufen werden. Gerne beraten wir Sie auch telefonisch.

HP-Textiles GmbH ~ Otto-Hahn-Str. 22 ~ D-48480 Schapen
www.hp-textiles.com info@hp-textiles.com
Tel.: +49 (0) 5905-94 598 70 Fax: +49 (0) 5905-94 598 74

Epoxidharz-Serie HP-E3000RI

- Härter HP-E30RI / HP-E120RI / HP-E300RI -

Basis der **Serie HP-E3000RI** bildet ein ungefülltes Epoxidharz, welches mit unterschiedlichen Härtern individuell für den jeweiligen Verwendungszweck eingestellt werden kann. Die Härter **HP-E30RI** und **HP-E300RI** erlauben die Einstellung der Topfzeit zwischen ca. 30 und 300 Minuten. Außerdem kann durch die Verwendung des Härters **HP-E120RI** die Temperaturbeständigkeit erhöht werden.

Die Injektions- / Infusionssysteme zeichnen sich aus durch eine besonders niedrige Viskosität. Daraus resultieren optimale Tränkungs- und Fließeigenschaften. Ein Einsatz im Handlaminierverfahren ist ebenfalls möglich.

Eigenschaften und Einsatzgebiete:

- sehr leichte Tränkung der Verstärkungsfasern im Infusions- und Injektionsverfahren
- warmhärtend, bei erhöhter Temperatur entformbar
- hohe statische und dynamische Festigkeiten
- besonders geeignet für RTM / RI - Verfahren
- Einsatz z.B. in Modellbau, KFZ, Yacht- und Bootsbau sowie Rotorblattherstellung
- Glasübergangstemperaturen bis 98 °C (Härter HP-E12 0RI)
- mit Thixotropiermittel HP-PK22 auch im Handlaminierverfahren einsetzbar

Verarbeitungsdaten:

		Harz	Härter		
		E3000RI	E30RI	E300RI	E120RI
Farbgebung		farblos	farblos bis leicht gelblich		
Farbzahl	[Gardner]	< 2	< 3		
Mischungsverhältnis *(Gewicht)*	[Teile]	100	30		
Topfzeit *(bei 20°C)*	[Minuten]		35	300	200
Topfzeit *(bei 25°C)*	[Minuten]		30	180	150
optimale Verarbeitungstemperatur	[°C]	→	20-25	20-30	20-30
minimale Verarbeitungstemperatur	[°C]	→	10	15	15

Optimaler Härtezyklus mit den Härtern HP-E30RI o. HP-E300RI	[h bei °C]	24h bei 20°C, dann 5h/60°C und 6h/80°C
Optimaler Härtezyklus HP-E120RI	[h bei °C]	24h bei 20°C, dann 5h/60°C und 6h/80°C und 2h/100°C

Beachten Sie auch die spezielle Vorgehensweise zur Entgasung und Warmhärtung in der Rubrik „Anwendungshinweise“!

Die Angaben in diesem Produktdatenblatt wurden nach bestem Wissen zusammengestellt und entsprechen unserem derzeitigen Erkenntnisstand. Eine Verbindlichkeit / Gewährleistung für das Verarbeitungsergebnis im Einzelfall, können wir jedoch aufgrund der Vielzahl der Anwendungsmöglichkeiten und der außerhalb unseres Einflusses liegenden Lagerungs- und Verarbeitungsbedingungen unserer Produkte nicht übernehmen. Wir raten generell zu Vorversuchen. Mit erscheinen des Datenblattes werden alle früheren Ausgaben und daraus resultierende Daten ungültig.

HP-Textiles ~ Otto-Hahn-Str. 22 ~ D-48480 Schapen ~ Tel.: +49 (0) 5905-94 598 70 ~ Fax.: +49 (0) 05905-94 598 74
www.hp-textiles.com info@hp-textiles.com
Revision 2011-09.3

Technisches Datenblatt

Injektionsharz - Serie HP-E3000RI

Spezifikationen:

Definierte und quantifizierte Merkmale unterliegen ständiger Kontrolle.

		Harz	Härter			
			E30RI	E300RI	E120RI	*Methode*
Dichte (20℃)	[g/cm³]	1.14 - 1.16	0.92 - 0.96	0.94 - 0.98	0.92 - 0.96	*PM.01.002*
Viskosität (25℃)	[mPa s]	400 - 600	30 - 50	8 - 13	40 - 60	*PM.01.003*
(NH)-Equivalent	[g/EQ]		50 - 55	50 - 55	50 - 55	*berechnet*
Epoxid-Equivalent	[g/EQ]	170 - 180				*berechnet*

Die Härter der drei Varianten sind untereinander kombinierbar, um so die Topfzeit, bzw. Wärmestandfestigkeit flexibel einstellen zu können.

Mechanische Daten / Normklima [1])

		HP-E30RI	HP-E300RI	HP-E120RI	*Methode*
Dichte	[g/cm³]	1.1	1.1	1.1	*PM.01.002*
Zugfestigkeit	[MPa]	72	72	71	*PM.01.004*
Bruchdehnung	[%]	4 - 5 *1	5 - 6	4 - 5 *1	*PM.01.004*
Biegefestigkeit	[MPa]	110 *1	110	110 *1	*PM.01.005*
E-Modul (Zug)	[kN/mm²]	3	3	2.9	*PM.01.004*
Glasübergangstemperatur	[℃]	90	83	98	*PM.01.011*
Härte	[Shore D]	82	83	83	*PM.01.009*

Physikalische Daten ermittelt am ungefüllten Probekörper / 20℃. Temperung variiert je nach Härtervarian te.
HP-E30RI, HP-E300RI: Härtung erfolgte 24h bei 20℃ + 5h bei 60℃ + 6h bei 80℃.
HP-E120RI: Härtung erfolgte 24h bei 20℃ + 5h bei 60℃ + 6h bei 80℃ + 2h bei 10 0℃.

**1) Erwartungswerte werden nach Validierung durch externes Labor ersetzt*

Referenzen

Das Infusionsharz HP-E3000RI wurde in enger Kooperation mit der Hochschule Osnabrück entwickelt und getestet.
Durch das Ignition-Racing Team der Hochschule Osnabrück wird es u. a. erfolgreich für den Bau der Formelfahrzeuge (Kohlefaser-Monocoque) der Formula Student eingesetzt.

IGNITION RACING TEAM

Hochschule Osnabrück
University of Applied Sciences

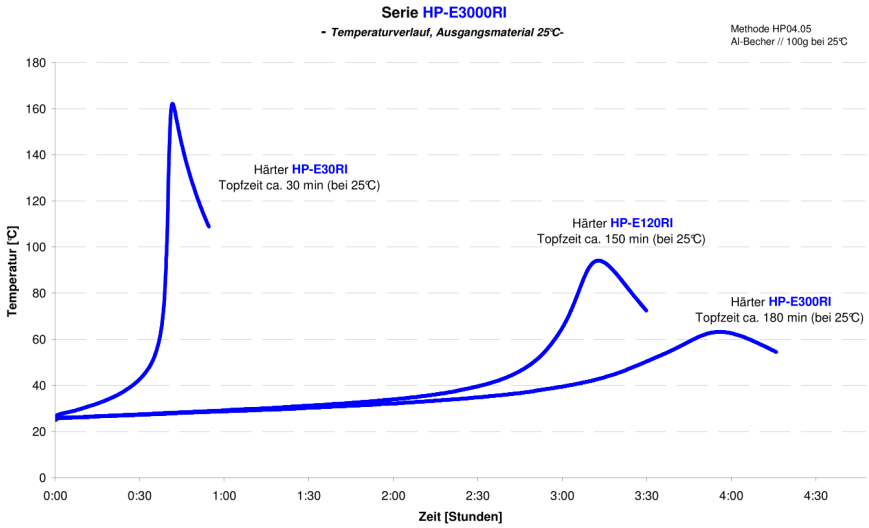

Bem.: Höhere Temperaturen oder größere Ansätze verkürzen die Topfzeiten deutlich!

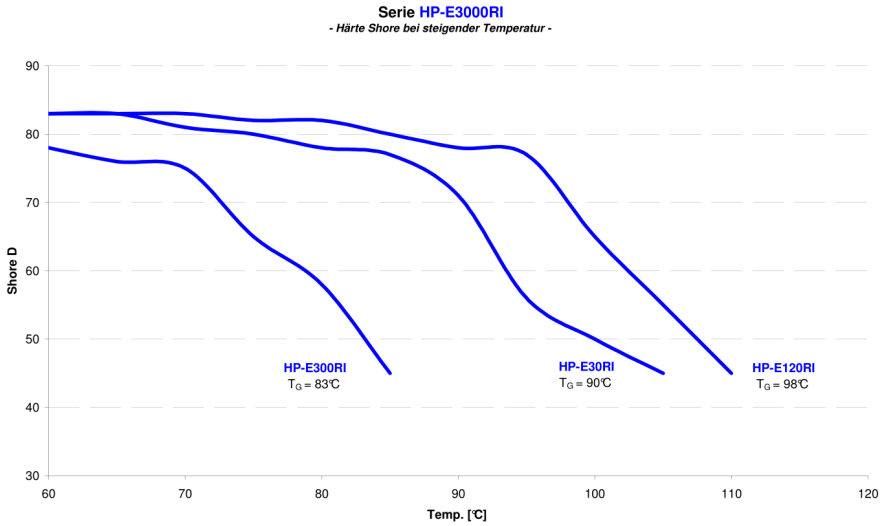

Bem.: Dargestellt ist die Abnahme der Festigkeit (über die Härte Shore D) mit zunehmender Temperatur.

HP-Textiles ~ Otto-Hahn-Str. 22 ~ D-48480 Schapen ~ Tel.: +49 (0) 5905-94 598 70 ~ Fax.: +49 (0) 05905-94 598 74
www.hp-textiles.com info@hp-textiles.com *Revision 2011-09.3*

Sicherheitshinweise:

Die Sicherheitshinweise sind den jeweiligen Gebinden zu entnehmen.
Nicht in die Hände von Kindern gelangen lassen. Einatmen von Dämpfen und Produktkontakt mit der Haut vermeiden. Geeignete Schutzhandschuhe und Schutzbrille tragen.
Bei Anwendung nicht essen oder rauchen.
Während der Aushärtung wird Energie abgegeben, daher zur Vermeidung von Hitzestaus für ausreichende Wärmeabführung sorgen. Mengen der Einzelansätze auf den jeweiligen Arbeitsschritt abstimmen.

Anwendungshinweise:

Wir empfehlen Vorversuche zur Prüfung auf Tauglichkeit für den jeweiligen Anwendungsfall.
Vor der Verarbeitung sollte das angemischte Harz ruhen und anschließend im Exsikkator unter Vakuum und leichtem Rühren ausreichend lange bei maximal 20℃ entlüftet werden.

Infusionsverfahren (RI) / Harztransferpressen (RTM):

Vor der Infusion werden die zugeschnittenen Verstärkungslagen und geeignete Kernmaterialien in die Form eingelegt. Das sorgfältig vermischte und entlüftete Harz wird über Anschlüsse mittels Vakuum oder leichtem Überdruck in die Form geleitet. Bei mehrschichtigen Lagenaufbauten, bzw. kompakten Verstärkungsfasern mit höherem Flächengewicht, sollten mehrere Anschlüsse geschaffen werden.
Zum Erreichen optimaler Bauteileigenschaften sollte im Anschluss getempert werden.

Arbeitsmittelreinigung:

Nicht ausgehärtete Produktreste können mit Aceton oder Verdünner XB von Werkzeugen abgelöst werden. Arbeitsgeräte müssen nach dem Auswaschen mit dem Lösungsmittel gründlich ausgelüftet werden, um ein Eintragen des Reinigers in Folgemischungen zu vermeiden.
Ausgehärtetes Material kann nur mechanisch, z.B. durch Abschleifen entfernt werden.

Lagerung:

Schraubverschluss von Produktresten befreien. Deckel nicht vertauschen. Angebrochene Gebinde fest verschließen. Kühl und trocken lagern. Haltbarkeit bei optimaler Lagerung mindestens 12 Monate.
Bei niedrigen Temperaturen kann es zur Kristallisation des Härters kommen. Der Vorgang ist reversibel, z.B. durch Erwärmen des Behälters im Wasserbad auf 40℃. Dabei auf vollständiges Aufschmelzen achten.
Lagerung und Verarbeitung des Systems unter Luftzutritt kann zur Carbamatbildung (Weißfärbung) führen.

Liefergebinde:

Kunststoffbehälter mit Sicherheitsverschluss in unterschiedlichen Liefermengen
Größere Gebinde (z. B. Fassware, Container) nach Absprache.

Entsorgung:

Nicht in die Kanalisation, in Gewässer oder ins Erdreich gelangen lassen. Nicht ausgehärtete Produktreste sind Sonderabfall. Das ausgehärtete System ist Baustellenabfall/ Hausmüll.

Weiterführende Informationen:

Weitere anwendungsspezifische Informationen können angefordert oder auf unserer Internetseite unter Produktinfo abgerufen werden. Gerne beraten wir Sie auch telefonisch.

HP-Textiles ~ Otto-Hahn-Str. 22 ~ D-48480 Schapen ~ Tel.: +49 (0) 5905-94 598 70 ~ Fax.: +49 (0) 05905-94 598 74
www.hp-textiles.com info@hp-textiles.com *Revision 2011-09.3*

APPENDIX B PRODUCTION DETAILS FOR THE HYBRID TEST SAMPLES

Surface Preparation For Aluminium Plates

i. Al plate is rinsed with distilled water, then wiped with acetone.

ii. Aluminium plate is soaked in beaker filled with acetone and heated up to 30°C for 15 minutes in the ultrasonic bath.

iii. Before sand blasting the plate is taped to expose only the bonding area of 12.5 mm length and protect the rest of the surface.

iv. The open surface is sand blasted for 25 to 30 seconds, until the surface looks homogeneous.

v. After adhesive tape is removed, remaining sand on the plate is air brushed, and plate is cleaned again in US bath at 30°C for 15 minutes.

vi. It is important to do bonding procedure within 4 hours after surface preparation, otherwise the surface will be contaminated and will be no longer active to provide proper bonding (DIN EN 13887) .

Preparation of Carbon Fiber Fabrics and Aluminium Plate for Vacuum Infusion Process

i. Two layers of plain 1x1 weave and two layers of +45/-45/0 triaxial carbon fabrics are cut into 140 mm x 160 mm rectangles.

ii. Release agent is applied to entire surface of aluminium plate except the bonding area. The reason is to ease the removing of excess adhesive cured on the test sample.

iii. Aluminium plate is placed in the mould. The surface next to bonding area is covered with PTFE tape, in order to prevent unwanted bonding between fabric and aluminium outside the bonding area. (Figure 57)

iv. Carbon fabric layers are placed in the mould, with stacking sequence $[(+45/-45/0)/0]_s$ when resin flow direction is considered 0°. (Figure 57)

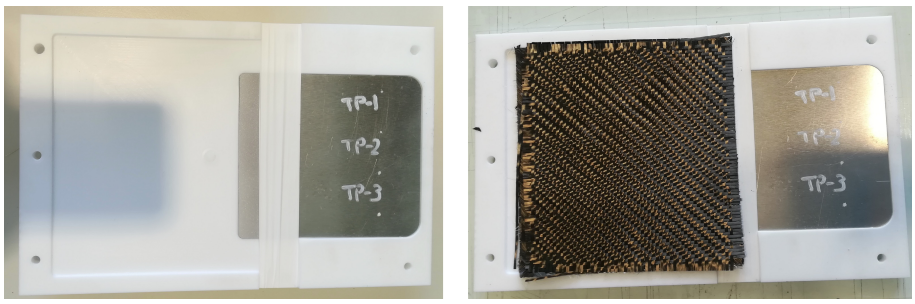

Figure 57. Mould with aluminium and carbon fabrics

Resin Preparation

Two types of resin was used; Elium 150 thermoplastic resin and HP-E3000 Epoxy-Hardener system. The data sheet instructions are followed.

Thermoplastic Resin

i. A pot is filled with water, and brought to 30°C on a hotplate stirrer (VWR VMS-C7).

ii. Peroxide, compound that initiates the polymerization process, is mixed with resin with 1.5% ratio in a cup. Two small magnet rods are placed in the mixture. Top of the cup is closed.

iii. Mixture is placed in the water filled pot and mixed for 3 minutes at 30°C and 100 rpm with the help of magnets and hotplate stirrer.

iv. After mixing, resin is let to settle for 2 minutes before infusion process.

Epoxy Resin

i. A pot is filled with water, and brought to 40°C on a hotplate stirrer (VWR VMS-C7).

ii. Epoxy Hardener (HP-E300RI) is mixed with Epoxy resin (HP-E3000GL) with weight ratio 30:100 in a cup. Two small magnet rods are placed in the mixture. Top of the cup is closed.

iii. Mixture is placed in the water filled pot and mixed for 3 minutes at 40°C and 100 rpm with the help of magnets and hotplate stirrer.

iv. The epoxy resin mixture is degassed for 6 minutes.

v. After mixing, resin is let to settle for 2 minutes before infusion process.

Vacuum Infusion Process

i. Inlet spiral tube and outlet spiral tubes are placed on the mould. Outlet tube is covered with membrane, therefore there is no need for resin trap to capture the excess resin.

ii. Peel ply, breather and flow mesh are placed on top of the carbon fabrics. (Figure 58)

iii. After sealing vacuum bag, vacuum is initiated to check any air leakage.

iv. When vacuum is established (around 4 mbar), inside the mould is dehumidified for 1 minute using silica pearls.

v. Inlet tube is release to let the resin flow. When complete wetting of fabrics is succeeded, resin flow is cut and mould is left for curing.

Figure 58. Peel ply, flow mesh and spiral tube configuration in VIP

Tempering and Cutting of Hybrid Samples

i. Hybrid plates with thermoplastic resin is tempered at 80°C for 4 hours. Epoxy resin plate is tempered first at 60°C for 6 hours and 80°C for 4 hours.

ii. Samples are cut using table cutting wheel (Struers Discotom-6) at 0.5 mm/s feeding speed following the DIN EN 2243-1 standard as much as possible.

iii. CFRP edge is cut out to have 100 mm long CFRP part. (Figure 59)

iv. 8 mm from the long edge of aluminium is cut away along the whole length of hybrid structure. (Figure 59)

v. Three 25 mm thick test objects are cut out from the hybrid stucture.

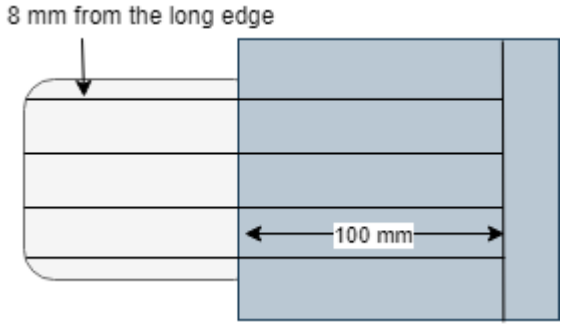

Figure 59. Cutting the hybrid structure into test samples

APPENDIX C ULTRASONIC SYSTEM PARAMETERS

Signal Generator Parameters				
	Nominal	Minimum	Optimum	Maximum
Frequency (MHz) :	0.75	0.20	1.60	3.00
Pulse Length :	4	1	8	15
Pulse Distance (μs) :	12500			
Pulse Rate (Hz) :	80			
* *Internal Trigger is used.*				
Probe Parameters (Probe Name: Probe8/45)				
	Nominal	Minimum	Optimum	Maximum
Scanning Angle :	45	45	65	90
Frequency (MHz) :	0.75	0.20	1.60	3.00
Pulse Length :	4	1	8	15
Transmitter & Receiver Parameters *				
Transmitter Delay Time (ns) :	0			
Receiver Delay Time (ns) :	0			
Receiver Filter Range (MHz) :	0.20-1.40			
* *Only one channel is used (Channel 1).*				
Angle Scanning Parameter				
Sample Number :	46			
Minimum Angle :	45			
Maximum Angle :	90			
Delta Angle :	10			
Data Acquisition Parameters				
Start Time of Data Acquisition (μs)	Minimum	Maximum	Δt	
Input Chanel A :	5.000	30.588	0.025	
Input Chanel B :	10.000	35.888	0.025	

APPENDIX D MOUNTING OF EMAT HOLDER

In order to keep the positions of the EMATs relative to the test sample, tolerances of each part were kept minimum. The contact of EMATs to the test samples are ensured by using springs (Part 16) to pull them on the sample.

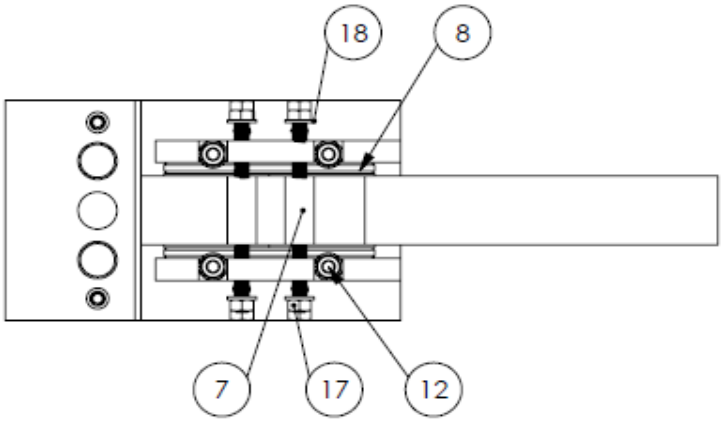

Figure 60. Front view of the EMAT holder tool

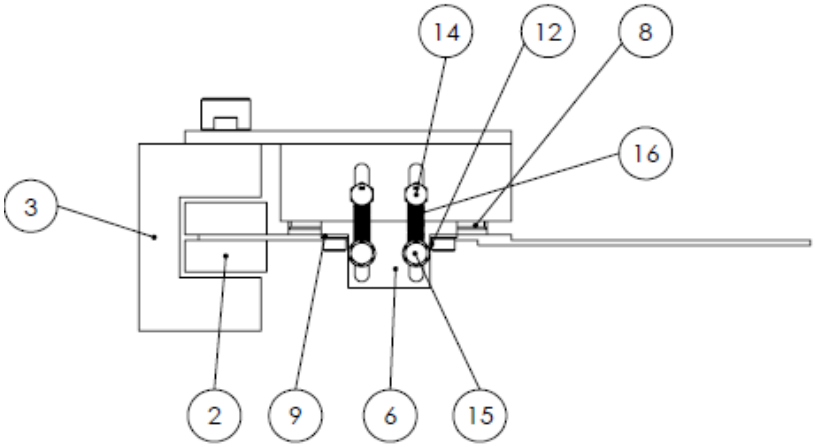

Figure 61. Side view of the EMAT holder tool

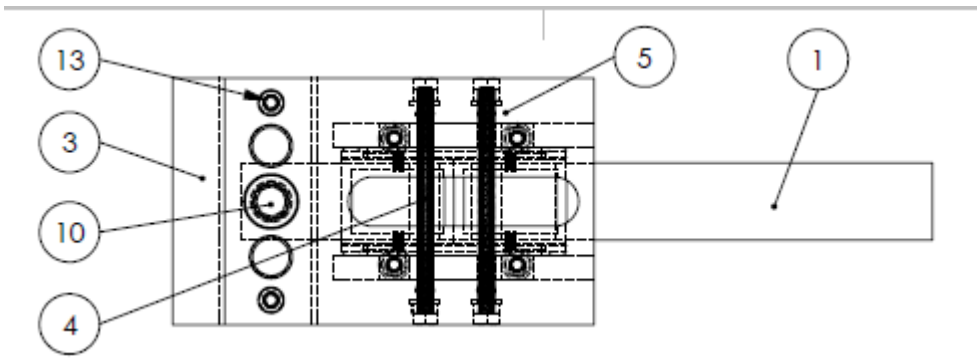

Figure 62. Back view of the EMAT holder tool

- Part 8 is fastened on the EMATs with DIN 7991 M3x6 socket head countersunk screws on both sides. The edge of sender EMAT is aligned with the plate (Part 8), where the edge of receiver is 1 mm away from the edge of the plate. Care must be taken the level both sender and receiver EMATs and Part 8.
- If the positions of the EMATs are to be changed, slot with 10 mm length allows increasing the distance between EMATs up to 20 mm. However, for the assembly of complete EMAT Holder, EMAT on the left hand side can be moved to the left maximum to 9 mm.
- EMATs that are held by plates (2 x Part 8) are put into Part 5 as shown in figure. Then Part 6 is fastened on Part 5 by DIN 912 M5x10 socket head screws and M5 washers.
- DIN 912-M5 x 20 screws are passed through the springs hook and through the slots of Part 5 and fastened to the M5 threaded holes on Part 8.
- The assembled parts are mounted on the upper cross head of the tensile test machine by first fastening two DIN 912 M5 x 25 screws, then DIN912-M12 x 20 screw in the middle hole.
- At this point, test sample should be fixed to the clamps on tensile test machine.
- DIN 933- M5 x 70 screws are covered with PTFE tape to prevent extra friction during the movement of the springs. Finally, the screws are passed through the spring hooks and the plastic hollow rod.

APPENDIX E RESULTS-Initial State of Hybrid Samples

Parameter:	Amplitude (V)					
# of Wave Packet:	1st Wave Packet		2nd Wave Packet		3rd Wave Packet	
Statistics:	μ	σ	μ	σ	μ	σ
Aluminium:	1.835	0.114	1.580	0.014	1.596	0.109
TP1-1:	1.879	0.073	0.390	0.023	1.640	0.056
TP1-2:	1.904	0.094	0.236	0.029	1.630	0.049
TP1-3:	1.807	0.267	0.227	0.043	1.539	0.265
TP2-1:	1.959	0.014	0.888	0.029	1.603	0.030
TP2-2:	1.975	0.018	0.961	0.029	1.666	0.034
TP2-3:	1.880	0.029	0.712	0.034	1.496	0.090
Ep1:	1.775	0.129	1.035	0.060	1.542	0.145
Ep2:	1.800	0.121	1.035	0.058	1.545	0.122
Ep3:	1.841	0.045	1.199	0.034	1.564	0.049

Parameter:	Time of Flight (μs)					
# of Wave Packet:	1st Wave Packet		2nd Wave Packet		3rd Wave Packet	
Statistics:	μ	σ	μ	σ	μ	σ
Aluminium:	12.653	0.026	28.426	0.221	46.358	0.218
TP1-1:	12.653	0.026	27.389	1.039	46.070	0.774
TP1-2:	12.653	0.026	29.798	2.301	45.840	0.630
TP1-3:	12.379	0.004	29.168	0.694	45.838	0.076
TP2-1:	12.379	0.004	29.168	0.694	45.838	0.076
TP2-2:	12.387	0.012	29.597	0.600	45.642	0.040
TP2-3:	12.379	0.012	28.635	0.523	45.749	0.069
Ep1:	12.643	0.026	29.933	1.104	45.926	0.802
Ep2:	12.653	0.026	29.002	0.593	46.330	0.171
Ep3:	12.662	0.021	29.702	0.086	46.118	0.645

Parameters	Normalized Amplitude			
# of Wave Packet	A2/A1		A3/A1	
Statistics	μ	σ	μ	σ
Aluminium:	0.864	0.056	0.871	0.059
TP1-1:	0.208	0.011	0.874	0.047
TP1-2:	0.125	0.022	0.857	0.030
TP1-3:	0.128	0.029	0.849	0.030
TP2-1:	0.453	0.015	0.818	0.013
TP2-2:	0.486	0.015	0.844	0.018
TP2-3:	0.379	0.016	0.795	0.038
Ep1:	0.584	0.017	0.868	0.025
Ep2:	0.576	0.021	1.545	0.122
Ep3:	0.651	0.012	1.564	0.049